

Using eDNA to Track Microbial and Meiofaunal Communities in the  
Environment Surrounding Coastal Finfish Aquaculture in Nova Scotia

by

Connor Mackie

Submitted in partial fulfilment of the requirements  
for the degree of Master of Science

at

Dalhousie University  
Halifax, Nova Scotia  
March 2021

© Copyright by Connor Mackie, 2021

# TABLE OF CONTENTS

LIST OF TABLES.....	i
LIST OF FIGURES .....	i
ABSTRACT .....	viii
LIST OF ABBREVIATIONS USED .....	ix
ACKNOWLEDGEMENTS.....	xi
CHAPTER 1: INTRODUCTION .....	1
1.1. Aquaculture .....	1
1.2. Fallowing.....	2
1.3. Environmental Monitoring .....	3
1.4. Aquaculture in Canada .....	3
1.5. Environmental DNA.....	4
CHAPTER 2: TRACKING CHANGES IN MICROBIAL AND MEIOFAUNAL COMMUNITIES IN THE WATER COLUMN AND SEDIMENTS AROUND COASTAL FINFISH AQUACULTURE.....	7
2.1. Introduction .....	7
2.1.1 Environmental Monitoring.....	7
2.1.2. Microbiota in Environmental Monitoring.....	7
2.2. Materials and Methods .....	8
2.2.1. Sample Collection.....	8
2.2.2. DNA Extraction .....	10
2.2.3. DNA Sequencing .....	11
2.2.4. Bioinformatics.....	11
2.2.5. Statistical Analysis.....	12
2.3. Results .....	13
2.3.1. Site Characteristics.....	13
2.3.2. Alpha Diversity of Microbial and Meiofaunal Communities .....	14
2.3.3. Beta Diversity of Microbial and Meiofaunal Communities Across the Sampling Period	16
2.3.4. Beta Diversity of Microbial and Meiofaunal Communities Within Sampling Days.....	19
2.3.5. Eukaryotic Community Composition .....	23
2.3.6 Prokaryotic Community Composition .....	28
2.3.7. Potential Indicator Organisms for Organic Loading.....	33
2.4. Discussion.....	36

2.4.1. Patterns in Water Column and Sediment Community Composition During the Study Period .....	36
2.4.2. Daily Patterns at Individual Sampling Sites .....	37
2.4.3. Effects of Aquaculture and Fallowing on Benthic Communities .....	39
2.5. Conclusions .....	41
CHAPTER 3: SHOTGUN METAGENOMIC ANALYSIS OF SULFUR METABOLIZING BACTERIA .....	42
3.1. Introduction .....	42
3.1.1 Sulfur Cycle .....	42
3.1.2. Shotgun Metagenomics and the Sulfur Cycle in Aquaculture.....	44
3.2. Materials and Methods .....	46
3.2.1. Sample Collection.....	46
3.2.2. DNA Extraction and Analysis .....	47
3.3. Results .....	49
3.3.1. Distribution of Metabolic Pathways Across Sampling sites.....	49
3.3.2. Distribution of Sulfur Cycling Genes Across Sampling sites.....	50
3.3.3 Taxonomy of SOB Associated with the <i>rdsrC</i> Gene.....	52
3.3.4. Taxonomy of SRB Associated with the <i>dsrC</i> Gene.....	56
3.3.5. Taxonomy of SOB Associated with the <i>soxB</i> Gene .....	60
3.4. Discussion.....	65
3.4.1. Metagenomic Results Relating back to Amplicon Sequencing.....	65
3.4.2. SOB and SRB Identified Through the Dsr Pathway.....	65
3.4.3. SOB Identified Through the Sox Pathway.....	68
3.5. Conclusions .....	68
CHAPTER 4: EVALUATION OF QPCR ASSAYS FOR QUANTIFICATION OF ALEXANDRIUM SP. IN THE SEDIMENT SURROUNDING FINFISH AQUACULTURE IN SHELBURNE, NOVA SCOTIA .....	70
4.1. Introduction .....	70
4.1.1. Effect of HABs on Aquaculture in the North Atlantic .....	70
4.1.2. Monitoring HABs .....	71
4.1.3. qPCR Monitoring.....	73
Materials and Methods .....	74
4.2.1. Sample Collection.....	74
4.2.2. DNA Processing.....	75
4.2.3. qPCR Optimization and Application .....	75

4.3. Results .....	77
4.3.1. Initial Testing .....	77
4.3.2. sxtA4 Optimization .....	79
4.3.3. LSU Optimization .....	79
4.4. Discussion .....	81
4.5. Conclusions .....	82
CHAPTER 5: CONCLUSIONS .....	83
REFERENCES .....	86
APPENDIX A: SUPPLEMENTAL MATERIAL .....	96

## LIST OF TABLES

Table 2.1: Primers used for Illumina MiSeq amplicon sequencing. All primers are reported 5'-3' in orientation .....	11
Table 3.1: Table of references to confirm sulfur metabolism in the top 10 most abundant oxidizers (rDsr) and reducers (Dsr) and the corresponding direction of Dsr pathway.....	56
Table 4.1: LSU and <i>sxtA4</i> qPCR primers from Murray <i>et al.</i> (2019).....	76
Table 4.2: Conditions for initial 2 optimization runs of each assay. Note: Only variables that differ amongst optimization runs are recorded in this table, mainly the concentration of primers, the addition of BSA and the elongation time. ....	77
Table 4.3: Primer combinations and the corresponding efficiencies for the first 2 tests of both assays. Primer concentrations recorded in this table are the stock concentrations.....	78
Table S1: Outline of McNutt's stations sampled at each timepoint for sediment.....	96
Table S2: Outline of McNutt's stations sampled at each timepoint for water. ....	96
Table S3: Overview of sediment samples taken at the McNutt's site on each sampling day. Highlighted and bolded samples were sequenced using shotgun metagenomics. ....	97
Table S4: Most significant bacterial ASV for the different station types on each sampling date as determined by indicpecies analysis. No ASVs were found to be significantly associated with any station type on Day 2, nor with barge or buoy stations on Day 3. ....	99
Table S5: Prokaryotic taxa from Figure 2.13 and the taxonomic families they belong to. Families denoted by a * are plotted in the previous sediment taxonomic bar plot (Figure 2.10).....	102
Table S6: Prokaryotic taxonomic families found in the sediment (Figure 2.10) and the phylum to which they belong, as well as a description of their metabolism and other relevant information. ....	103
Table S7: Outline of Hartz and Sandy Points stations sampled at each timepoint for sediment.....	118
Table S8: Conditions for each optimization run of each assay. Note: Only variables that differ amongst optimization runs are recorded in this table. * Denotes runs where PowerUp SYBR was used. ....	118

Table S9: Primer combinations and the corresponding efficiencies for the 3 <sup>rd</sup> test of the sxt assay. Primer concentrations recorded in this table are the final concentration in the PCR tube.....	121
Table S10: Primer combinations and the corresponding efficiencies for the 4 <sup>th</sup> test of the sxt assay. Primer concentrations recorded in this table are the final concentration in the PCR tube. ....	122
Table S11: Primer combinations and the corresponding efficiencies for the 3 <sup>rd</sup> and 4 <sup>th</sup> tests of the LSU assay. Primer concentrations recorded in this table are the final concentration in the PCR tube. ....	123
Table S12: Primer combinations and the corresponding efficiencies for the 5 <sup>th</sup> test of the LSU assay. Primer concentrations recorded in this table are the final concentration in the PCR tube. ....	124
Table S13: Primer combinations and the corresponding efficiencies for the 6 <sup>th</sup> test of the LSU assay. Primer concentrations recorded in this table are the final concentration in the PCR tube. ....	125
Table S14: Primer combinations and the corresponding efficiencies for the 7 <sup>th</sup> test of the LSU assay. Primer concentrations recorded in this table are the final concentration in the PCR tube. ....	125
Table S15: Results from LSU assay test 3. Quantities were calculated using the formula from the line of best fit for the standard curve.....	126

## LIST OF FIGURES

- Figure 2.1: Map of the McNutt’s sampling area in relation to (a) all of Nova Scotia and (b) close up of the farm area, indicated by red dashed lines, and sampling layout. In (b), stations beginning with C are cages, those beginning with B are farm buoys, and Bg represents the on-site barge. Black dots represent cage and barge samples, while blue dots represent buoy stations. .... 10
- Figure 2.2: Shannon diversity index of eukaryotes (18S V4) in the a) sediment and b) water column and prokaryotes (16S V6V8) in the c) sediment and d) water column across the sampling period. For each day, the samples are reported in the order seen in the legend: barge, buoy, cage, except for September 2018 where there are no buoy samples. Red vertical dotted lines show the time fallowing occurred and split the plots into the three time periods outlined in the methods: production cycle 1 (P1), mid-fallowing (F), and production cycle 2 (P2). Tukey results for each plot are labelled above each day and days that share the same letter are not significantly different. .... 16
- Figure 2.3: nMDS plots of a) sediment 18S V4, b) water column 18S V4, c) sediment 16S V6V8, and d) water column 16S V6V8 amplicon sequencing for all days of sampling. Ellipses outline the time periods described in the methods: production cycle 1 (P1), mid-fallowing (F), and production cycle 2 (P2). Note: depth only applies to water column samples as all sediment samples are from approximately the same depth. .... 18
- Figure 2.4: nMDS plots of 18S V4 amplicon sequencing of sediment eukaryote communities from each sampling day. Plot A is from time period P1, B from time period F, and C-F from time period P2. Communities from September 2018 are not represented because there were too few samples to conduct a robust nMDS analysis. .... 20
- Figure 2.5: nMDS plots of 18S V4 amplicon sequencing of water column eukaryote communities from each sampling day. Plots A-B are from time period P1, C from time period F, and D-F from time period P2. Communities from November 2019 are not represented because there were too few samples to conduct a robust nMDS analysis. .... 21
- Figure 2.6: nMDS plots of 16S V6V8 amplicon sequencing of sediment prokaryote communities from each sampling day. Red ellipses on plots (d), (e), and (f) indicate samples from the two cages at the open-ocean end of the farm (C5 & C6). Plot A is from time period P1, B from time period F, and C-F from time period P2. Communities from September 2018 are not represented because there were too few samples to conduct a robust nMDS analysis. .... 22
- Figure 2.7: nMDS plots of 16S V6V8 amplicon sequencing of water column prokaryote communities from each sampling day. Plots A-B are from time period P1, C from time period F, and D-F from time period P2. .... 23

Figure 2.8: Bubble plot of the top 10 eukaryotic ASVs with the highest relative abundance in the sediment from each sampling day. ASVs for each day were compiled into one list, run through BLAST and taxonomy was recorded down to the lowest possible level. In cases where more than one ASV came back as the same organism the counts were added together within each sample. .... 25

Figure 2.9: Bubble plot of the top 10 dominant eukaryotic ASVs with the highest relative abundance in the water column from each sampling day. ASVs for each day were compiled into one list, run through BLAST and taxonomy was recorded down to the lowest possible level. In cases where more than one ASV came back as the same organism the counts were added together within each sample. Note that there was a sequencing issue with 10m samples from stations B2, C5, and C6 in August 2019, as well as B2 and Bg 10m, and C1 5m stations in November 2019 and blank columns are not indicative the listed ASVs were not present. .... 27

Figure 2.10: Relative abundance of the top 5 prokaryotic taxonomic families present in the sediment on each sampling date as determined by 16S V6V8 sequencing. Buoy and Farm samples are ordered left to right from inland (I) to seaward (S). ASV's unclassified to the family level were excluded and represented by white space on the y-axis. The letters ABC in x-axis labels indicate sediment replicates. Plots A-B are from time period P1, C from time period F, and D-G from time period P2..... 30

Figure 2.11: Relative abundance of the top 5 prokaryotic taxonomic families present in the water column on each sampling date as determined by 16S V6V8 sequencing. In each section, samples are ordered left to right from inland to open ocean. ASV's unclassified to the class levels were excluded and represented by white space on the y-axis. In the x-axis labels, samples ending in A are from 10m water, and those ending in B are from 5m water. Plots A-B are from time period P1, C from time period F, and D-G from time period P2. .... 32

Figure 2.12: Alluvial plot of the percent of the a) farm sediment community and b) buoy sediment community that is made up of 3 potential meiofaunal indicators of organic loading levels. Percent community was calculated using the relative abundance of each at each samples date. Black lines indicate the approximate time of fallowing and separate the 3 time periods defined in the methods. .... 34

Figure 2.13: Alluvial plot of the percent of the a) farm sediment community and b) buoy sediment community that is made up of potential microbial indicators (Vanhoeveen *et al.* 2018) of organic loading levels. Percent community was calculated using the relative abundance on each sampling date as determined by 16S V6V8 amplicon sequencing. Black lines indicate the approximate time of fallowing and separate the 3 time periods defined in the methods..... 35

Figure 3.1: Overview of the sulfur cycle pathways relevant to this study and the proteins involved. Genes investigated are highlighted in orange. The red S signifies the sulfur that is being reduced/oxidized throughout the cycle. .... 43

Figure 3.2: Map of the McNutt’s sampling area in relation to (a) all of Nova Scotia and (b) close up of the farm area, indicated by red dashed lines, and sampling layout. In (b), stations beginning with C are cages, those beginning with B are farm buoys, and Bg represents the on-site barge. Black dots represent cage and barge samples, while blue dots represent buoy stations. .... 47

Figure 3.3: A) Reads per kilobase million (RPKM) and B) Relative abundance (%) of overarching gene categories before (July 2018) and during (March 2019) following as determined by the Metacyc database (Caspi *et al.* 2014). Relative abundance was calculated for each sample by adding together raw reads of all pathways and determining the percentage of each pathway..... 50

Figure 3.4: Reads per kilobase million (RPKM) of unstratified sulfur cycling genes before (July 2018) and during (March 2019) following in the A) cage sediments and B) buoy sediments. .... 52

Figure 3.5: Reads per kilobase million (RPKM) of the *rdsrC* gene for sulfur oxidation separated by taxonomy before (July 2018) and during (March 2019) following in the A) cage sediments and B) buoy sediments. Reads are separated into reads per phylum aside from Proteobacteria which, when possible, were separated into the different classes due to abundance compared to other phyla. .... 53

Figure 3.6: Reads per kilobase million (RPKM) of Top 10 most abundant Gammaproteobacteria taxa that have the ability to perform sulfur oxidation via the *rdsrC* gene before (July 2018) and during (March 2019) following in the A) cage sediments and B) buoy sediments. Reads are separated into the lowest taxonomy level possible from the stratified table. References supporting that these taxa are sulfur oxidizers are listed in Table 3.1. .... 55

Figure 3.7: Reads per kilobase million (RPKM) of the *dsrC* gene for sulfur reduction separated by taxonomy before (July 2018) and during (March 2019) following in the A) cage sediments and B) buoy sediments. Reads are separated into reads per phylum aside from Proteobacteria which, when possible, were separated into the different classes due to abundance compared to other phyla. .... 58

Figure 3.8: Reads per kilobase million (RPKM) of Top 10 most abundant Deltaproteobacteria taxa that have the ability to perform sulfur reduction via the *dsrC* gene before (July 2018) and during (March 2019) following in the A) cage sediments and B) buoy sediments. Reads are separated into the lowest taxonomy level possible from the stratified table. References supporting that these taxa are sulfur reducers are listed in Table 3.1..... 59

Figure 3.9: Reads per kilobase million (RPKM) of the <i>soxB</i> gene separated by taxonomy before (July 2018) and during (March 2019) following in the A) cage sediments and B) buoy sediments. Reads are separated into reads per phylum aside from Proteobacteria which, when possible, were separated into the different classes due to abundance compared to other phyla. ....	61
Figure 3.10: Reads per kilobase million (RPKM) of Top 10 most abundant Alphaproteobacteria taxa that have the ability to perform sulfur oxidation via the <i>soxB</i> gene before (July 2018) and during (March 2019) following in the A) cage sediments and B) buoy sediments. Reads are separated into the lowest taxonomy level possible from the stratified table.....	62
Figure 3.11: Reads per kilobase million (RPKM) of Top 10 most abundant Gammaproteobacteria taxa that have the ability to perform sulfur oxidation via the <i>soxB</i> gene before (July 2018) and during (March 2019) following in the A) cage sediments and B) buoy sediments. Reads are separated into the lowest taxonomy level possible from the stratified table.....	64
Figure 4.1: Map of the sample areas (a) in relation to all of Nova Scotia and (b) close up of the farm areas, Hartz Point (HP) and Sandy Point (SP), indicated by red dashed lines, and sampling layout. In (b), stations beginning with C and marked by a black dot are cages, B and marked by a blue dot are farm buoys, and Ref represents off-site reference stations, marked by a green dot.....	75
Figure 4.2: Plot of the mean Ct values against the log <sub>10</sub> quantity of the standard curve for LSU assay test 3. The formula of the line of best fit ( $y = -4.7279x + 50.608$ ) was used to calculate the quantities in the samples from the Ct values. ....	80
Figure S1: Depth profile of temperature collected using a seacast ctd. Dotted lines at 5m and 10m indicate depths at which samples were taken. ....	98
Figure S2: Relative abundance of the top 5 prokaryotic taxonomic classes present in the sediment on each sample date as determined by 16S V6V8 sequencing. Buoy and Farm samples are ordered left to right from inland (I) to seaward (S). ASV's unclassified to the family level were excluded and represented by white space on the y-axis. The letters ABC in x-axis labels indicate sediment replicates. Plots A-B are from time period P1, C from time period F, and D-G from time period P2.....	101
Figure S3: Shannon diversity index of prokaryotes (16S V4V5) in the water column and sediment across the sampling period. Red dotted lines show the approximate time following occurred. Labels in plots represent the 3 time periods outlined in the methods: production cycle 1 (P1), mid-fallowing (F), and production cycle 2 (P2).....	104

Figure S4: nMDS plots of A) water column 16S V4V5 and B) sediment 16S V4V5 amplicon sequencing for all days of sampling. Ellipses in plots represent the 3 time periods outlined in the methods: production cycle 1 (P1), mid-fallowing (F), and production cycle 2 (P2). Note: depth only applies to water column samples as all sediment samples are from approximately the same depth. .... 105

Figure S5: nMDS plots of 16S V4V5 amplicon sequencing of sediment samples by day, with the exception of September 2018 as there were too few samples to conduct a robust nMDS analysis. Red ellipses on plots (d), (e), and (f) indicate samples from the two cages at the open-ocean end of the farm (C5 & C6). Plot A is from time period P1, B from time period F, and C-F from time period P2..... 106

Figure S6: nMDS plots of 16S V4V5 amplicon sequencing of water column samples by day, with the exception of September 2018 as there were too few samples to conduct a robust nMDS analysis. Plot A is from time period P1, B from time period F, and C-F from time period P2. .... 107

Figure S7: Relative abundance of the top 5 prokaryotic taxonomic families present in the sediment on each sample date as determined by 16S V4V5 sequencing. Buoy and Farm samples are ordered left to right from inland (I) to seaward (S). ASV's unclassified to the family level were excluded and represented by white space on the y-axis. The letters ABC in x-axis labels indicate sediment replicates. Plots A-B are from time period P1, C from time period F, and D-G from time period P2..... 108

Figure S8: Relative abundance of the top 5 prokaryotic taxonomic families present in the water column on each sample date as determined by 16S V4V5 sequencing. In each section, samples are ordered left to right from inland to open ocean. ASV's unclassified to the class levels were excluded and represented by white space on the y-axis. In the x-axis labels, samples ending in A are from 10m water, and those ending in B are from 5m water. Plots A-B are from time period P1, C from time period F, and D-G from time period P2..... 109

Figure S9: Percent relative abundance of unstratified sulfur cycling genes before (July 2018) and during (March 2019) fallowing in the A) cage sediments and B) buoy sediments. Relative abundance was calculated for each sample by adding together raw reads of all pathways and determining the percentage of each pathway.... 110

Figure S10: Percent relative abundance of the *rdsrC* gene separated by taxonomy before (July 2018) and during (March 2019) fallowing in the A) cage sediments and B) buoy sediments. Reads are separated into reads per phylum aside from Proteobacteria which, when possible, were separated into the different classes due to abundance compared to other phyla. Relative abundance was calculated for each sample by adding together raw reads of all pathways and determining the percentage of each pathway..... 111

Figure S11: Percent relative abundance of Top 10 most abundant Gammaproteobacteria taxa that have the ability to perform sulfur oxidation via the *rdsrC* gene before (July 2018) and during (March 2019) following in the A) cage sediments and B) buoy sediments. Reads are separated into the lowest taxonomy level possible from the stratified table. References confirming these taxa are oxidizers can be found in Table 3.1. Relative abundance was calculated for each sample by adding together raw reads of all pathways and determining the percentage of each pathway..... 112

Figure S12: Percent relative abundance of the *dsrC* gene separated by taxonomy before (July 2018) and during (March 2019) following in the A) cage sediments and B) buoy sediments. Reads are separated into reads per phylum aside from Proteobacteria which, when possible, were separated into the different classes due to abundance compared to other phyla. Relative abundance was calculated for each sample by adding together raw reads of all pathways and determining the percentage of each pathway..... 113

Figure S13: Percent relative abundance of Top 10 most abundant Deltaproteobacteria taxa that have the ability to perform sulfur reduction via the *dsrC* gene before (July 2018) and during (March 2019) following in the A) cage sediments and B) buoy sediments. Reads are separated into the lowest taxonomy level possible from the stratified table. References confirming these taxa are reducers can be found in Table 3.1. Relative abundance was calculated for each sample by adding together raw reads of all pathways and determining the percentage of each pathway..... 114

Figure S14: Percent relative abundance of the *soxB* gene separated by taxonomy before (July 2018) and during (March 2019) following in the A) cage sediments and B) buoy sediments. Reads are separated into reads per phylum aside from Proteobacteria which, when possible, were separated into the different classes due to abundance compared to other phyla. Relative abundance was calculated for each sample by adding together raw reads of all pathways and determining the percentage of each pathway..... 115

Figure S15: Percent relative abundance of Top 10 most abundant Alphaproteobacteria taxa that have the ability to perform sulfur oxidation via the *soxB* gene before (July 2018) and during (March 2019) following in the A) cage sediments and B) buoy sediments. Reads are separated into the lowest taxonomy level possible from the stratified table. Relative abundance was calculated for each sample by adding together raw reads of all pathways and determining the percentage of each pathway..... 116

Figure S16: Percent relative abundance of Top 10 most abundant Gammaproteobacteria taxa that have the ability to perform sulfur oxidation via the <i>soxB</i> gene before (July 2018) and during (March 2019) following in the A) cage sediments and B) buoy sediments. Reads are separated into the lowest taxonomy level possible from the stratified table. Relative abundance was calculated for each sample by adding together raw reads of all pathways and determining the percentage of each pathway.....	117
Figure S17: Plot of the mean Ct values against the log <sub>10</sub> quantity of the standard curve for the LSU assay test 4. The formula of the line of best fit was used to calculate the quantities in the sample dilutions from the Ct values. SPS2 corresponds to Sandy Point station C2 in July 2018, while SPS22 corresponds to Sandy Point reference station in October 2019. ....	130
Figure S18: Alpha rarefaction curves for sediment (S) and water column (W) samples from Run 1 of 16S V4V5 sequencing.....	131
Figure S19: Alpha rarefaction curves for sediment (S) and water column (W) samples from Run 2 of 16S V4V5 sequencing.....	132
Figure S20: Alpha rarefaction curves for sediment (S) and water column (W) samples from Run 3 of 16S V4V5 sequencing.....	133
Figure S21: Alpha rarefaction curves for sediment (S) and water column (W) samples from Run 4 of 16S V4V5 sequencing.....	134
Figure S22: Alpha rarefaction curves for sediment (S) and water column (W) samples from Run 1 of 16S V6V8 sequencing.....	135
Figure S23: Alpha rarefaction curves for sediment (S) and water column (W) samples from Run 2 of 16S V6V8 sequencing.....	136
Figure S24: Alpha rarefaction curves for sediment (S) and water column (W) samples from Run 3 of 16S V6V8 sequencing.....	137
Figure S25: Alpha rarefaction curves for sediment (S) and water column (W) samples from Run 4 of 16S V6V8 sequencing.....	138
Figure S26: Alpha rarefaction curves for sediment (S) and water column (W) samples from Run 1 of 18S V4 sequencing. ....	139
Figure S27: Alpha rarefaction curves for sediment (S) and water column (W) samples from Run 2 of 18S V4 sequencing. ....	140
Figure S28: Alpha rarefaction curves for sediment (S) and water column (W) samples from Run 3 of 18S V4 sequencing. ....	141
Figure S29: Alpha rarefaction curves for sediment (S) and water column (W) samples from Run 4 of 18S V4 sequencing. ....	142

## ABSTRACT

Finfish aquaculture has increased globally in recent years, which has led to concerns about the effect on the surrounding environment. Traditional biological environmental monitoring techniques such as examining OPC's and percent coverage of the sulfur oxidizing *Beggiatoa sp.* are often time consuming and expensive, therefore eDNA has been investigated as an alternative method for monitoring the biological communities around aquaculture farms. The work described in this thesis looks at using three molecular techniques: amplicon sequencing, shotgun metagenomic sequencing, and qPCR to study eDNA in the sediment and water column around fish farms off the coast of Nova Scotia. Amplicon sequencing results were able to track changes in the microbial and meiofaunal communities as the farm transitioned from production, to fallowing, and into the subsequent production cycle. Results also identified potential indicator organisms: Monhysterid nematode worms and sulfur metabolizing bacteria *Sulfurovum* and *Desulfobacteraceae*. Shotgun metagenomic analysis of the sulfur genes *dsrC* and *soxB* shows that Gammaproteobacteria and Deltaproteobacteria were the dominant sulfur metabolizing bacteria in the sediments at time points before and during fallowing. They also reinforced amplicon sequencing results and provided further evidence that *Desulfobacter* species have potential to be important indicator bacteria. Lastly, qPCR assays for quantification of the HAB *Alexandrium sp.* were able to confirm its presence in the sediment, but low efficiencies showed the need for further optimization in order to produce reliable quantifications. Overall, all of the techniques used in this thesis work demonstrate the huge potential eDNA provides for monitoring the environment around finfish aquaculture sites.

## **LIST OF ABBREVIATIONS USED**

16S rRNA: 16S Ribosomal RNA

18S rRNA: 18S Ribosomal RNA

AEM: Aquaculture Environmental Monitoring

ASV: Amplicon Sequence Variant

BLAST: Basic Local Alignment Search Tool

Dsr: Dissimilatory Sulfur Reductase

eDNA: Environmental DNA

HAB: Harmful Algal Bloom

IMR: Integrated Microbiome Resource

LSU: Large Ribosomal Subunit

nMDS: Non-metric Multi-dimensional Scaling

OPC: Opportunistic Polychaete Complex

PCR: Polymerase Chain Reaction

PSP: Paralytic Shellfish Poisoning

qPCR: Quantitative PCR

rDsr: Reverse Dissimilatory Sulfur Reductase

RPKM: Reads per Kilobase per Million Mapped Reads

SOB: Sulfur Oxidizing Bacteria

SOO: Sulfur Oxidizing Organism

SOP: Standard Operating Procedure

Sox: Sulfur Oxidation (pathway)

SRB: Sulfur Reducing Bacteria

SRO: Sulfur Reducing Bacteria

SSU: Small Ribosomal Subunit

SxtA4: Saxitoxin Biosynthesis Pathway Protein A Domain 4

## ACKNOWLEDGEMENTS

First, I'd like to acknowledge and thank my supervisor, Dr. Julie LaRoche for the opportunity to work on this project as well as all her time, support, and guidance over the years I have been fortunate enough to be a part of her lab.

I'd also like to thank the rest of the members of the LaRoche Lab for all their help and support in making my thesis possible. In particular I'd like to acknowledge Dr. Jennifer Tolman for helping me in the field and teaching me various laboratory techniques, Dhvani Desai for his guidance regarding bioinformatics, and for processing my metagenomic data, and Brent Robicheau and Sonja Rose for their help in solving all my R script issues and constructive feedback on various figures and ideas.

My field sampling would not have been possible without the support from members of the Grant lab in Oceanography. In particular I'd like to thank Hart Koepke and Anne McKee for all of their help in scheduling trips to the field and hauling up many, many niskins of water.

Thank you to my committee members, Dr. Ramón Filgueira and Dr. Morgan Langille for their input and help in shaping my project.

I'd also like to acknowledge and thank the Ocean Frontier Institute for providing the funding that made my project possible.

My final thank yous go out to all of my friends and family who constantly give me all of their love and support. I am incredibly lucky and grateful to have so many people in my life who helped me in whatever way they could, whether it was lending me an ear, or distracting me when I needed to take a break. Lastly, a very special thank you to my parents, Shaun and Joanna, my sister Caelin, and my uncles Blair and Scott for helping me get to where I am today. None of this would have been possible without you.

# CHAPTER 1: INTRODUCTION

## 1.1. AQUACULTURE

The use of open water finfish aquaculture has increased in recent years to ensure food security due to the increasing seafood demands of the human population (Flaherty *et al.* 2019), particularly the increasing consumption of fish (Bastos Gomes *et al.* 2017). Aquaculture also creates jobs, particularly in rural, coastal areas, and is an important economic sector (Flaherty *et al.* 2019). In Canada, aquaculture production has increased four-fold since the early 1990's and, in 2018, brought in an economic contribution of \$487.4 million (Government of Canada 2013). On the East coast of Canada, New Brunswick is the leader in salmon aquaculture, however the industry in Nova Scotia is established and has been growing over the years (Flaherty *et al.* 2019).

With the increase in aquaculture comes an increased concern about how intensive farms and high production levels are affecting the surrounding aquatic environment. It has been shown that organic matter falling from cages (fecal matter and excess food) can overload the sediment biological oxygen demand and cause anoxia as well as H<sub>2</sub>S buildup (Moncada *et al.* 2019). These conditions not only affect the biodiversity and species composition of the benthos but, when unmitigated, can also cause adverse conditions for the farmed species if high concentrations of H<sub>2</sub>S diffuse up in the water column (Bentzon-Tillia *et al.* 2016, Strain and Hargrave 2005). Although the overall effect on the environment is highly dependent on the physical structure of each individual site (Carroll *et al.* 2003), there are recommended approaches and guidelines in place to minimize impact to the environment.

## 1.2. FALLOWING

In order to try and circumvent the effects of organic loading on the surrounding environment, fallowing regulations are implemented. Fallowing is a process through which cages are left empty for a length of time after a full production cycle (Werkman *et al.* 2011). This practice was historically implemented as a way to control fish die offs from disease and parasites but has been adapted over time with the goal of allowing the environment to recover from changes caused by intensive farming (Werkman *et al.* 2011, Wheatley *et al.* 1995). It can be difficult to create overarching regulations when it comes to fallowing, as every site is different. Hydrological conditions such as flow rate, depth, bottom type, and cage orientation can all play a role in how the environment responds to intensive aquaculture, as well as how quickly it recovers during fallowing. For example, the fallowing time for salmon farms in Norway operating on a 2-year production cycle is approximately 6-8 weeks (Black *et al.* 2008), while in other countries fallowing can last 6 months (Spain, USA, Canada) to years (Scotland, Australia, Canada) depending on the farm (Lin and Bailey-Brock 2008). In Nova Scotia, fallowing time varies among sites but, in terms of the environment, regulations indicate that it should be long enough to ensure sufficient oxic conditions on the site (Aquaculture Management Regulations 2019), a guideline which mainly pertains to the sediments under the farm. In many cases fallowing can be sufficient to prevent further progressive deterioration of sediments, however the usual fallowing periods may not be sufficient for complete recovery, leading to irreversible changes on the long-term (Zhuley *et al.* 2015, Guo *et al.* 2009, Lin and Bailey-Brock 2008).

### **1.3. ENVIRONMENTAL MONITORING**

In order to monitor the benthic environment and ensure mitigation techniques such as fallowing are working, a combination of chemical and biological measurements is used, including measurements of H<sub>2</sub>S, pH, and total organic carbon (TOC), as well as percent (%) cover of bacterial mats and taxonomic classification of macrofauna (Fernandes *et al.* 2001, Zhuley *et al.* 2015). Undisturbed sediments are typically classified as having high species diversity with a few dominant species, while impacted sediments are characterized by a reduction in species diversity and increase in opportunistic species such as opportunistic polychaete complexes (OPCs) (Fernandes *et al.* 2001, Zhuley *et al.* 2015). If organic matter is allowed to build up, the sediment may become severely affected, leading to very few macro- and meiofaunal species and in some cases large percent cover of white bacterial mats of *Beggiatoa sp.*, a sulfide oxidizing bacteria (SOB) (Fernandes *et al.* 2001). The typical model of environmental impact is that based on the Pearson Rosenberg model which shows a bullseye-like pattern of disturbance, with the most heavily impacted sediments directly under the cages and the impact lessening in a uniform distribution radiating out from the cages (Pearson and Rosenberg 1978, Lin and Bailey-Brock 2008).

### **1.4. AQUACULTURE IN CANADA**

In Canada, aquaculture environmental monitoring (AEM) program specifics vary among provinces, but all have similar components including video surveying of the benthos, sediment grab sampling, visual identification and counting of opportunistic polychaete complexes (OPCs) and percent (%) cover of sulfur metabolizing *Beggiatoa sp.*

which form the characteristic bacterial mat mentioned above (Wade *et al.* 2015, Schmidt *et al.* 1987). In Nova Scotia, environmental regulations on finfish aquaculture state that farms must take benthic samples at least once during the production cycle, ideally during maximum production (July-October) (Government of Canada 2015a) and submit a yearly report. Included in the report are measurements such as: *Beggiatoa* percent (%) cover, OPC percent (%) cover, sediment colour, pH, redox, and flocculent material, and the presence of un-eaten feed, gas bubbles, fish feces and free sulfides, (Government of Canada 2015b). However, there are pitfalls to some of these monitoring procedures, particularly the biological measurements, in terms of time involvement and costs. Therefore, there are suggestions to increase the use of eDNA in multiple areas of aquatic monitoring, including environmental monitoring of coastal aquaculture facilities in Canada (Baille *et al.* 2019).

## **1.5. ENVIRONMENTAL DNA**

Environmental DNA, or eDNA, refers to all DNA present in the environment, whether it be from organisms currently in the area, or DNA that sloughed off organisms passing through the environment. Once this DNA is extracted, there are a multitude of molecular techniques that can be used to study it, each with its own purpose as well as advantages and disadvantages. The work in this thesis applies three such techniques to study eDNA specifically in the water and sediment surrounding a coastal finfish farm. In Chapter 2, amplicon sequencing is used to study prokaryotic and eukaryotic DNA in the environment. This process involves sequencing a specific, taxonomically informative marker gene (Sharpton *et al.* 2014) in order to identify organisms in the sample and their relative abundance. The development of this type of analysis has allowed for

characterization of microbes from many different environments and can be used to compare diversity and community composition of microbes across samples (Sharpton *et al.* 2014). Multiple studies in other countries have used amplicon sequencing to study the microbiota in aquaculture sediments in order to assess the use of eDNA to monitor changes in the environment (Santander de Leon *et al.* 2017, Stoeck *et al.* 2018a, Stoeck *et al.* 2018b).

Although amplicon sequencing is the most widely used method for characterizing the diversity of microbiota, it is not without its limitations, particularly in the marine environment (Sharpton 2014). In some cases, amplicon sequencing of taxonomic markers may not have enough resolution to distinguish between closely related strains and may not be able to classify organisms down to a taxonomic level appropriate for monitoring due to a lack of representative groups in DNA sequence databases. This lack of representative groups leads to many species being undescribed or described as unclassified in scientific databases (Sharpton 2014, Garlapati *et al.* 2019).

As well, while amplicon sequencing is able to give information on the taxonomic composition of a community, it does not resolve biological functions associated with the taxa (Sharpton 2014). This is particularly important when studying the change in microbial communities, as rapid changes occur in the metabolic potential of a community (Fuhrman *et al.* 2015), meaning even if there is no apparent shift in the taxonomic composition of a community, there may be a noticeable shift in which biological functions are present in the eDNA (Moncada *et al.* 2019).

In Chapter 3 of this thesis, shotgun metagenomics is used to study the eDNA from sediments in the environment surrounding the same aquaculture farm studied in Chapter 2. This technique can be used to supplement the amplicon sequencing approach, as it

resolves the aforementioned disadvantages of amplicon sequencing. Instead of certain sections of DNA being amplified and sequenced, in shotgun metagenomics all of the DNA in a sample is sheared into small fragments which are sequenced, allowing genes for many biological functions to be sampled (Sharpton 2014). Although shotgun metagenomics is fairly new, it is quickly becoming a more accessible and useful tool for analyzing environmental microbial communities (Sharpton 2014).

Despite all the information to be gained from amplicon sequencing and shotgun metagenomics, they are both relative, not quantitative, measurements. In Chapter 4, two qPCR assays are tested in an attempt to quantify the potentially harmful algae *Alexandrium sp.*, which was initially found in amplicon sequencing results of sediments from a fish farm further inland. This work builds upon that previously performed by Murray *et al.* (2019) which looked at two *Alexandrium catenella* qPCR assays. Unlike a standard PCR reaction where only the final product is analyzed, qPCR uses fluorescent dyes that emit a fluorescence when bound to double stranded DNA at each amplification cycle (Antonella and Luca 2013). Fluorescence levels in samples can be compared to a standard curve, allowing for quantification of the gene that is being amplified (Antonella and Luca 2013). In order for qPCR results to be accurate and reliable, primers must be highly specific, therefore Chapter 3 is aimed at testing primers and assays as opposed to focusing on the results.

Through the use of these different molecular techniques, the work presented in this thesis demonstrates the several approaches in which eDNA can be used in environmental monitoring, and the potential it holds for monitoring the environment surrounding coastal aquaculture farms in particular.

# **CHAPTER 2: TRACKING CHANGES IN MICROBIAL AND MEIOFAUNAL COMMUNITIES IN THE WATER COLUMN AND SEDIMENTS AROUND COASTAL FINFISH AQUACULTURE**

## **2.1. INTRODUCTION**

### *2.1.1 Environmental Monitoring*

Traditional taxonomic identification and enumeration of macrofauna is a time consuming and expensive process requiring dedicated, trained personnel (Goodwin *et al.* 2017). However, it has remained the standard approach for environmental monitoring on aquaculture farms until recently, when eDNA became a viable alternative. Previously, eDNA studies have been conducted using PCR and cloning, as well as pyrosequencing to study the environment around fish farms (Kawahara *et al.* 2009, Hornick and Buschmann 2018), with more recent studies using DNA metabarcoding via Illumina sequencing (Kolda *et al.* 2020). eDNA metabarcoding is shown to be a robust analysis among different labs (Dully *et al.* 2020), and with the decreasing costs of high-throughput sequencing, this type of analysis is rapidly becoming a widespread tool for environmental monitoring (Goodwin *et al.* 2017).

### *2.1.2. Microbiota in Environmental Monitoring*

The growing acceptance of eDNA-based monitoring approaches has streamlined biological sample collection and enables the targeting of an expanded suite of metazoans,

including those that are not distinguishable or identifiable with standard microscopy, as well as microbiota in the environment. In particular, amplicon sequencing of the prokaryotic 16S rRNA gene is widely used for taxonomic identification of marine bacteria and archaea, while the eukaryotic 18S rRNA gene is used to identify phytoplankton and microeukaryotes (Goodwin *et al.* 2017). Smaller organisms such as bacteria, archaea and unicellular eukaryotes are more closely linked to the biogeochemical processes that degrade organic matter and can therefore provide increased resolution of changes due to organic loading on a faster time scale than macrobiota (Bentzon-Tillia *et al.* 2016, Moncada 2019, Stoeck *et al.* 2018a, Stoeck *et al.* 2018b). These changes can present as either changes in just the metabolic pathways, or an entire shift in community composition (Bentzon-Tillia *et al.* 2016, Moncada 2019) and can be affected by organic matter loading from aquaculture (Santander de Leon *et al.* 2017).

The main goal of the study described in this chapter is to use amplicon sequencing of eDNA to describe changes in the meiofaunal and microbial communities present in the environment of a Canadian finfish aquaculture facility before fallowing, during fallowing, and into the subsequent production cycle. In order to provide a complete overview of the environment, changes in both sediment and water column communities were studied and compared in order to determine the main drivers of each.

## **2.2. MATERIALS AND METHODS**

### *2.2.1. Sample Collection*

Sampling for this study took place intermittently from July 2018 – November 2019 at the Cooke Aquaculture facility's McNutt's site outside of Shelburne, NS

(Figure 2.1), which houses between 19-20 cages of Atlantic salmon (*Salmo salar*), as well as a large onsite barge that houses staff and the automatic feeder. During this time the farm was fallowed from approximately November 2018 – June 2019, splitting sampling dates into 3 categories: production cycle 1 (P1) from July 2018 – September 2018, mid-fallowing (F) in March 2019, and production cycle 2 (P2) from July 2019 – November 2019.

Water and sediment samples were taken at three types of stations: barge, cage, and buoy, according to Figure 2.1 when possible (Table S1, Table S2). Water was collected from both 5m and 10m depths using a 5L niskin bottle, then filtered for 2 minutes through 0.2µm Isopore™ polycarbonate membrane filters (47mm diameter) in duplicate on deck and immediately frozen. On average, the volume of water filtered for each duplicate was 590ml. Sediment samples were taken using a van veen grab and 2ml of sediment from the grab was immediately frozen in cryo tubes on deck. Samples were frozen in a cryoshipper that had been primed with liquid nitrogen the day before. Due to the rough nature of the water at the site, buoy sites were the farthest locations from cages that could be sampled. Therefore, buoy sites were considered reference sites relative to the cage sites on this farm.

On average, between 9-10 stations were sampled each sampling day, with the exception of September 2018, when harsh weather conditions limited sampling. Initial results from sediment sampling in 2018 indicated that the sediment was spatially heterogeneous, so sampling was increased to include duplicate and triplicate samples from the same sediment grab in 2019 (Table S1, Table S2). Replicates were taken from different sections of the grab; however, all replicates were taken from the top layer of the grab.

Water column temperature was recorded using an AML SeaCast CTD during 5 out of the 7 sampling days due to technical issues on the other 2 days (Figure S1).

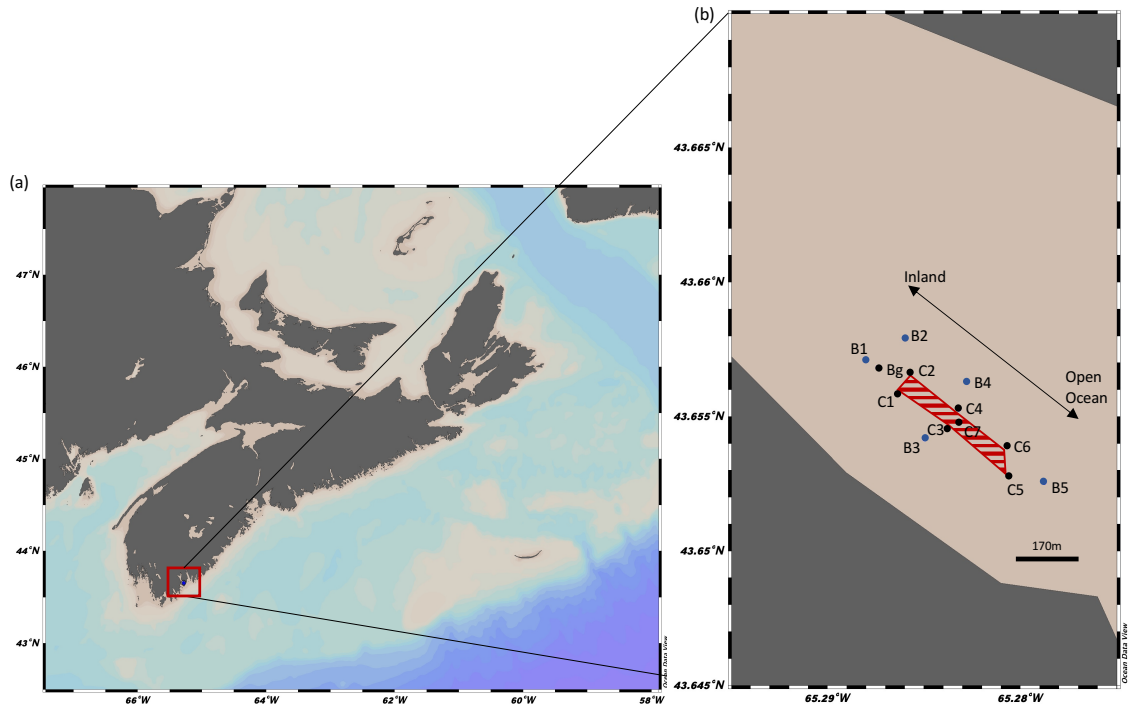


**Figure 2.1: Map of the McNutt's sampling area in relation to (a) all of Nova Scotia and (b) close up of the farm area, indicated by red dashed lines, and sampling layout. In (b), stations beginning with C are cages, those beginning with B are farm buoys, and Bg represents the on-site barge. Black dots represent cage and barge samples, while blue dots represent buoy stations.**

### *2.2.2. DNA Extraction*

DNA from water samples was extracted using the DNeasy plant mini kit from Qiagen<sup>®</sup> according to the manufacturer's instructions with the following modifications as per the LaRoche lab SOP: after adding the buffer AP1 and proteinaseK, samples were incubated for 1hr at 52°C instead of 10 minutes at 65°C, and 50µl of buffer AE was used to elute the DNA instead of 100µl. For the sediments, DNA was extracted from 0.25g of sediment using the Qiagen<sup>®</sup> PowerSoil kit according to manufacturer's instructions.

### 2.2.3. DNA Sequencing

Concentration of extracted DNA was measured using a nanodrop, after which the DNA was sent for Illumina amplicon sequencing of the V4V5 and V6V8 variable regions of the prokaryotic 16S rDNA, and of the V4 region of the eukaryotic 18S rDNA. Primer sequences for the amplification of these variable regions are listed in Table 2.1.

**Table 2.1: Primers used for Illumina MiSeq amplicon sequencing. All primers are reported 5'-3' in orientation**

Target Gene	Region	Forward Primer	Reverse Primer	Source
16S	V6V8	B969F = ACGCGHNRAAC CTTACC	BA1406R = ACGGGCRGTGWGT RCAA	Comeau 2011
16S	V4V5	515FB = GTGYCAGCMGC CGCGGTAA	926R = CCGYCAATTYMTT RAGTTT	Parada 2015 / Walters 2015
18S	V4	E572F = CYGCGGTAATT CCAGCTC	E1009R = AYGGTATCTRATCR TCTTYG	Comeau 2011

### 2.2.4. Bioinformatics

In total, 141 sediment samples and 125 water samples were sequenced at the Integrated Microbiome Resources (IMR) laboratory according to Comeau *et al.* (2017). Read quality of raw amplicon sequencing data was first assessed using a combination of FASTQC (Andrews 2010) and MULTIQC (Ewels *et al.* 2016), then processed through the Qiime 2 2019.7 pipeline (Boylen *et al.* 2019) according to the protocol by Comeau *et al.* (2019). Reads underwent denoising using Deblur (Amir *et al.* 2017) during which reads were trimmed to the same length for each amplicon, after which taxonomy was assigned using the SILVA database (Glöckner *et al.* 2017, Quast *et al.* 2013, Yilmaz *et al.* 2014). Trim lengths for the different amplicons were as follows: 16S rRNA gene variable

region V4V5 sequences were trimmed to 255bp, 16S V6V8 to 300bp, and 18S V4 to 290bp. The resulting amplicon sequence variant (ASV) tables were rarefied to 1000 reads and used in all further analyses. Some samples failed during sequencing, and a full list of the remaining samples is presented in Tables S1 & S2. 16S V6V8 results are reported in the results, while 16S V4V5 data is presented in the supplemental material. This is because V6V8 primers are less susceptible to eukaryotic contamination and therefore recommended for studying the bacterial diversity in samples that are expected to have substantial eukaryotic contamination (Comeau *et al.* 2011, IMR 2014).

#### 2.2.5. Statistical Analysis

Alpha rarefaction curves (presented in the supplemental material) and Shannon diversity index values were calculated as part of the Qiime2 2019.7 pipeline (Boyle *et al.* 2019), while all other analyses, as well as all visualizations, were performed in RStudio version 1.2.5042 (R Core Team 2020). ANOVA and subsequent Tukey tests were performed using the basic R stats package (R Core Team 2020), while nMDS analysis using the Bray-Curtis method as well as the ADONIS analysis of variance were performed using Vegan version 2.5-6 (Oksanen *et al.* 2019). Taxonomy bar plots were made using the `group.abundance.meta` function of the RAM package version 1.2.1.7 (Chen *et al.* 2018) and alluvial plots were made using the `ggalluvial` package (Brunson 2020). `Indicspecies` (De Caceres and Legendre 2019) was used to determine taxa significantly associated with specific time periods. All plots were visualized using `ggplot2` (Wickham 2016), `tidyverse` (Wickham *et al.* 2019), `lubridate` (Grolemund and Wickham 2011), `ggpubr` version 0.3.0 (Kassambara 2020), `reshape2` (Wickham 2007),

gridExtra version 2.3 (Auguie 2017), cowplot version 1.0.0 (Wilke 2019), and viridis version 0.5.1 (Garnier 2018).

## **2.3. RESULTS**

### *2.3.1. Site Characteristics*

The Cooke Aquaculture farm investigated in this study is situated on the southeast coast of Nova Scotia, close to the open ocean in an environment influenced by a semi-diurnal tide ranging from 0.2m low to 2.6m high (Burke *et al.* 2020). This exposed location led to a very dynamic water column, with large swells and wind driven waves occurring on multiple occasions. The layout of the rectangular farm was parallel to the direction of the tidal flushing, with one end inland, and the other towards the ocean (Figure 2.1). Sediment below the farm was a coarse sand, however the hydrodynamics of the water column and tidal current exposed the rocky bottom at specific sites in July 2019 (C4) and August 2019 (C3), preventing sediment samples from being taken. Initial analysis indicated a heterogenous benthos and therefore replicates were taken, however sequencing results show minimal differences between replicates, particularly when looking at prokaryotic data, therefore it may be more beneficial to take multiple grabs along the farm instead of multiple samples from the same grab. Despite the relatively shallow depth of the farm (about 12-15m on average) the water column was stratified in the July 2018 (Burke *et al.* 2020), which led to a weak thermocline in the water column during spring and late summer/early fall (September 2018, March 2019). Mixing of the water column occurred in late fall/early winter (October and November 2019).

### *2.3.2. Alpha Diversity of Microbial and Meiofaunal Communities*

In the sediment, eukaryotic Shannon diversity index values had a noticeably wider range (2-6) compared to the prokaryotes (Figure 2.2a and c) and showed a noticeable increase after fallowing. Unlike the eukaryotes, prokaryotic sediment samples had the most uniform and highest Shannon index values (Figure 2.2c) and did not show a noticeable increase in the sediments after fallowing, however there was a visible separation of the buoy and cage samples in November 2019 (Figure 2.2c).

These visible patterns were reflected in the Tukey results that compared the sediment alpha diversity values between the sampling days, although it should be noted that the lack of buoy samples and low sample numbers in general in September 2018 may have affected the statistics for this day. For eukaryotic samples, the majority of the days during and after fallowing were significantly different from July 2018, with the exception of July 2019, likely due to the low alpha diversity of cage samples (Figure 2.2a). Among the prokaryotic sediment samples, there were few significant differences between the sampling days reflecting the uniformity of the alpha diversity. Those days that were significantly different were as follows: October 2019 and November 2019, October 2019 and March 2019, and March 2019 and August 2019.

Both eukaryotic and prokaryotic water column Shannon diversity index values formed a sinusoidal curve across time, which was more pronounced in the prokaryotes (Figure 2.2b and d). Interestingly, Tukey results for water column eukaryotes and prokaryotes showed different patterns. In eukaryotes there was a lot of overlap and very few significantly different days. The main exception was March 2019 which was significantly different from all days except July 2019 (Figure 2.2b). Since prokaryotic

alpha diversity values followed a more pronounced sinusoidal curve, the Tukey values reflected this, with the majority of consecutive days being significantly different. The only exception was that September 2018 and March 2019 were not significantly different, which could be because it was the longest time gap between sampling dates, or because September 2018 had so few samples (Figure 2.2d).

As for differences in alpha diversity between station types on the same day, Tukey test results showed there were no significant differences except in the post fallowing prokaryotic sediment samples. In samples from July, August, and October 2019, the barge samples were significantly different from the buoy and cage samples, and in November 2019 the buoy and cage samples were significantly different, though on this date neither was significantly different from the barge samples. This difference between station types during P2 is more pronounced in the V4V5 data (Figure S3).

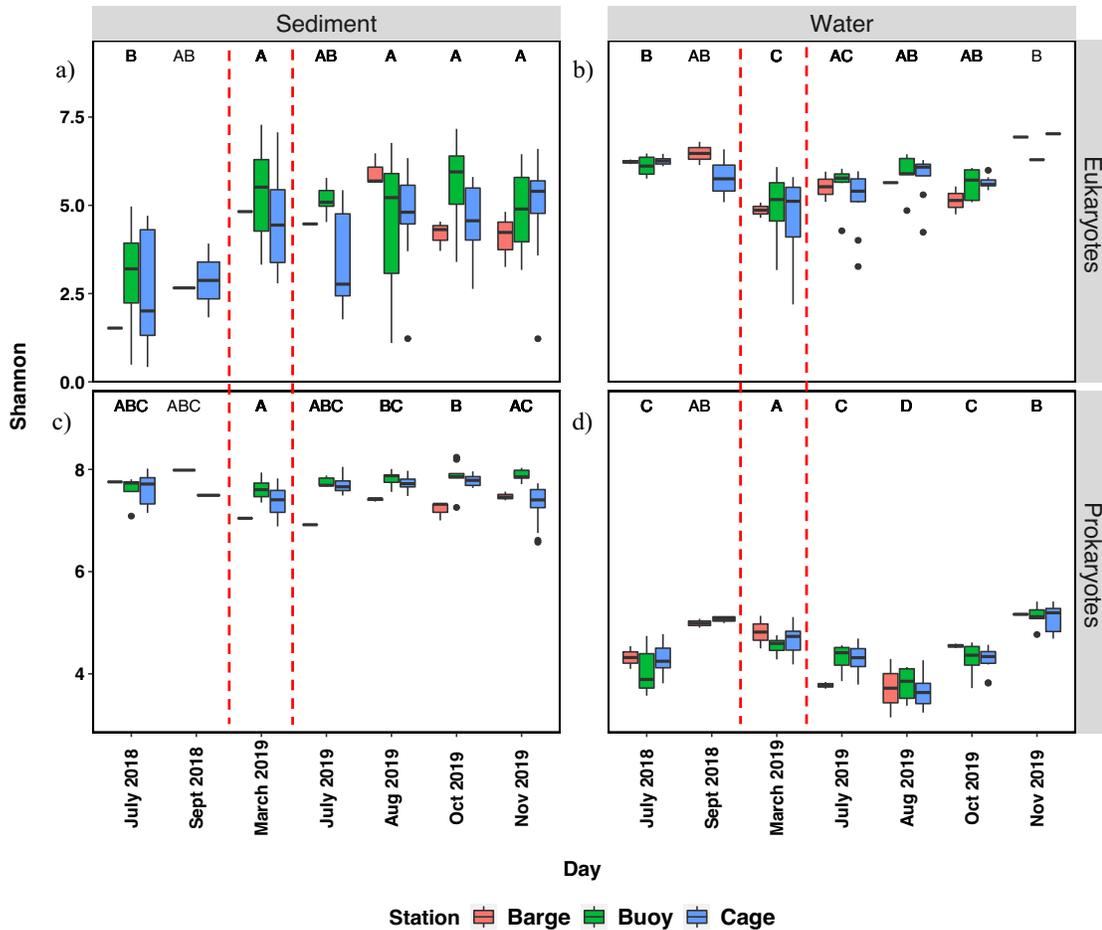


**Figure 2.2: Shannon diversity index of eukaryotes (18S V4) in the a) sediment and b) water column and prokaryotes (16S V6V8) in the c) sediment and d) water column across the sampling period. For each day, the samples are reported in the order seen in the legend: barge, buoy, cage, except for September 2018 where there are no buoy samples. Red vertical dotted lines show the time following occurred and split the plots into the three time periods outlined in the methods: production cycle 1 (P1), mid-fallowing (F), and production cycle 2 (P2). Tukey results for each plot are labelled above each day and days that share the same letter are not significantly different.**

### 2.3.3. Beta Diversity of Microbial and Meiofaunal Communities Across the Sampling Period

Non-metric multi-dimensional scaling (nMDS) plots of the Bray-Curtis distance measures demonstrate the beta diversity among samples. The nMDS plot of eukaryotes in

the sediments (Figure 2.3a) shows a pattern where P1 samples were widespread and variable, F samples clustered more tightly together, and P2 samples also clustered together, but overlapped with the P1 and F samples. ADONIS analysis indicated a significant difference [ $P = 0.001$ ] between these 3 groups.

In contrast to the sediment samples, the nMDS plot of eukaryotes in the water column (Figure 2.3b) shows tighter clustering based on days, appearing to capture the seasonal cycling in the area. There was a slight mismatch among the years with samples from July 2018 overlapping with August 2019 rather than July 2018, likely due to sampling in 2018 being later in July (26<sup>th</sup>) as opposed to 2019 when sampling was done earlier in the month (18<sup>th</sup>). ADONIS analysis showed a significant difference among following time points [ $P = 0.001$ ], however this is likely driven by the aforementioned seasonal cycle in the water column.

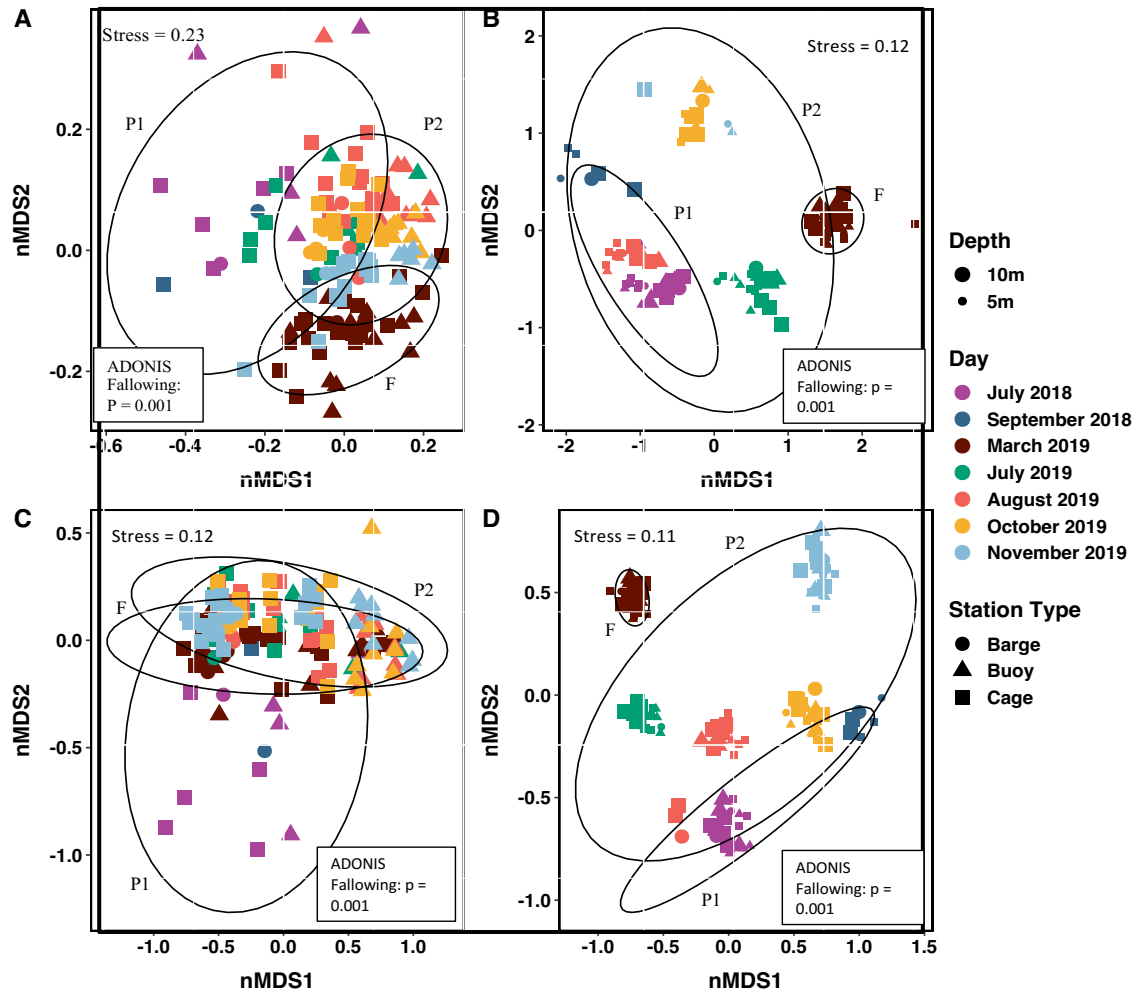


**Figure 2.3: nMDS plots of a) sediment 18S V4, b) water column 18S V4, c) sediment 16S V6V8, and d) water column 16S V6V8 amplicon sequencing for all days of sampling. Ellipses outline the time periods described in the methods: production cycle 1 (P1), mid-fallowing (F), and production cycle 2 (P2). Note: depth only applies to water column samples as all sediment samples are from approximately the same depth.**

On the nMDS plot for prokaryotes in the sediments (Figure 2.3c), the community structure of the P1 samples was more diverse and did not form a tight cluster, similarly to the eukaryotes (Figure 2.3a), while the F and P2 samples clustered together and had a large amount of overlap. ADONIS analysis showed there was a significant difference among these 3 groups [P= 0.001].

As with the eukaryotes, prokaryotic water column samples clustered tightly by sampling date in the V6V8 nMDS plot (Figure 2.3d) and ADONIS analysis showed significant difference among the 3 groups [ $P = 0.001$ ]. Both of these patterns (sediment and water column) were mirrored in the V4V5 data (Figure S4).

#### 2.3.4. *Beta Diversity of Microbial and Meiofaunal Communities Within Sampling Days*

nMDS plots of eukaryotes in the sediments on each sampling day (Figure 2.4) show a transition with time from no significant difference between station types to a significant difference between station types. Before and during fallowing, stations were intermixed, and ADONIS analysis showed no significant difference among station types in July 2018 [ $P = 0.31$ ] and March 2019 [ $P = 0.144$ ]. By July 2019, approximately a month into the next production cycle (P2), separation began to occur and there was a significant difference between the station types [ $P = 0.034$ ] as some cage samples clustered away from the buoy and barge samples (Figure 2.4). Further into P2, this significant difference was maintained, and samples began to separate into 2 distinct groups with barge and cage samples intermixing, while buoy samples clustered separately. Lastly, the lower alpha diversity of station C4 in August and November 2019 (Figure 2.2) was also reflected in the beta diversity by said cage sample not clustering with the rest of the cage samples on the August and November 2019 plots (Figure 2.4).

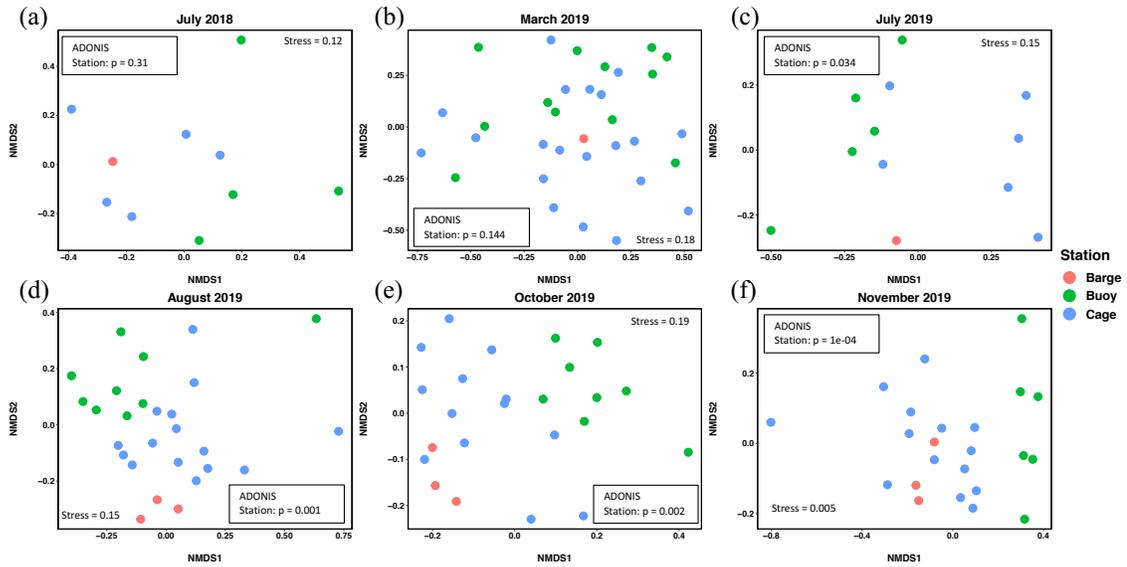


**Figure 2.4: nMDS plots of 18S V4 amplicon sequencing of sediment eukaryote communities from each sampling day. Plot A is from time period P1, B from time period F, and C-F from time period P2. Communities from September 2018 are not represented because there were too few samples to conduct a robust nMDS analysis.**

In contrast to the sediment, water column eukaryotes (Figure 2.5), showed no significant difference between the different station types [ $P > 0.05$ ]. Instead, there was a significant difference between the 10m and 5m samples in all sampling days except September 2018 [ $P = 0.1$ ], likely as a result of too few samples from September 2018. CTD data indicates that this may be the result of water column stratification, as indicated by the presence of a thermocline throughout the water column in July 2018, September 2018, and March 2019, though mixing occurred in October and November 2019 (Figure S1). Although the outliers from the Shannon diversity index plot (Figure 2.2) are not seen in the nMDS plots, there is a different outlier seen in March 2019, which was a sample from the seaward cage station C6 (Figure 2.5).

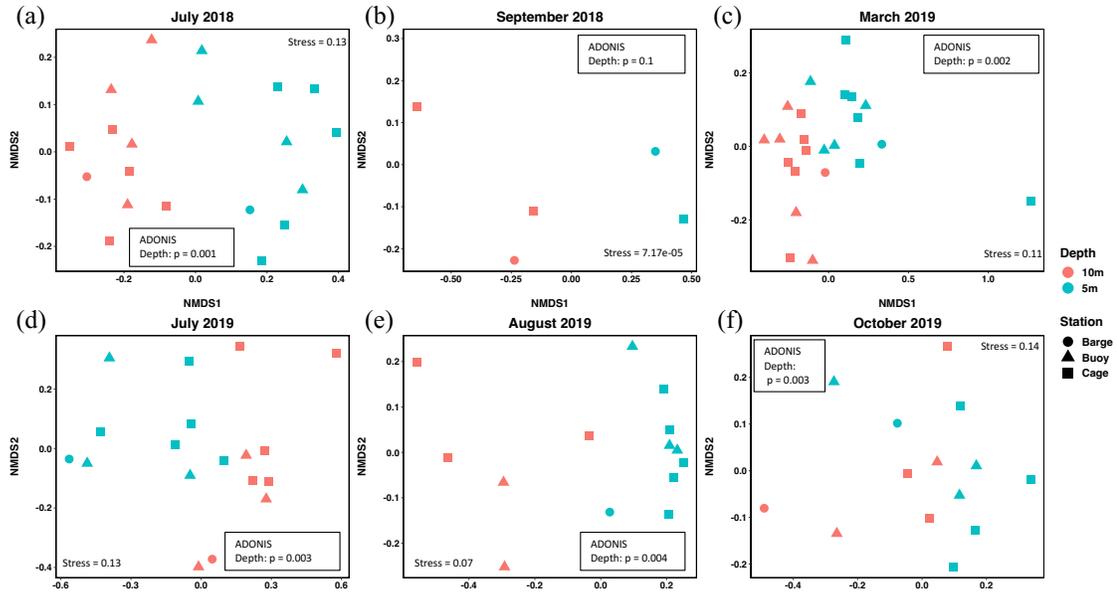


**Figure 2.5:** nMDS plots of 18S V4 amplicon sequencing of water column eukaryote communities from each sampling day. Plots A-B are from time period P1, C from time period F, and D-F from time period P2. Communities from November 2019 are not represented because there were too few samples to conduct a robust nMDS analysis.

Beta diversity of sediment prokaryotes demonstrated a slightly different pattern than the eukaryotes. In July 2018 (Figure 2.6), cage and barge prokaryotic communities were more separated from the buoy samples than in the eukaryotes, and ADONIS analysis showed there was a significant difference among the station types [ $P = 0.048$ ]. The rest of the nMDS plots follow the same pattern of significance as the eukaryotes with March 2019 stations showing no significant difference and all P2 sampling dates having a significant difference among station types (Figure 2.6). Interestingly, August, October and November 2019 plots show strong separation of most of the cage samples and buoy samples, with the exception of 6 cage samples that cluster between the two groups and correspond to triplicate samples from the two cages at the far end of the farm near the ocean (Figure 2.1). The separation and clustering of these 6 samples is more pronounced in the November 2019 V4V5 data (Figure S5).

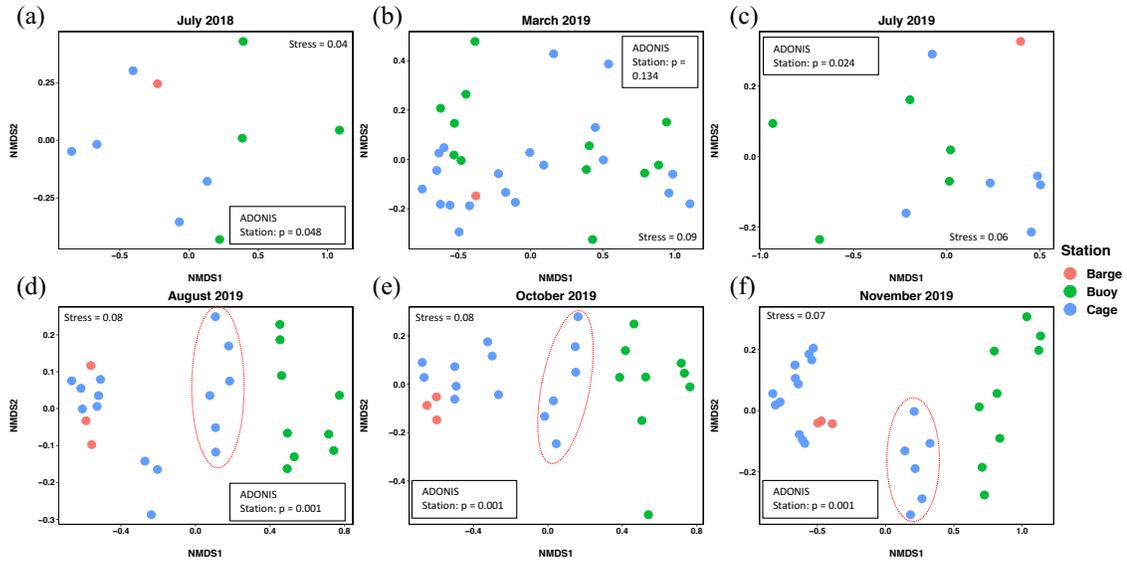


**Figure 2.6: nMDS plots of 16S V6V8 amplicon sequencing of sediment prokaryote communities from each sampling day. Red ellipses on plots (d), (e), and (f) indicate samples from the two cages at the open-ocean end of the farm (C5 & C6). Plot A is from time period P1, B from time period F, and C-F from time period P2. Communities from September 2018 are not represented because there were too few samples to conduct a robust nMDS analysis.**

Like the eukaryotic community composition from the water column samples, prokaryotic communities (Figure 2.7) showed few significant differences among stations with the exception of October 2019 [ $P = 0.017$ ]. In agreement with the eukaryotic communities, a significant difference between depths was observed on all sampling days except on September 2018 [ $P = 0.8$ ] and October 2019 [ $P = 0.271$ ]. September 2018 results may be explained by comparatively fewer samples and October 2019 results indicate that the water column was homogeneously mixed as previously mentioned (Figure S1).

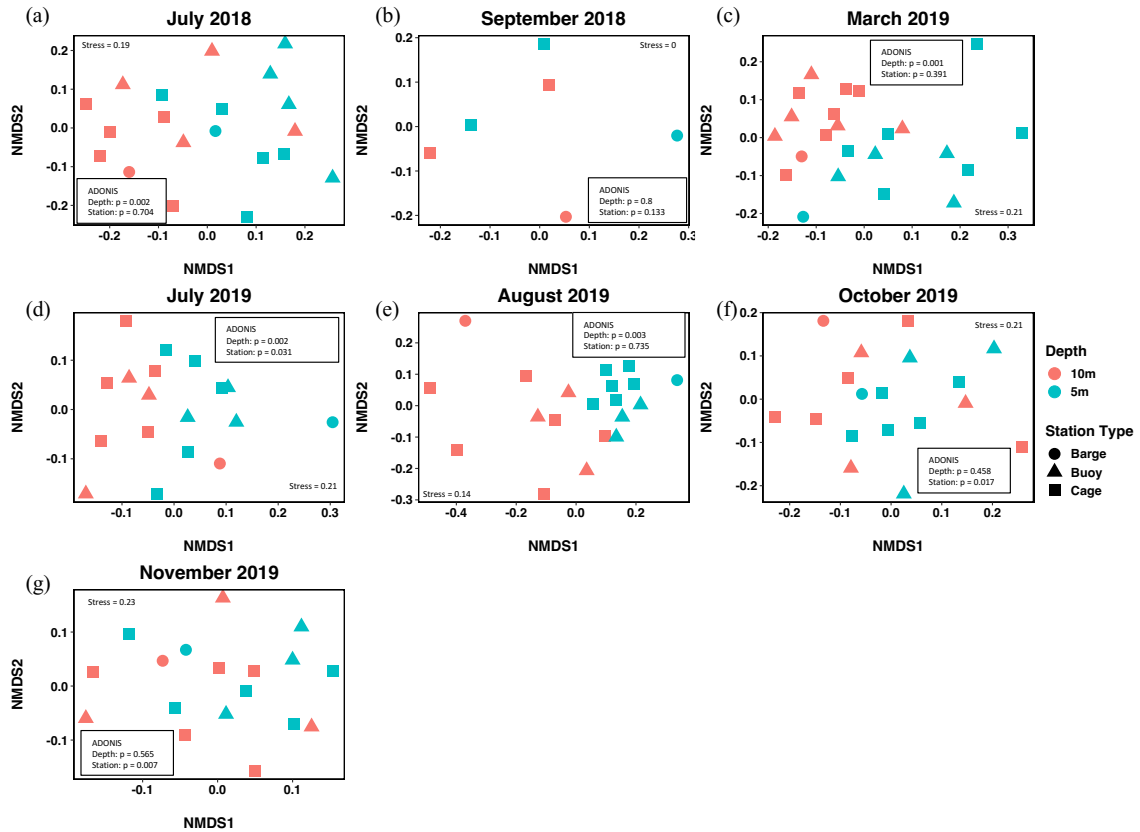


**Figure 2.7:** nMDS plots of 16S V6V8 amplicon sequencing of water column prokaryote communities from each sampling day. Plots A-B are from time period P1, C from time period F, and D-F from time period P2.

### 2.3.5. Eukaryotic Community Composition

Bubble plots of the top 10 eukaryotic ASVs with the highest relative abundance in the sediment on each sampling date (Figure 2.8) show a pattern that relates back to and reinforces the Shannon diversity index values in these samples (Figure 2.2). July and September 2018 samples were less diverse, and each sample was dominated a few ASVs, as opposed to the later date samples where communities were dominated by more ASVs at similar relative abundances (Figure 2.8). In particular, 2018 farm (cage and barge) samples were dominated by the nematode worm *Halomonhysteria sp.* (Figure 2.8), which persists into the following period as seen in the March 2019 samples but is not a part of

the top 10 ASVs by July 2019. While July-November 2019 samples showed a more even relative abundance among top ASVs, there was a noticeable emergence of *Dichromadora* sp (nematode), *Gymnodium aureolum* (dinoflagellate), and Phytomyxea (group of obligate parasites of plants and algae).

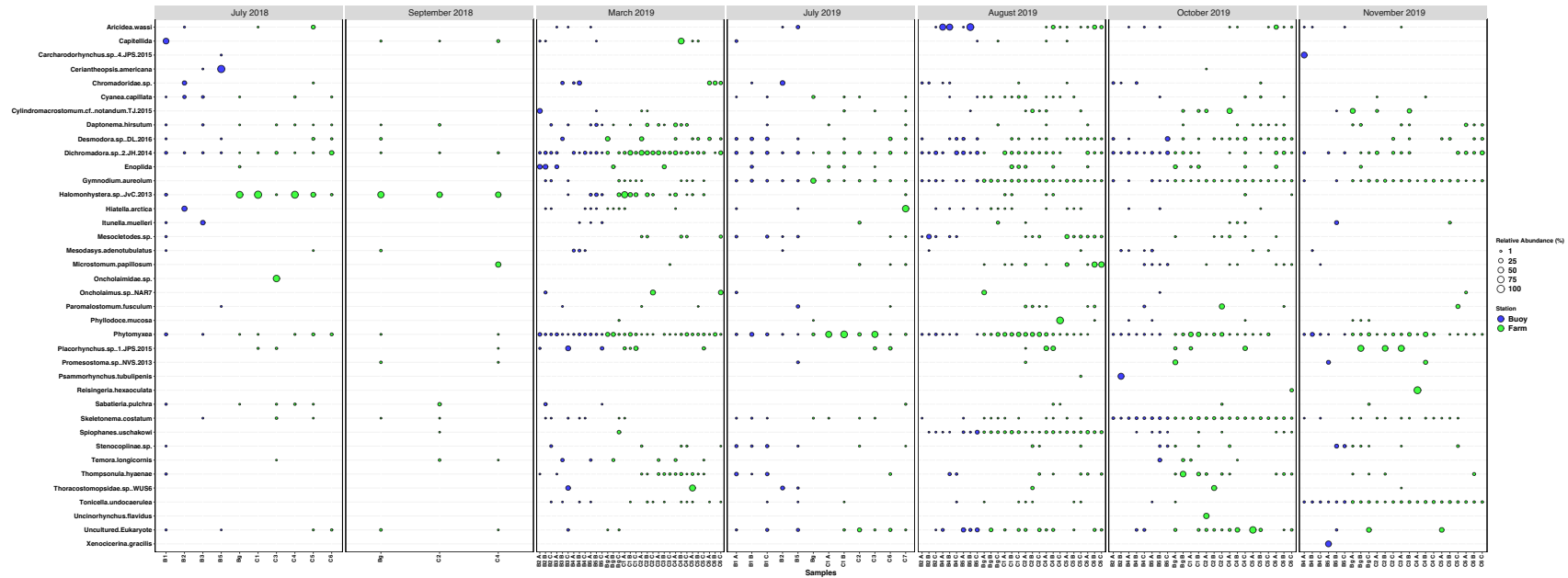


**Figure 2.8: Bubble plot of the top 10 eukaryotic ASVs with the highest relative abundance in the sediment from each sampling day. ASVs for each day were compiled into one list, run through BLAST and taxonomy was recorded down to the lowest possible level. In cases where more than one ASV came back as the same organism the counts were added together within each sample.**

In contrast to the sediments, the bubble plot of the top 10 eukaryotic ASVs with the highest relative abundance in the water column did not show a noticeable increase in ASVs present between the 2018 and 2019 samples, and the communities were not dominated by any one or two ASVs (Figure 2.9). There was, however, a shift in which ASVs were present between the days, reinforcing the seasonal community shift seen in the previous nMDS plot (Figure 2.3). Interestingly, there does not appear to be any evidence of the difference between 5m and 10m water seen previously (Figure 2.5), indicating that it is not the most abundant organisms driving that difference, but the community as a whole at each depth.

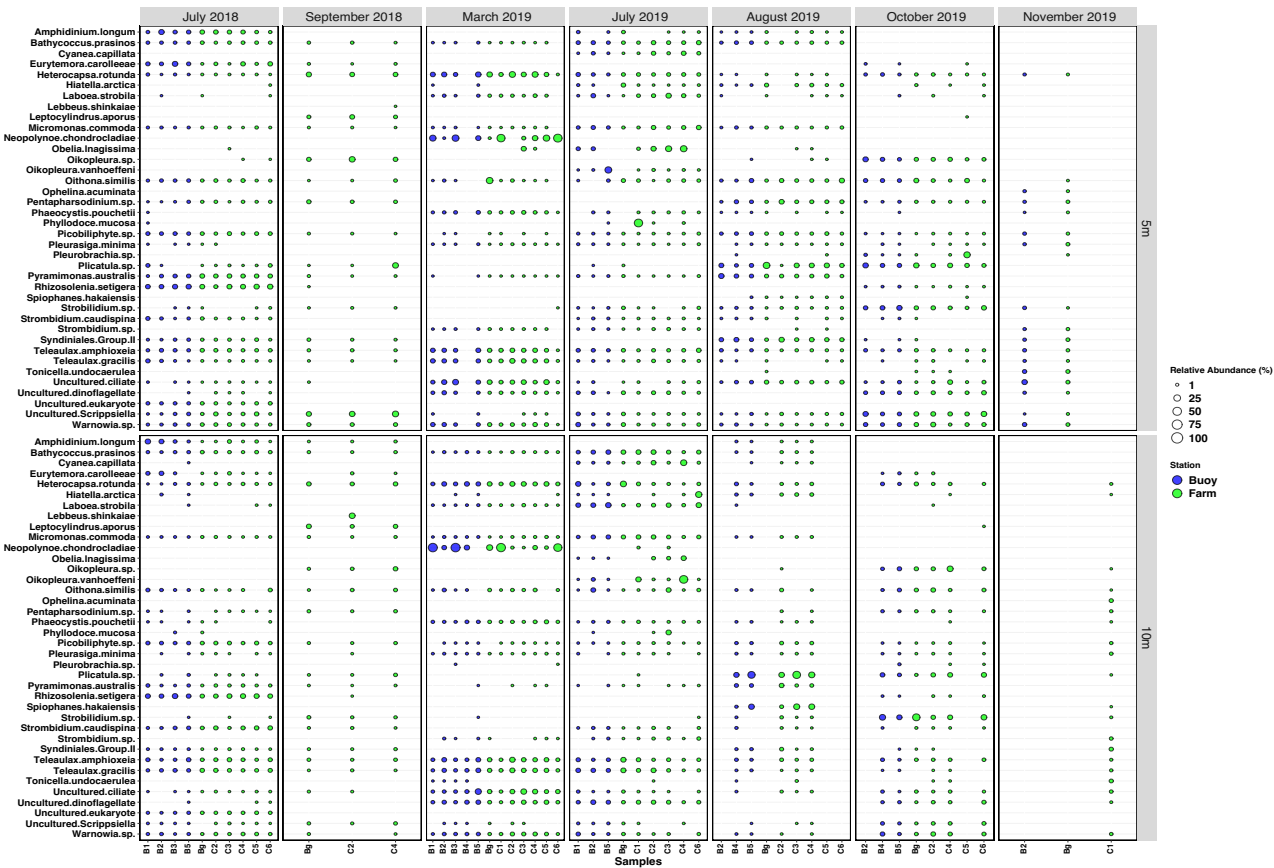


**Figure 2.9: Bubble plot of the top 10 dominant eukaryotic ASVs with the highest relative abundance in the water column from each sampling day. ASVs for each day were compiled into one list, run through BLAST and taxonomy was recorded down to the lowest possible level. In cases where more than one ASV came back as the same organism the counts were added together within each sample. Note that there was a sequencing issue with 10m samples from stations B2, C5, and C6 in August 2019, as well as B2 and Bg 10m, and C1 5m stations in November 2019 and blank columns are not indicative the listed ASVs were not present.**

### 2.3.6 Prokaryotic Community Composition

For the purpose of identifying more specific potential bioindicators, prokaryotic community composition of the sediment was plotted down to the family, however the majority of ASV's were not classified down to that taxonomic level, therefore a plot of the same samples at a higher taxonomy level (class) is presented in the supplemental information (Figure S2). Relative abundance bar plots show that Pre-fallowing sediments were marked by the presence of families whose members are sulfur cycling bacteria: *Desulfobacteraceae*, *Marinifilaceae* and *Desulfobulbaceae* (in July 2018), and *Sulfurovaceae* (in September 2018) (Figure 2.10). In particular, *Desulfobacteraceae* and *Desulfobulbaceae* families are composed of mainly anaerobic sulfur reducers, and *Sulfurovaceae* contains sulfur oxidizers (Table S6). Sediments from the fallowing period (March 2019) still contained *Sulfurovaceae*, however this family was not in the top 5 most abundant ASVs by July of the same year. Samples taken during production cycle 2 (July – November 2019) look similar in terms of the composition of the top 5 families, however there was a noticeable difference between the buoy and farm samples, which supports the results seen in the nMDS (Figure 2.6). Farm samples contained higher levels of *Thiotrichaceae* and *Rhodobacteraceae*, and buoy samples contained more unclassified ASVs at the family level over time. Further supporting the results from the nMDS plots, bars corresponding to the two cages at the seaward end of the farm are more similar to those of the buoy samples, particularly in November 2019. Also, in November 2019, the re-emergence of *Desulfobacteraceae* as one of the top 5 most abundant families was observed. The *Desulfobacteraceae* family was also picked up in the V4V5 sediment data and was a part of the top 5 bacterial families on all days, though there was a higher

relative abundance in cage samples compared to buoy samples during the P2 time period  
(Figure S7).

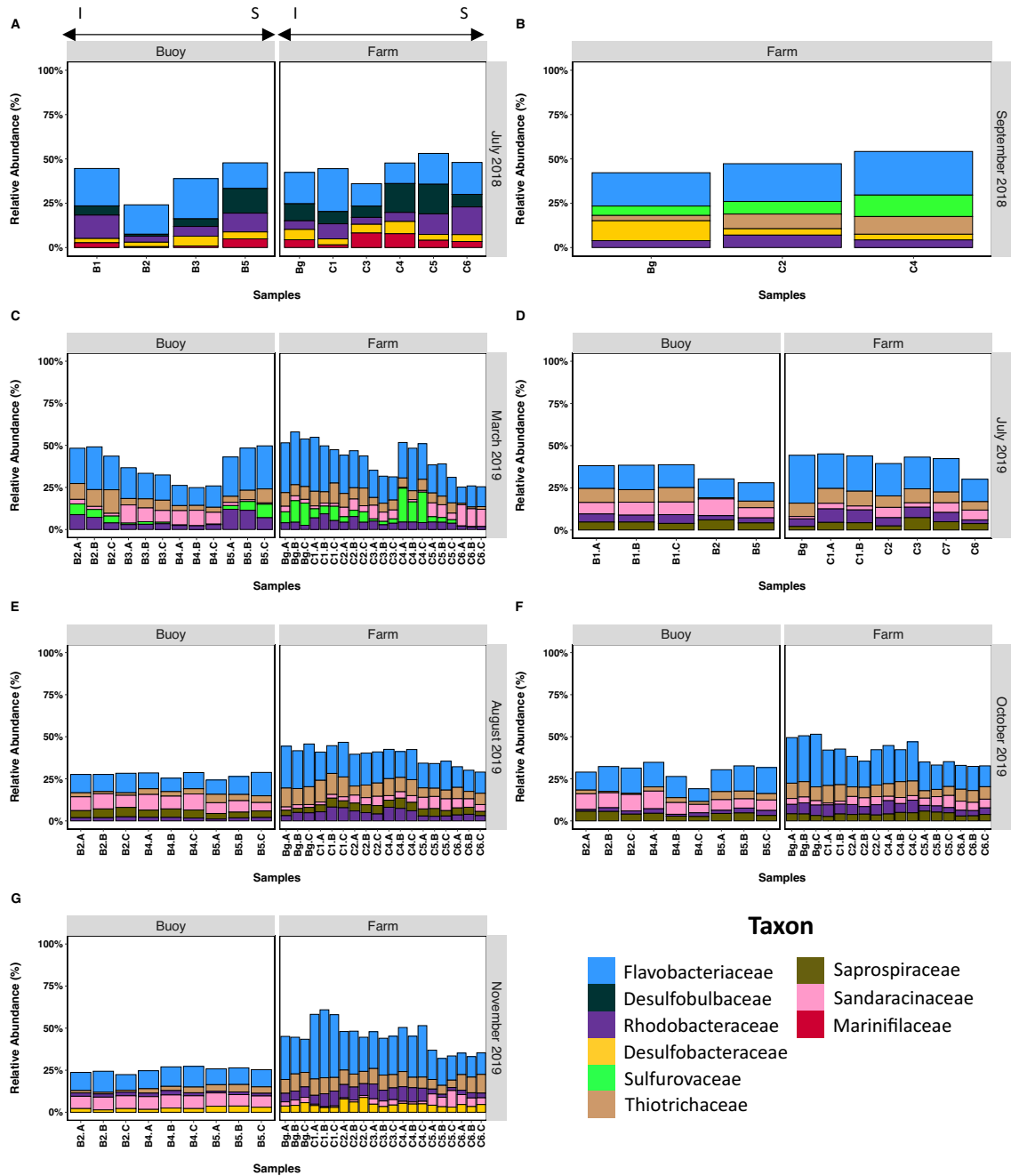


**Figure 2.10: Relative abundance of the top 5 prokaryotic taxonomic families present in the sediment on each sampling date as determined by 16S V6V8 sequencing. Buoy and Farm samples are ordered left to right from inland (I) to seaward (S). ASV's unclassified to the family level were excluded and represented by white space on the y-axis. The letters ABC in x-axis labels indicate sediment replicates. Plots A-B are from time period P1, C from time period F, and D-G from time period P2.**

The water column was dominated by 3 families throughout all of the sampling dates: *Rhodobacteraceae*, Clade I, and *Flavobacteriaceae*. in varying relative abundances (Figure 11). Clades I, II and III all refer to different clades of SAR11 bacteria, another widely distributed taxa that is abundant globally in the ocean. Two of these three families (*Rhodobacteraceae* and *Flavobacteraceae*) were also seen in the sediment, which is not surprising as they are two of the most widely distributed families and different members are known to be abundant in both water column and sediments.

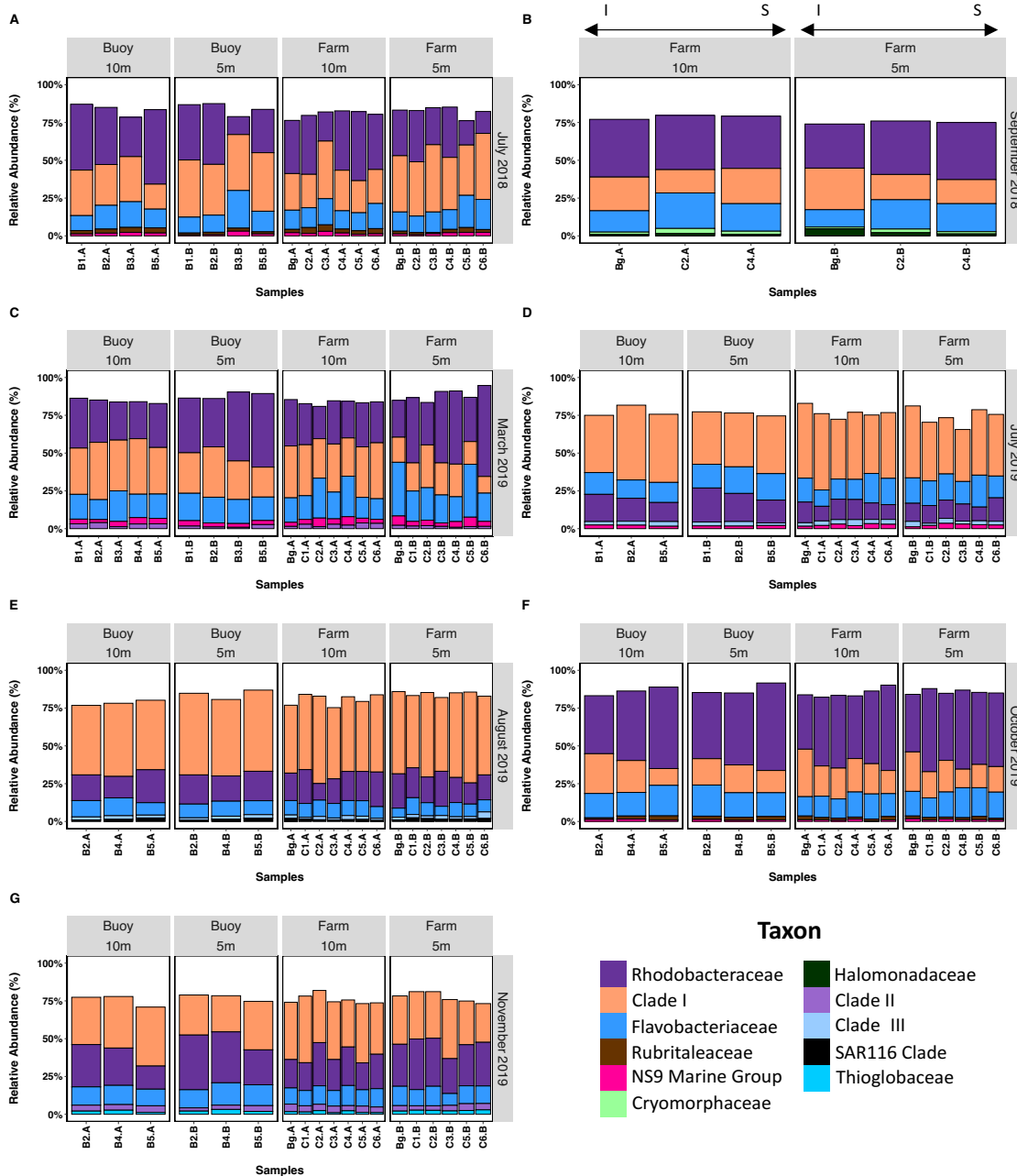


**Figure 2.11: Relative abundance of the top 5 prokaryotic taxonomic families present in the water column on each sampling date as determined by 16S V6V8 sequencing. In each section, samples are ordered left to right from inland to open ocean. ASV's unclassified to the class levels were excluded and represented by white space on the y-axis. In the x-axis labels, samples ending in A are from 10m water, and those ending in B are from 5m water. Plots A-B are from time period P1, C from time period F, and D-G from time period P2.**

### *2.3.7. Potential Indicator Organisms for Organic Loading*

Three eukaryotic taxa were chosen as potential organisms to indicate levels of organic loading (Figure 2.12). Capitellida polychaetes are already used as indicators in traditional monitoring techniques, while Monhysterids and Enoplids (colloquial names for members of the orders Monhysterida and Enoplida) are nematodes that made up a relatively large proportion of many samples. Under the cages, there was a low relative abundance of Capitellida in samples before and during fallowing, which disappeared after fallowing. Looking at the nematodes, pre-fallowing cage sediments were dominated by Monhysterids, which became lower in relative abundance during and after fallowing, during which Enoplids became the relatively dominant nematode taxa.

In buoy samples, relative abundance of Monhysterids was low. Instead, buoy sediments before fallowing had slightly higher levels of Capitellida, which again decreases in relative abundance after fallowing. Similarly, to the cage samples, Enoplids became the relatively dominant taxa after fallowing (Figure 2.12).

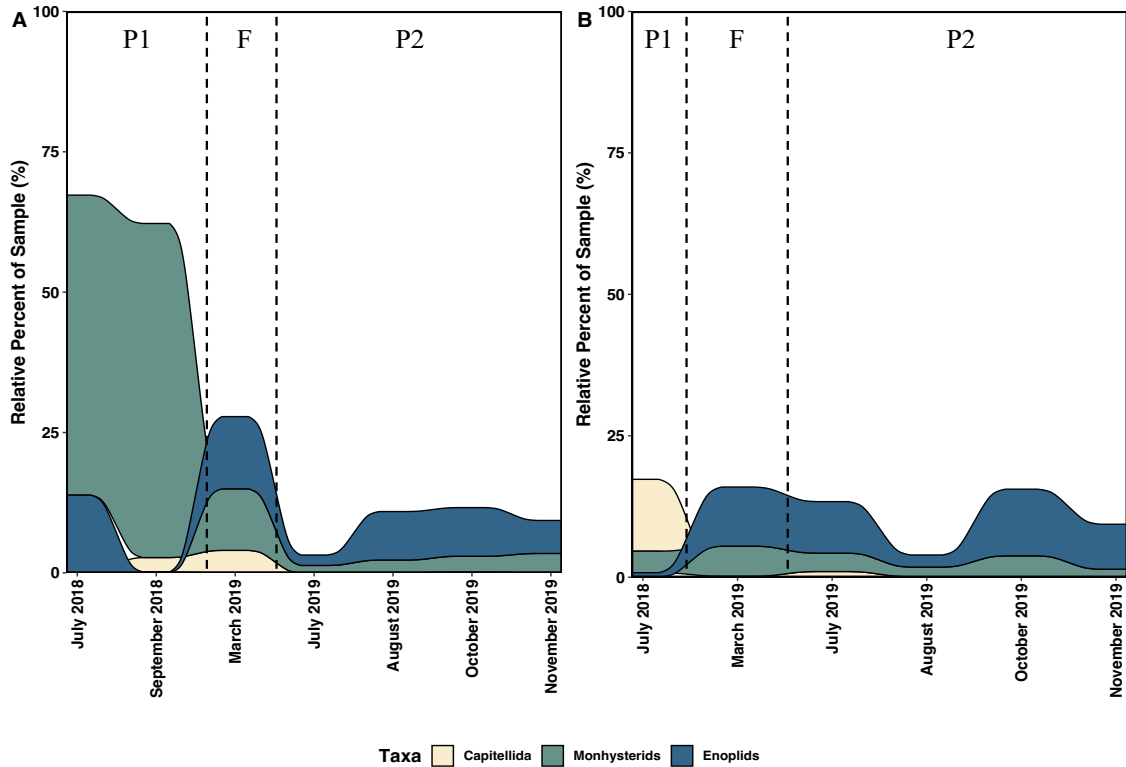


**Figure 2.12: Alluvial plot of the percent of the a) farm sediment community and b) buoy sediment community that is made up of 3 potential meiofaunal indicators of organic loading levels. Percent community was calculated using the relative abundance of each at each samples date. Black lines indicate the approximate time of fallowing and separate the 3 time periods defined in the methods.**

Indicator prokaryotic taxa were chosen based on a paper by Vanhoeveen *et al.* (2018), which identified bacterial taxa associated that could potentially be indicators of the degree of organic loading in the sediments. Relative abundance of *Beggiatoa*, the large bacterium used as a visual indicator in traditional monitoring, was also investigated, but it made up less than 1% of the relative abundance of the bacterial community in the samples and was therefore excluded from the plot. Many of these indicator bacteria belong the families seen above in the bar plots (Figure 2.10, Table S5). Relative abundance of these indicator bacteria decreased after fallowing in both cage and buoy sediments (Figure 2.13), however the buoy samples showed a much lower level of these

indicator bacteria, even before fallowing. Relative abundance of *Sulfurovum* in the cage samples is comparatively high, even after fallowing, and increased again in October and November 2019. Indicspecies analysis shows that, in November 2019, the ASV most significantly associated with cage samples was a bacterium species belonging to the *Sulfurovum* genus (Table S4).

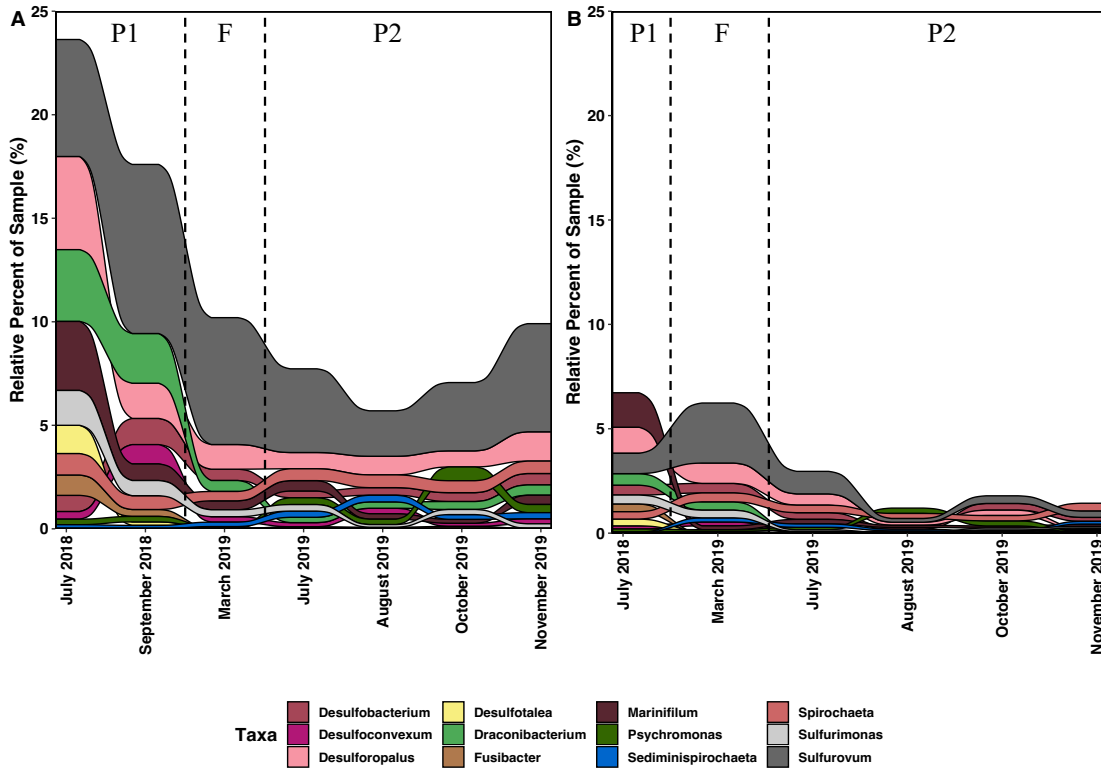


**Figure 2.13: Alluvial plot of the percent of the a) farm sediment community and b) buoy sediment community that is made up of potential microbial indicators (Vanhoeven *et al.* 2018) of organic loading levels. Percent community was calculated using the relative abundance on each sampling date as determined by 16S V6V8 amplicon sequencing. Black lines indicate the approximate time of fallowing and separate the 3 time periods defined in the methods.**

## 2.4. DISCUSSION

### 2.4.1. Patterns in Water Column and Sediment Community Composition During the Study Period

Over the course of the study period, eukaryotic Shannon diversity was comparable between the water column and sediment post-fallowing, with pre-fallowing sediment showing a lower diversity than the water column. Sediments subjected to high organic loading, displayed a lower diversity due to the dominance of a few, more tolerant organisms (Zhulay *et al.* 2015). As well, in this study benthic prokaryotic communities consistently had a much higher Shannon diversity index compared to the water column over the study period. Prokaryotes naturally have a high diversity in sediments (Li *et al.* 2013) and, unlike eukaryotes, prokaryote diversity does not always change with eutrophication (Bentzen-Tilia *et al.* 2016, Rubio-Portillo *et al.* 2019). Instead, changes are often seen in community composition (Bentzen-Tilia *et al.* 2016, Rubio-Portillo *et al.* 2019) as demonstrated with the findings in this study where prokaryotic families in the sediment changed in relative abundance but maintain a high Shannon diversity index throughout the study period.

In the water column, a sinusoidal pattern emerged in both the eukaryotic and prokaryotic Shannon diversity index values that was not seen in the sediment. Given the location of the site, close to the open ocean, it is not surprising that across sampling dates there appears to be a very strong seasonal cycle that occurs within the water column prokaryotic and eukaryotic communities. This type of seasonal cycle has been seen in the bacterial community of the North Atlantic Ocean across multiple years (Zorz *et al.* 2019). Unlike the water column, the microbial and meiofaunal communities in the sediment

were not influenced by seasonal trends and instead were more influenced by farm activity, with fallowing and post-fallowing sediments being different from pre-fallowing sediment communities. The classical sphere of influence model observed most often in regard to aquaculture production is the “bulls-eye” pattern of continuous succession first described in Pearson and Rosenberg 1978, with the most affected sediments being in the center of the farm with decreasing effects radiating out from the center (Zhulay *et al.* 2015). Here however, results showed that communities were patchy instead of forming a bullseye starting at the middle cages and radiating out, with samples from the same day differing in beta diversity instead of clustering tightly as seen in the water column. This could be because of the coarse-grained structure of the sediments, or the tidal flushing that occurs at the site (Burke *et al.* 2020). Though more sampling is needed to confirm, this pattern is seen in a study of a hard bottomed aquaculture site in Eastern Canada, off the coast of Newfoundland, which found indicators such as polychaetes and bacterial mats were patchy in nature along transects, as opposed to radiating out from the site in a predictable pattern (Armstrong *et al.* 2019).

#### *2.4.2. Daily Patterns at Individual Sampling Sites*

Although water column samples cluster more tightly by day when looking at the yearly cycle, data from individual days showed another, small scale pattern. During most months there is a slight thermocline in the water column, leading the 5m and 10m communities to differ significantly (Figure S1). These results indicate that communities and patterns across time in the water column were, at least in part, driven by water column stratification. Meanwhile, there is only a significant difference between farm and

buoy sample prokaryotes on two of the days, both during P2, with no concrete pattern to these differences. This supports the idea that overall, the farm is not the major driving force behind the microbial planktonic communities in the water column.

Unlike the water column, benthic communities, on individual sampling days, displayed differences between the 3 sample types (cage, buoy, barge), which showed a pattern connected to farm production. Over the course of the P2 cycle, there were significant difference among station types after approximately 4 months of production and became increasingly different over the rest of the P2 time period in both eukaryote and prokaryote communities. Interestingly, although the sediment communities were patchy, there was a distinct pattern that appeared during P2 where, as buoy and cage samples became increasingly different, communities under the two cages at the seaward end of the farm fell somewhere in between those at the buoy sites, and those under the rest of the cages. This pattern appeared in both eukaryotic and prokaryotic communities; however, it was much more pronounced in the prokaryotes. A parallel study performed at the same farm which monitored cage oxygen levels in the water column determined that as the tide flows into the bay, the outer cages closer to the open ocean are re-aerated, but a combination of fish respiration and cage infrastructure decreases the oxygen concentration by the time it reaches the inner cages (Figure 2.1) (Burke *et al.* 2020). Since oxygen depletion is considered one of the primary drivers of benthic community change at aquaculture sites (Wildish and Pohle 2005), the two cages at the seaward end of the farm receiving higher oxygen water on the incoming tide, may have offset some of the effects of organic matter recycling. Interestingly, although the reverse was observed on the outgoing tide where the inner cages received higher oxygen water (Burke *et al.* 2020), this was not reflected in the biological data. These results highlight both the importance

of hydrodynamics and increased spatial sampling, something that has been highlighted in previous studies (Beentjes *et al.* 2019, Macleod *et al.* 2006).

As for the samples from the end of P1 (July 2018), eukaryotic communities were not significantly different among station types, while prokaryotes were. This could be a result of prokaryotes and eukaryotes differing in how they react to organic loading, since prokaryotes are known to be more sensitive and respond faster to changes in their immediate environment (Bentzen-Tilia 2016). In samples collected during the fallowing period (March 2019), both eukaryotic and prokaryotic communities from different station types were not significantly different. This could indicate that the fallowing period was adequate enough to allow sediments to recover after the source of organic matter was removed, however more sampling is needed to confirm this.

#### 2.4.3. *Effects of Aquaculture and Fallowing on Benthic Communities*

The exact degree to which the fallowing period allowed the environment to recover was unfortunately not within the scope of this project, however from the data collected it was clear that fallowing had an effect on the benthic community. This was most noticeably seen in the reduced relative abundance of the anaerobic *Desulfobacteraceae* bacterial family in post-fallowing sediment samples (both V6V8 and V4V5), as well as an overall decrease in relative abundance of other sulfur-metabolizing bacteria, such as *Sulfurovum* sp. A previous experiment by Stoeck *et al.* (2018a) found *Desulfobacter* (a bacterial genus from the family *Desulfobacteraceae*) in the sediments under aquaculture cages, which decreased in relative abundance as distance away from the cages increased, reinforcing the findings from this study that this bacterial taxon is a

promising indicator for sediments affected by cage presence. Although the results from this study indicate that fallowing had the desired effect of allowing sediments to recover, it should be noted that the changes were short-lived as after less than a year into the next production cycle, *Desulfobacteraceae* appeared in the sediment samples again, although at much lower levels.

The sediment meiofaunal community under the cages also showed changes after the fallowing period, marked by a switch from sediment dominated by Monhysterida nematodes, to sediment where Enoplida nematodes were in higher relative abundance compared to Monhysterida. As well, there was a small amount of Capitellida polychaetes which mostly disappeared after the fallowing period. As Monhysterids are small and tolerant to pollution while Enoplids are larger and more sensitive to pollution (Mirto *et al.* 2002), a shift in the ratio of Monhysterida:Enoplida could indicate that there was a decrease in organic matter pollution during the fallowing period, though more sampling would be needed to confirm this.

Since every aquaculture site is unique, and this is the first study of its kind conducted in the area to the best of our knowledge, more research would need to be conducted in order to validate these organisms as indicators of organic loading. However, the prevalent presence of nematodes that have been previously associated with organic loading (Mirto *et al.* 2002) in combination with other eDNA research which found that sulfur metabolizing bacteria are good indicators of organic loading levels (Rubio-Portillo *et al.* 2019), not only indicates that these organisms are good bioindicator candidates in this area, but also validates the use of eDNA as a monitoring tool.

## **2.5. CONCLUSIONS**

Results from this study demonstrate that eDNA can be used to study both eukaryotic and prokaryotic communities around coastal aquaculture farms, revealing patterns and changes in the water and sediment. Environmental monitoring around aquaculture farms is usually preformed using visual counts and taxonomic ID based on microscopy, however this is a time consuming and expensive process. eDNA has the potential to make monitoring easier, and allow for a higher volume of sampling which, as this research shows, is important due to the spatial variability in sediment communities. Overall, the results from this study both reinforce the idea that monitoring the environmental on coastal farms is paramount and demonstrate how the use of eDNA has potential to become an integral part of making aquaculture more sustainable in the future.

# CHAPTER 3: SHOTGUN METAGENOMIC ANALYSIS OF SULFUR METABOLIZING BACTERIA

## 3.1. INTRODUCTION

### 3.1.1 Sulfur Cycle

Sulfur reducing bacteria (SRB) and sulfur oxidizing bacteria (SOB) are important drivers of the global sulfur cycle (Muyzer and Stams 2008, Paterson 2012). In particular, sulfur oxidation is considered one of the most important microbial chemosynthetic processes (Cao *et al.* 2014), while genes responsible for sulfite reduction are considered to catalyze the rate-limiting step in the global sulfur cycle (Anantharaman *et al.* 2018).

The dissimilatory sulfur reductase (Dsr) pathway (Figure 3.1) is one of the major pathways responsible for sulfur metabolism (Venceslau *et al.* 2014). When operating in the forward direction, this pathway performs sulfur reduction, however it can also function in the reverse to perform sulfur oxidation (rDsr) and the *dsr* genes are found in both SRBs and SOBs (Anantharaman *et al.* 2018, Pereira *et al.* 2011). Within the Dsr pathway, the *dsrC* gene codes for a protein that is essential for the final reduction step yielding hydrogen sulfide (H<sub>2</sub>S) (Pereira *et al.* 2011, Venceslau *et al.* 2014). Additionally, *dsrC* is strictly conserved in all sulfate reducing organisms (SRO) (Pereira *et al.* 2011) and phylogenetic analysis of the *dsrC* gene shows a clear split between SRB and SOB groups in the phylogenetic tree (Venceslau *et al.* 2014), allowing a distinction for the forward and reverse reaction based on taxonomic grounds.

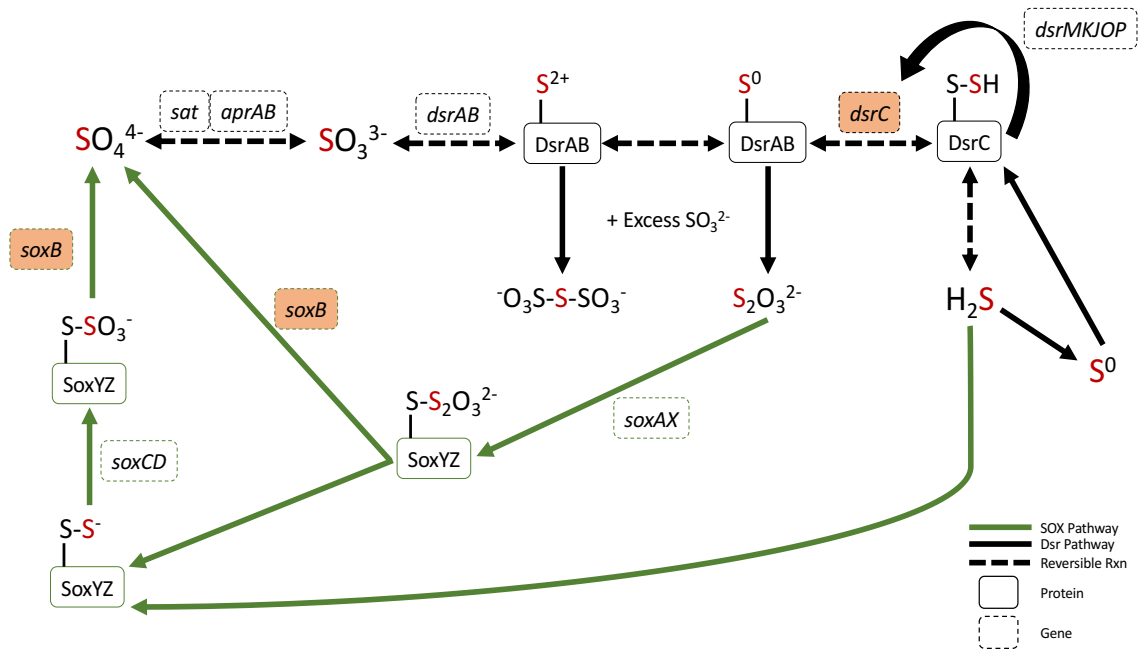


**Figure 3.1: Overview of the sulfur cycle pathways relevant to this study and the proteins involved. Genes investigated are highlighted in orange. The red S signifies the sulfur that is being reduced/oxidized throughout the cycle.**

Another important pathway in SOB is the Sox sulfur oxidation pathway (Figure 3.1), which unlike the Dsr pathway, is a unidirectional pathway for the oxidation of reduced sulfur compounds. One important aspect of the Sox pathway is that it can oxidize not only elemental sulfur and sulfides, but thiosulfate (S<sub>2</sub>O<sub>3</sub><sup>2-</sup>) as well (Dahl *et al.* 2008), which can be a by-product of the Dsr pathway under excess sulfate conditions (Venceslau *et al.* 2014). Though there are multiple *sox* genes involved in the oxidation cycle, *soxB* is of particular interest as it codes for the SoxB protein which directly produces sulfate, the end product of the oxidation process (Dahl *et al.* 2008).

### 3.1.2. Shotgun Metagenomics and the Sulfur Cycle in Aquaculture

With developments in technology and subsequent accessibility of DNA sequencing, shotgun metagenomics is increasingly being applied to many studies of microbial eDNA in the environment (Garlapati *et al.* 2019). One of the areas where increasing the use of shotgun metagenomics would be beneficial is in aquaculture monitoring of the benthic environment. It is well established that organic waste from coastal aquaculture can accumulate in the sediments, leading to anoxic conditions (Holmer *et al.* 2005). Due to the abundance of sulfate in overlying and pore water, sulfate reduction rapidly becomes the predominant driver of organic matter respiration in anaerobic coastal sediments, particularly in organic-enriched fish farm sediments (Anantharaman *et al.* 2018, Choi *et al.* 2018, Choi *et al.* 2020). This process produces toxic, reactive sulfides (H<sub>2</sub>S), which are harmful to the benthic flora and fauna (Choi *et al.* 2018, Choi *et al.* 2020, Moncada *et al.* 2019). In some cases, the resulting sulfides can diffuse into the sediment pore water and be transported up to the surface of the benthos where it can diffuse into the overlying water column, (Holmer *et al.* 2005, Moncada *et al.* 2019). Sulfides released into the water column can be harmful to the gills, liver, and metabolic enzymes of Atlantic salmon (Holmer *et al.* 2005). As well, other anaerobic benthic processes can release nutrients such as nitrogen and phosphorus into the overlying water, which can cause eutrophication of the water column and stimulate harmful algal blooms in shallow ecosystems (Choi *et al.* 2020).

Since a high rate of sulfate reduction is one of the most prominent outcomes of organic loading on finfish farms, measuring sulfide levels is a widely used monitoring tool for assessing the effects of Atlantic salmon farming on the benthic environment in

Canada (Holmer *et al.* 2005). In particular, a survey that looked at many different parameters used for monitoring purposes showed that total sulfide was the most sensitive and practical variable used to detect organic enrichment in the Bay of Fundy (Hargrave *et al.* 1997, Holmer *et al.* 2005). Examples showing a decrease in the sulfate reduction rate with increasing distance from cages concluded that both the locality of farm effects and an increasing presence of large benthic macrofauna oxygenating the sediments through bioturbation were suppressing sulfate reduction (Holmer *et al.* 2005).

Despite many studies on the sulfur cycle and its importance, little is known about the microorganisms that are directly linked to and responsible for the biogeochemical cycling of sulfur in fish farm sediments specifically (Choi *et al.* 2018). Organisms in this group generally fall into two categories: SRB, which perform anaerobic sulfur reduction (Pereira *et al.* 2011), and SOB, which can perform either aerobic or anaerobic sulfur oxidation (Dahl *et al.* 2008). The most studied bacterium in relation to fish farm sediments is the sulfur oxidizer *Beggiatoa sp.* due to its large size, which makes it visible to the naked eye as large, white bacterial mats on the sediment surface. The presence of *Beggiatoa sp.* is usually correlated with a buildup of sulfides in the sediment which has diffused up to the sediment/water interface, where the bacteria oxidize it back to sulfate. It has also been shown that *Beggiatoa sp.* can concentrate nitrate which is then transported down into the sediment where it is reduced to dinitrogen or ammonia in combination with oxidation of sulfides (Dahl *et al.* 2008), further demonstrating how changes in the sulfur cycle driven by organic loading can affect other biogeochemical cycles. Although *Beggiatoa sp.* is fairly well studied, it is only one bacterial genus of many that are present in marine sediment and is one whose presence is linked with a degraded benthic state, high in sulfides. While *Beggiatoa* is easily seen on the sediment

surface when present, other taxa involved in the sulfur cycle may also provide an earlier warning signal sulfide accumulation. Due to the lack of knowledge regarding microbial communities associated with sediments below aquaculture cages, shotgun metagenomics would be a valuable tool to use as it not only allows for sulfur cycling genes to be used to taxonomically identify organisms but provide information on the general metabolic potential of the microbiome and possible interaction between the cycling of elements, for example between the sulfur and nitrogen cycles.

The purpose of this study is to assess the use of shotgun metagenomics as a tool for studying microbes that contribute to sulfur cycling by tracking the genes present in the sediment surrounding a finfish farm off the coast of Nova Scotia. In particular, looking at the genes involved in the Dsr and Sox pathway before and during the fallowing period in order to improve the taxonomic assignment of microbes involved in key metabolic pathways in the sulfur cycle and, as a secondary goal, assess the change in metabolic potential for sulfur cycling in the sediments.

## **3.2. MATERIALS AND METHODS**

### *3.2.1. Sample Collection*

Samples for this study were collected at the Cooke aquaculture facility's McNutt's site outside of Shelburne, NS which houses between 19-20 cages of Atlantic salmon (*Salmo salar*) as well as a large onsite feeding barge. Sampling occurred intermittently from July 2018 – November 2019, with fallowing taking place from approximately November 2018 – June 2019. Samples used in this metagenomic study were taken in July

2018 and March 2019 (Table S3). More information on all sampling dates can be found in the supplemental material.

Sediment samples were taken using a van der veen grab at cage and buoy samples according to Figure 3.2 when weather and farm activity permitted. Table S3 outlines which stations were sampled in July 2018 and March 2019. Samples were immediately frozen on deck in liquid nitrogen following collection.

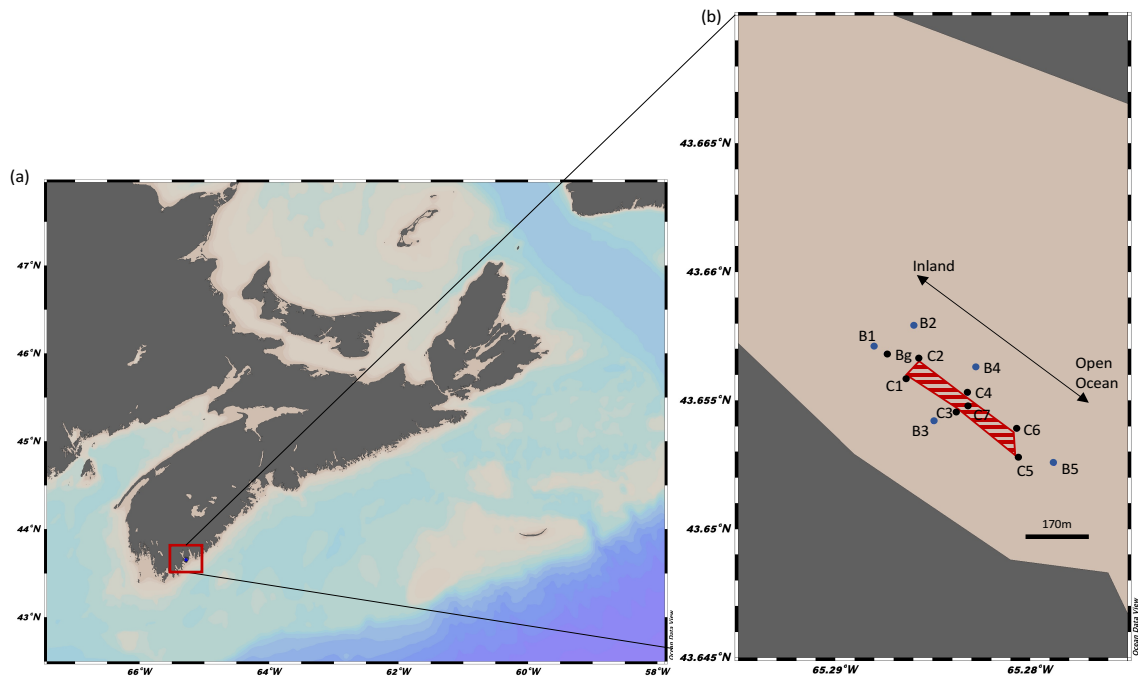


**Figure 3.2:** Map of the McNutt's sampling area in relation to (a) all of Nova Scotia and (b) close up of the farm area, indicated by red dashed lines, and sampling layout. In (b), stations beginning with C are cages, those beginning with B are farm buoys, and Bg represents the on-site barge. Black dots represent cage and barge samples, while blue dots represent buoy stations.

### 3.2.2. DNA Extraction and Analysis

DNA from sediment samples was extracted according to the methods described in Chapter 1. Extracted DNA from 2 cage stations (C3, C6) and 2 buoy stations (B2, B3) was sent off for metagenomic sequencing at Dalhousie's IMR lab. Shotgun metagenomic

sequencing was performed on IMR's Illumina NextSeq machine at 4X sampling depth as per their protocol (Commeau *et al.* 2017).

The following analysis of raw sequences up to the creation of RPKM tables was performed by Dhvani Desai in the LaRoche lab. Raw sequences were first screened for contaminating sequences using Bowtie2 (Langmead *et al.* 2009). Kraken2 (Wood *et al.* 2019) was then run to determine functions by mapping reads against the UniRef90 (Suzek *et al.* 2014) gene families. The resulting gene abundances were normalized to gene length and number of reads that mapped to a reference gene, resulting in the units of reads per kilobase million (RPKM). RPKM reads were split into two tables: unstratified (functional profile and taxonomy of reference gene) and stratified (includes the taxa associated with each functional gene). Using taxonomy of the assigned reference genes, *DsrC* reads were separated into known sulfur oxidizers and reducers. As the Sox pathway only performs sulfur oxidation, such confirmation is not needed for these reads. Lastly, the unstratified RPKM table was used to match genes to MetaCyc (Caspi *et al.* 2020) pathways. The table of genes that were matched to pathways was uploaded to the MetaCyc dashboard in order to get a rough visualization of the distribution of metabolic pathways among samples (Caspi *et al.* 2020).

Bar plots were created in RStudio version 1.2.5042 (RStudio Team 2020) using the following packages: Reshape2 (Wickham 2007), tidyverse (Wickham *et al.* 2019), lubridate (Grolemund and Wickham 2011), ggplot2 (Wickham 2016), gridExtra version 2.3 (Auguie 2017), ggpubr version 0.3.0 (Kassambara 2020), and cowplot version 1.0.0 (Wilke 2019).

### **3.3. RESULTS**

#### *3.3.1. Distribution of Metabolic Pathways Across Sampling sites*

The distribution of metabolic pathways shows that the majority of the genes successfully mapped to the metacyc database were related to biosynthesis, for example fatty acid/lipid, amino acid, and secondary metabolite biosynthesis (Figure 3.3). The sediments from the mid-fallowing sampling time point (March 2019) had the highest number of reads from genes assigned to a Metacyc pathway, while pre-fallowing cage sediments, C3 in particular, had the lowest (Figure 3.3). Relative abundance of reads showed a consistent percentage of each pathway across samples with a dominance for reads assigned to biosynthesis pathways in all samples (Figure 3.3).

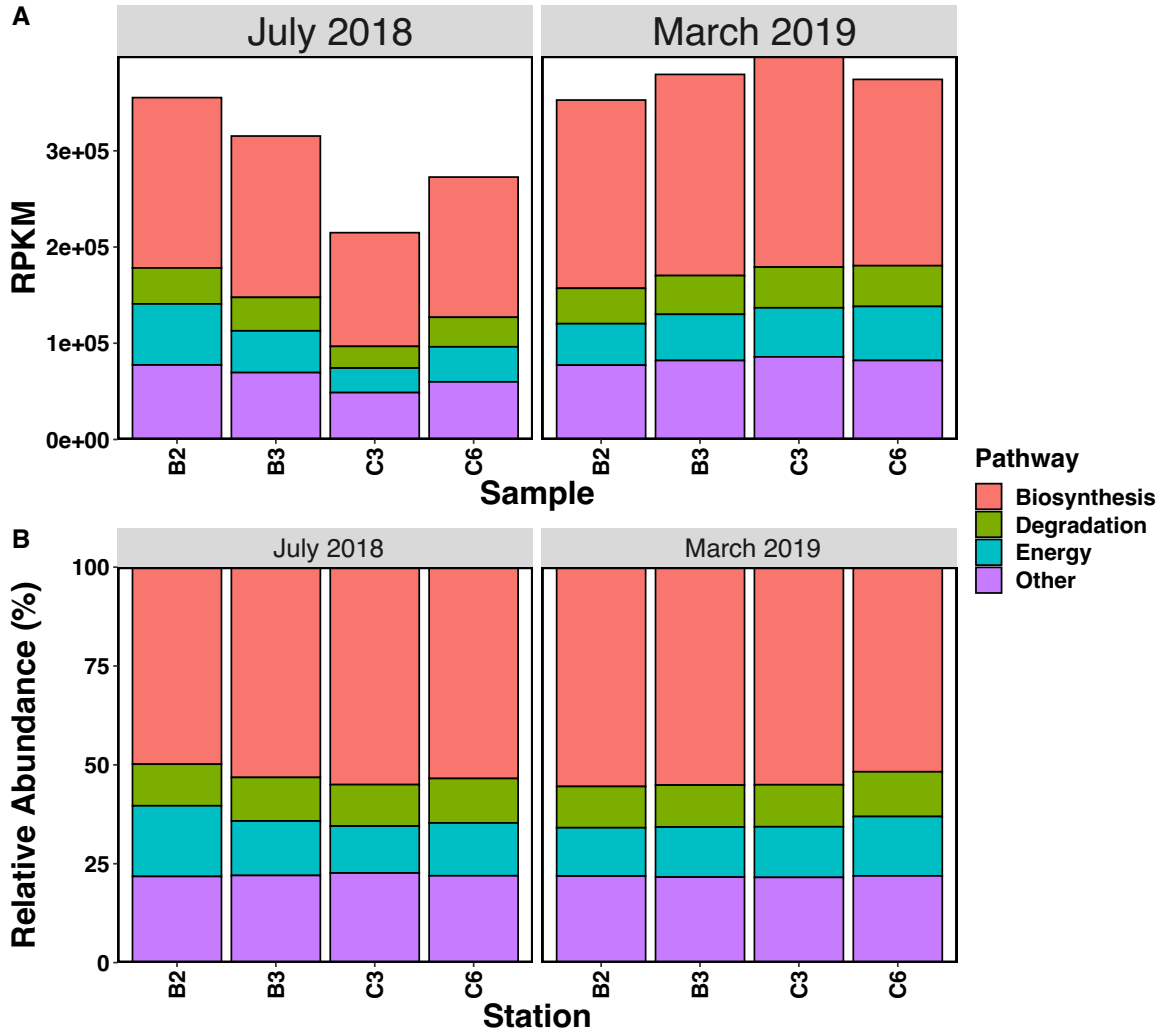


**Figure 3.3: A) Reads per kilobase million (RPKM) and B) Relative abundance (%) of overarching gene categories before (July 2018) and during (March 2019) following as determined by the Metacyc database (Caspi *et al.* 2014). Relative abundance was calculated for each sample by adding together raw reads of all pathways and determining the percentage of each pathway.**

### 3.3.2. Distribution of Sulfur Cycling Genes Across Sampling sites

All bar plots of sulfur cycle genes in the chapter are plots of normalized RPKM values. These numbers are also presented as relative abundances in the supplemental material. Results from unstratified RPKM tables show that, overall, the *dsrC* gene (oxidizers and reducers combined) had a higher count than the *soxB* gene in all samples.

In total, 209 were assigned to oxidizers, 104 to reducers, and 86 were not confidently assigned. Comparing cage samples across sampling days, there was a noticeable difference between samples from pre-fallowing sediments and mid-fallowing sediments (Figure 3.4). There were lower reads of *dsrC* genes for oxidation (*rdsrC*) and slightly elevated reads of *dsrC* genes for reduction (*dsrC*). In the C3 sediments, there were more *dsrC* than *rdsrC* reads, while in C6 there was slightly more *rdsrC*, although the number of *rdsrC* reads was still lower than mid-fallowing sediments (Figure 3.4). Mid fallowing cage samples showed a similar pattern to the buoy samples, with increased *rdsrC* reads and reduced *dsrC* compared to pre-fallowing, particularly in the C6 sediment (Figure 3.4). Buoy sediment samples did not show much difference between days compared to the cages. However, there was a noticeably higher amount of *dsrC* reads in B2 sediment in March 2019 (Figure 3.4). Presence of the *soxB* gene did not show as noticeable a pattern between before and during fallowing as the *dsrC* and *rdsrC* genes, with levels in the buoy stations being almost the same between the two in the majority of samples (Figure 3.4). Most noticeably there were elevated levels of *soxB* with elevated levels of *dsrC* at the B2 station in March 2019 (Figure 3.4). *soxB* was also the dominant oxidation gene in the C3 sediments during pre-fallowing, when *rdsrC* reads were lower than *dsrC* (Figure 3.4).

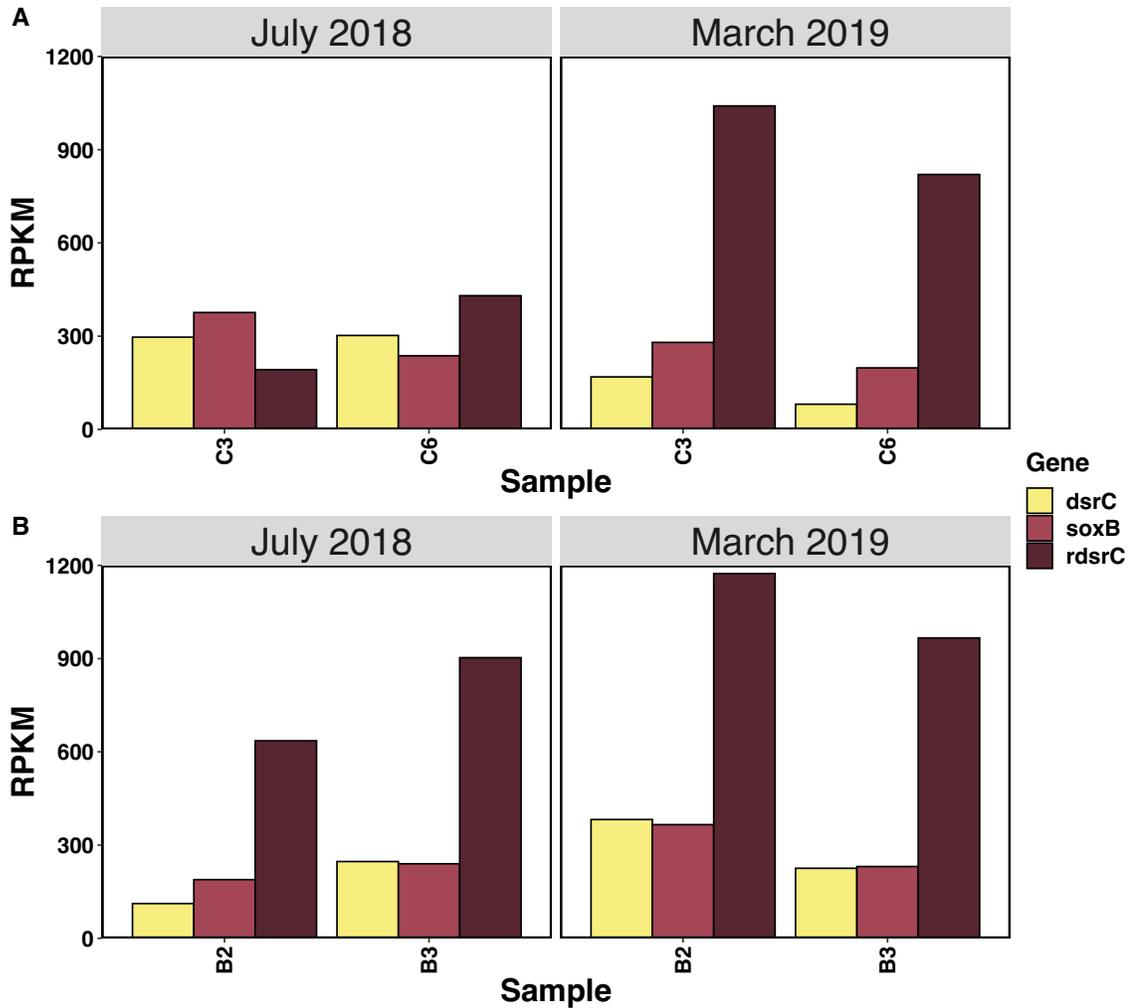


**Figure 3.4: Reads per kilobase million (RPKM) of unstratified sulfur cycling genes before (July 2018) and during (March 2019) following in the A) cage sediments and B) buoy sediments.**

### 3.3.3 Taxonomy of SOB Associated with the *rdsrC* Gene

Using the stratified RPKM table to assess the number of reads and relative abundance of different taxa responsible for sulfur oxidation via the rDsr pathway, it is clear that the majority of SOB taxa belonged to Gammaproteobacteria (Figure 3.5). Figure 3.5 also reinforces the pattern seen in the unstratified gene totals (Figure 3.4) of lower *rdsrC* reads in the pre-fallowing cage sediments and higher reads in the mid-

fallowing cage sediments which was more similar to the levels seen in the buoy sediments. Relative abundance (Figure S10) confirms that even in the pre-fallowing cage sediments with low *rdsrC* reads, Gammaproteobacteria was still the classified taxa with the highest relative abundance.

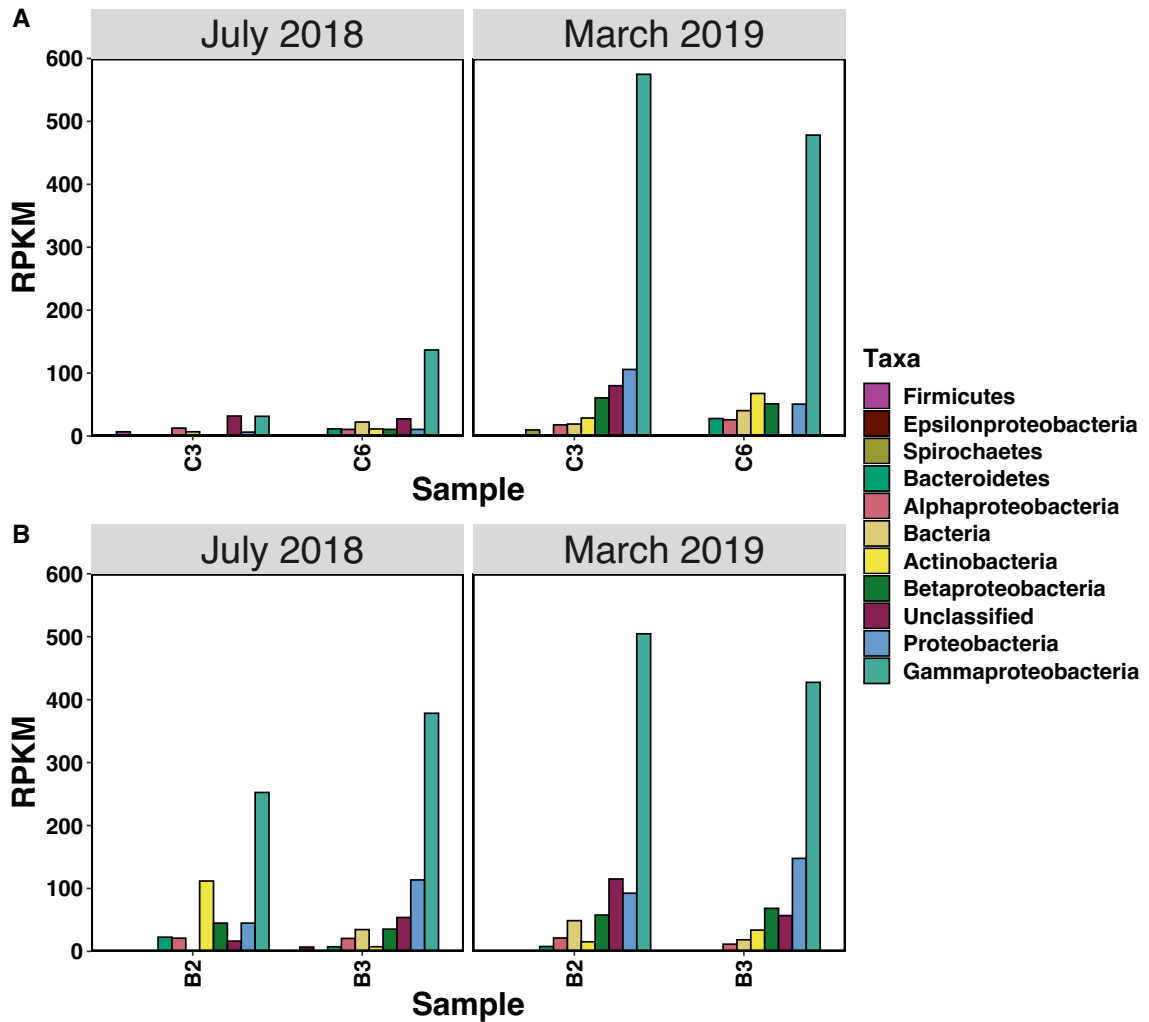


**Figure 3.5: Reads per kilobase million (RPKM) of the *rdsrC* gene for sulfur oxidation separated by taxonomy before (July 2018) and during (March 2019) fallowing in the A) cage sediments and B) buoy sediments. Reads are separated into reads per phylum aside from Proteobacteria which, when possible, were separated into the different classes due to abundance compared to other phyla.**

Gammaproteobacteria were rare in the pre-fallowing cage sediments in comparison to cage sediments during fallowing, though there were more at the C6 station compared to the C3. Mid-fallowing sediments had much higher levels of Gammaproteobacteria, but relative abundance plots show they were dominated by 2 main identified taxa: Chromatiales and *Thioalkalivibrio*, and a pool of unclassified Gammaproteobacteria (Figure 3.6). The buoy samples in contrast were dominated by the unclassified Gammaproteobacteria and, in 2 out of 4 samples, by Chromatiales (Figure 3.6). In particular, the mid-fallowing buoy sediments showed a wider variety and more evenly distributed relative abundance among the other Top 10 Gammaproteobacteria (Figure 3.6).

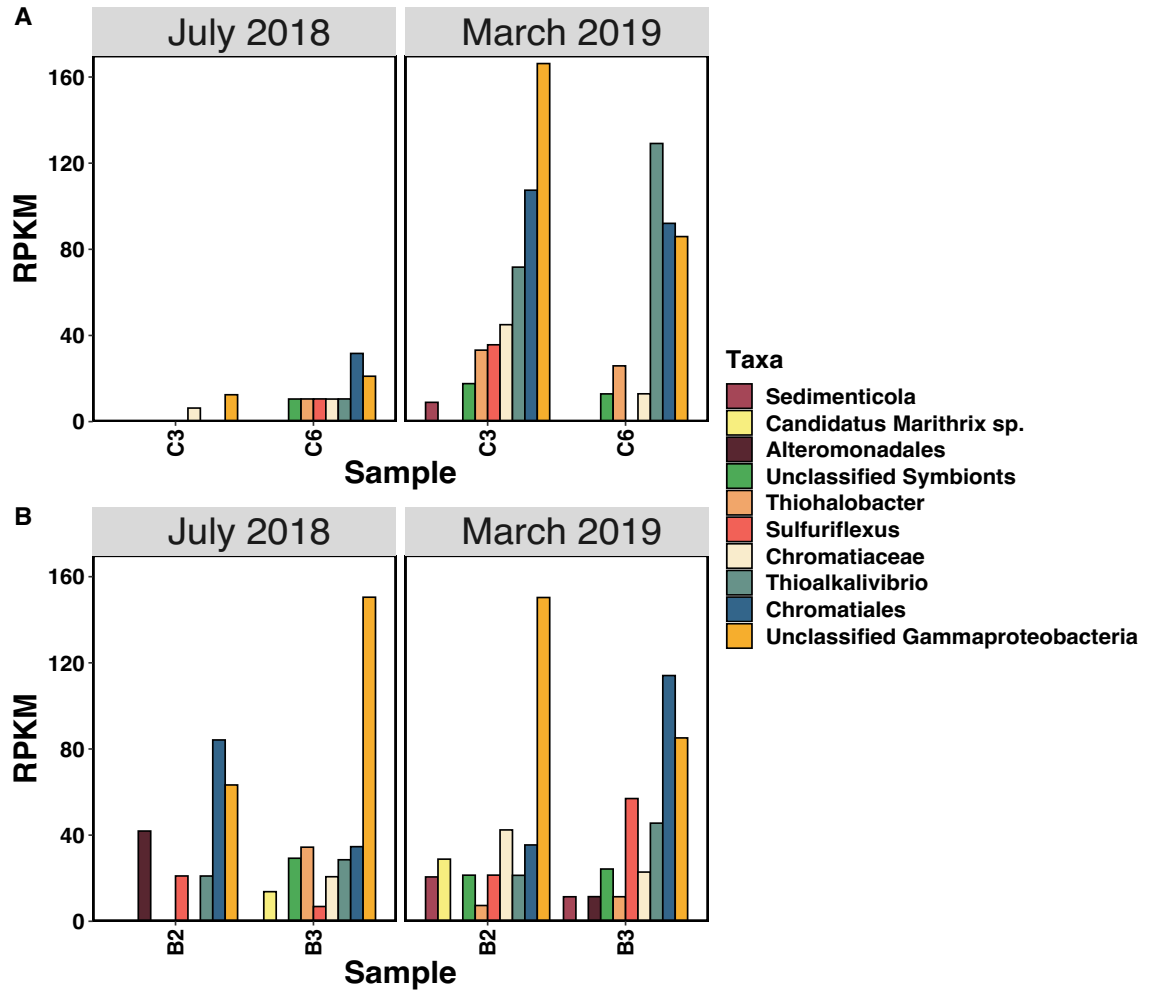


**Figure 3.6: Reads per kilobase million (RPKM) of Top 10 most abundant Gammaproteobacteria taxa that have the ability to perform sulfur oxidation via the *rdsrC* gene before (July 2018) and during (March 2019) following in the A) cage sediments and B) buoy sediments. Reads are separated into the lowest taxonomy level possible from the stratified table. References supporting that these taxa are sulfur oxidizers are listed in Table 3.1.**

**Table 3.1: Table of references supporting the sulfur metabolism in the top 10 most abundant oxidizers (rDsr) and reducers (Dsr) and the corresponding direction of Dsr pathway.**

<b>Taxa</b>	<b>Phylum</b>	<b>rDsr/Dsr</b>
Unclassified Gammaproteobacteria	Gammaproteobacteria	rDsr (Anantharaman <i>et al.</i> 2018)
Chromatiales	Gammaproteobacteria	rDsr (Lavy <i>et al.</i> 2018)
<i>Thioalkalvibrio</i>	Gammaproteobacteria	rDsr (Anantharaman <i>et al.</i> 2018)
<i>Chromatiaceae</i>	Gammaproteobacteria	rDsr (Lavy <i>et al.</i> 2018)
<i>Sulfuriflexus</i>	Gammaproteobacteria	rDsr (Kojima and Fukui 2016)
<i>Thiohalobacter</i>	Gammaproteobacteria	rDsr (Tsallagov <i>et al.</i> 2019)
Unclassified Symbionts	Gammaproteobacteria	rDsr (König <i>et al.</i> 2017)
Alteromonadales	Gammaproteobacteria	rDsr (Lavy <i>et al.</i> 2018)
<i>Candidatus Marithrix</i> <i>sp.</i>	Gammaproteobacteria	rDsr (Salman-Carvalho <i>et al.</i> 2016)
<i>Sedimenticola</i>	Gammaproteobacteria	rDsr (Petersen <i>et al.</i> 2016)
<i>Desulfovibrio</i>	Deltaproteobacteria	Dsr (Anantharaman <i>et al.</i> 2018)
<i>Desulfobacter</i>	Deltaproteobacteria	Dsr (Anantharaman <i>et al.</i> 2018)
Unclassified Deltaproteobacteria	Deltaproteobacteria	Dsr (Anantharaman <i>et al.</i> 2018)
Desulfovibrionales	Deltaproteobacteria	Dsr (Wang <i>et al.</i> 2015)
<i>Desulfobacteraceae</i>	Deltaproteobacteria	Dsr (Anantharaman <i>et al.</i> 2018)
Desulfobacterales	Deltaproteobacteria	Dsr (Wang <i>et al.</i> 2015)
<i>Desulfobulbus</i>	Deltaproteobacteria	Dsr (Anantharaman <i>et al.</i> 2018)
<i>Desulfampus</i>	Deltaproteobacteria	Dsr (Anantharaman <i>et al.</i> 2018)
<i>Desulfonatronum</i>	Deltaproteobacteria	Dsr (Anantharaman <i>et al.</i> 2018)
<i>Desulfobacterium</i>	Deltaproteobacteria	Dsr (Anantharaman <i>et al.</i> 2018)

### 3.3.4. Taxonomy of SRB Associated with the *dsrC* Gene

Assessing the taxa responsible for sulfur reduction via the Dsr pathway revealed that one taxonomic group of SRB, Deltaproteobacteria, was responsible for the majority

of reads (Figure 3.7). There were higher reads of Deltaproteobacteria in the cage sediments pre-fallowing, that decreased during fallowing, when reads became to those seen in the buoy sediments (Figure 3.7). In pre-fallowing buoy samples, B3 sediments showed more Deltaproteobacteria than B2, though not at the high levels seen in cage sediments (Figure 3.7). The spike in reads seen in the March 2019 B2 sediments (Figure 3.7), is reflective of the results seen in the unstratified gene numbers (Figure 3.4).

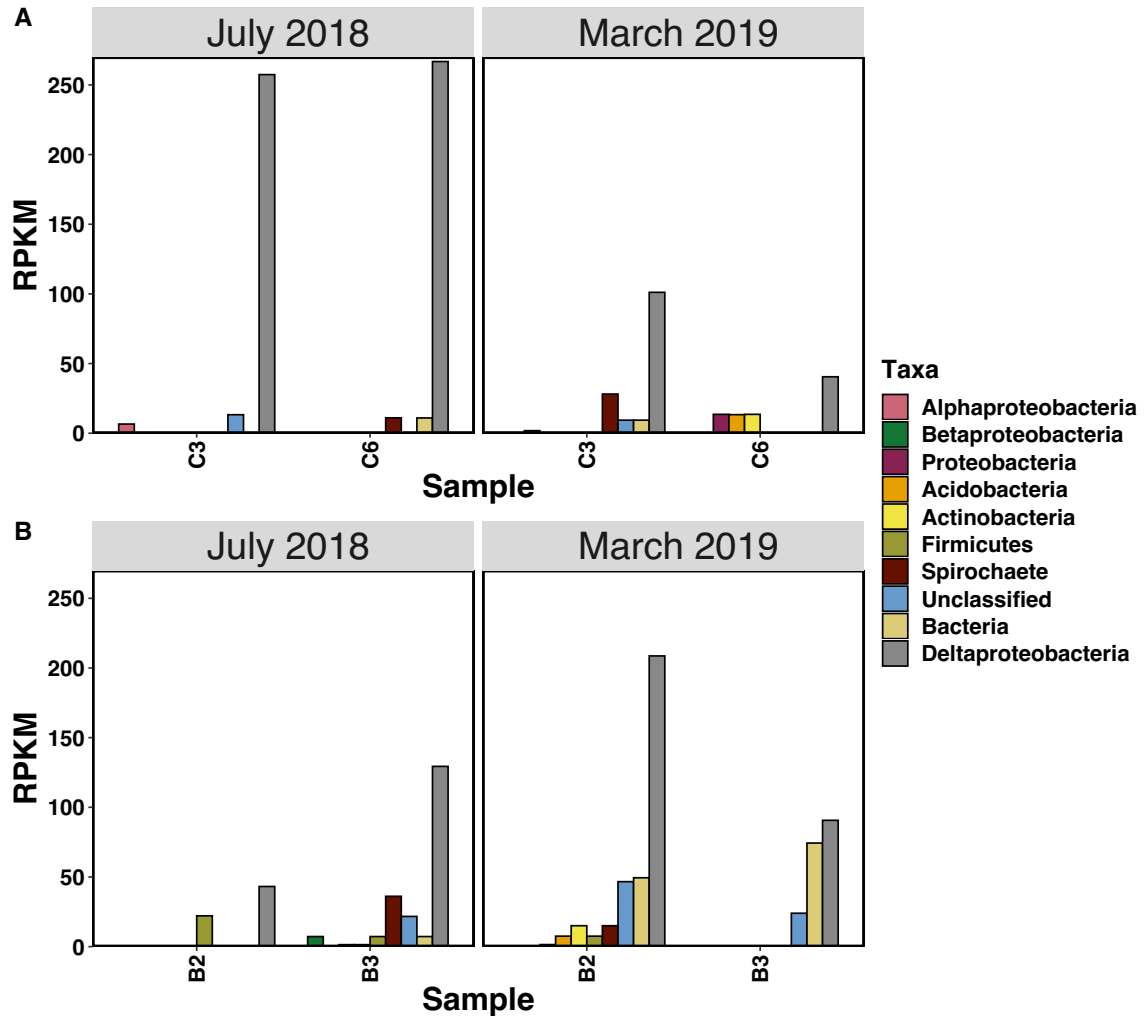


**Figure 3.7: Reads per kilobase million (RPKM) of the *dsrC* gene for sulfur reduction separated by taxonomy before (July 2018) and during (March 2019) following in the A) cage sediments and B) buoy sediments. Reads are separated into reads per phylum aside from Proteobacteria which, when possible, were separated into the different classes due to abundance compared to other phyla.**

Within the top 10 Deltaproteobacteria present, there was a fairly even relative abundance of the taxa when they were present in samples (Figure S13). The pre-fallowing C3 sediments were an exception and showed a high read count and relative abundance of *Desulfobacter* not seen in other samples (Figure 3.8, Figure S13). This dominance of *Desulfobacter* disappeared during fallowing; however, the sample was still dominated by *Desulfovibrio* and Desulfovibrionales (Figure 3.8). As well, C6 sediment pre-fallowing

contained only 2 taxa: Unclassified Deltaproteobacteria and *Desulfobacter* (Figure 3.8).

Interestingly, pre-fallowing B2 sediments did not contain any of the top 10

Deltaproteobacteria taxa (Figure 3.8).

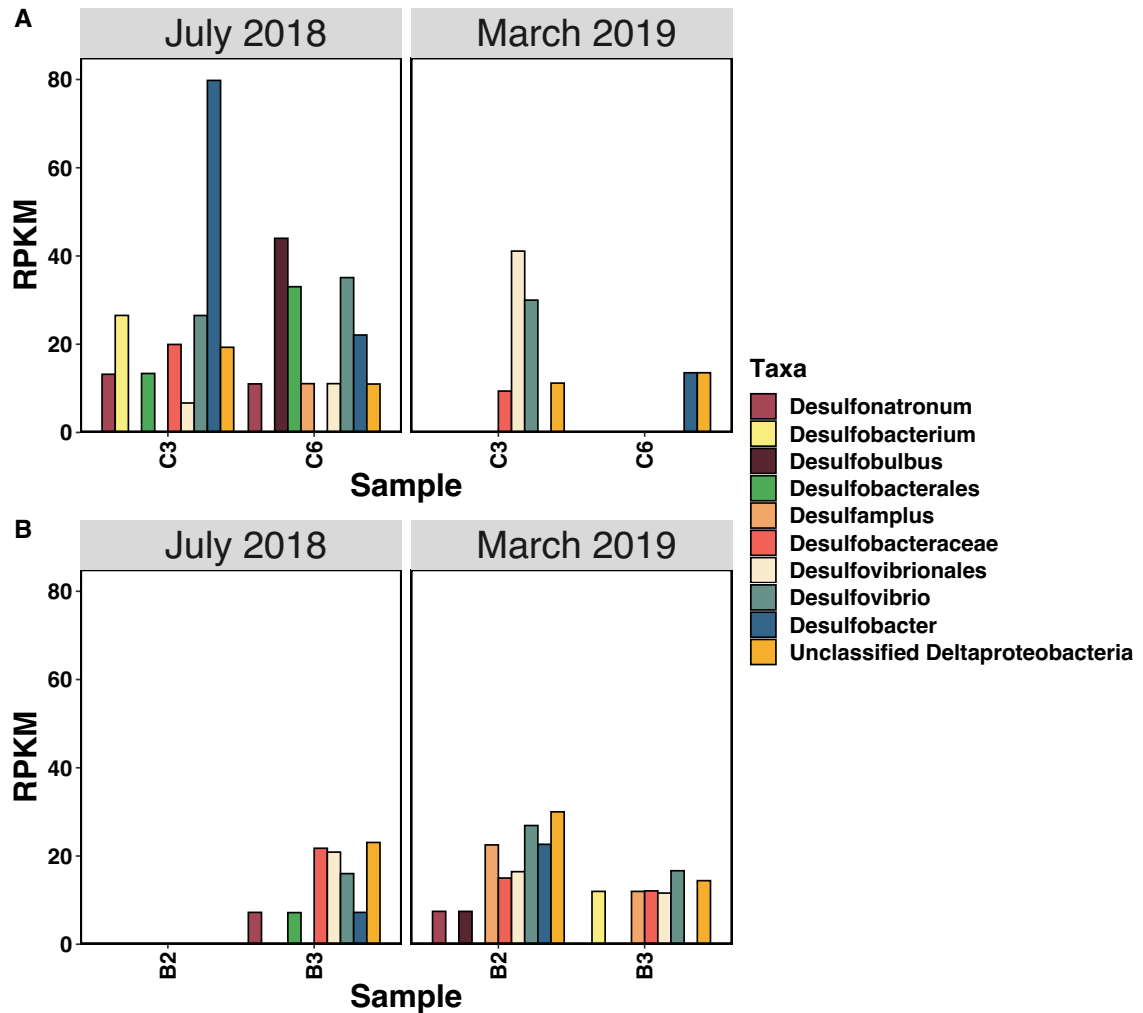


**Figure 3.8: Reads per kilobase million (RPKM) of Top 10 most abundant Deltaproteobacteria taxa that have the ability to perform sulfur reduction via the *dsrC* gene before (July 2018) and during (March 2019) fallowing in the A) cage sediments and B) buoy sediments. Reads are separated into the lowest taxonomy level possible from the stratified table. References supporting that these taxa are sulfur reducers are listed in Table 3.1.**

### 3.3.5. Taxonomy of SOB Associated with the *soxB* Gene

Unlike the *dsrC* gene, a taxa breakdown of the *soxB* genes present does not show a definitive pattern of one taxon dominating in the samples. Instead, it seems both Alpha and Gammaproteobacteria were the taxa with the highest relative abundance (Figure 3.9). There were fewer reads in the sediments below the cages in the pre-fallowing sediments, with the exceptions of higher Alphaproteobacteria reads and relative abundance in the C6 sediment, and a high number of Epsilonproteobacteria reads in the C3 sediment where it was the most relatively abundant taxa (Figure 3.9, Figure S14). Further investigation shows this spike in Epsilonproteobacteria was due to a large number of *Arcobacter* in that particular sample.

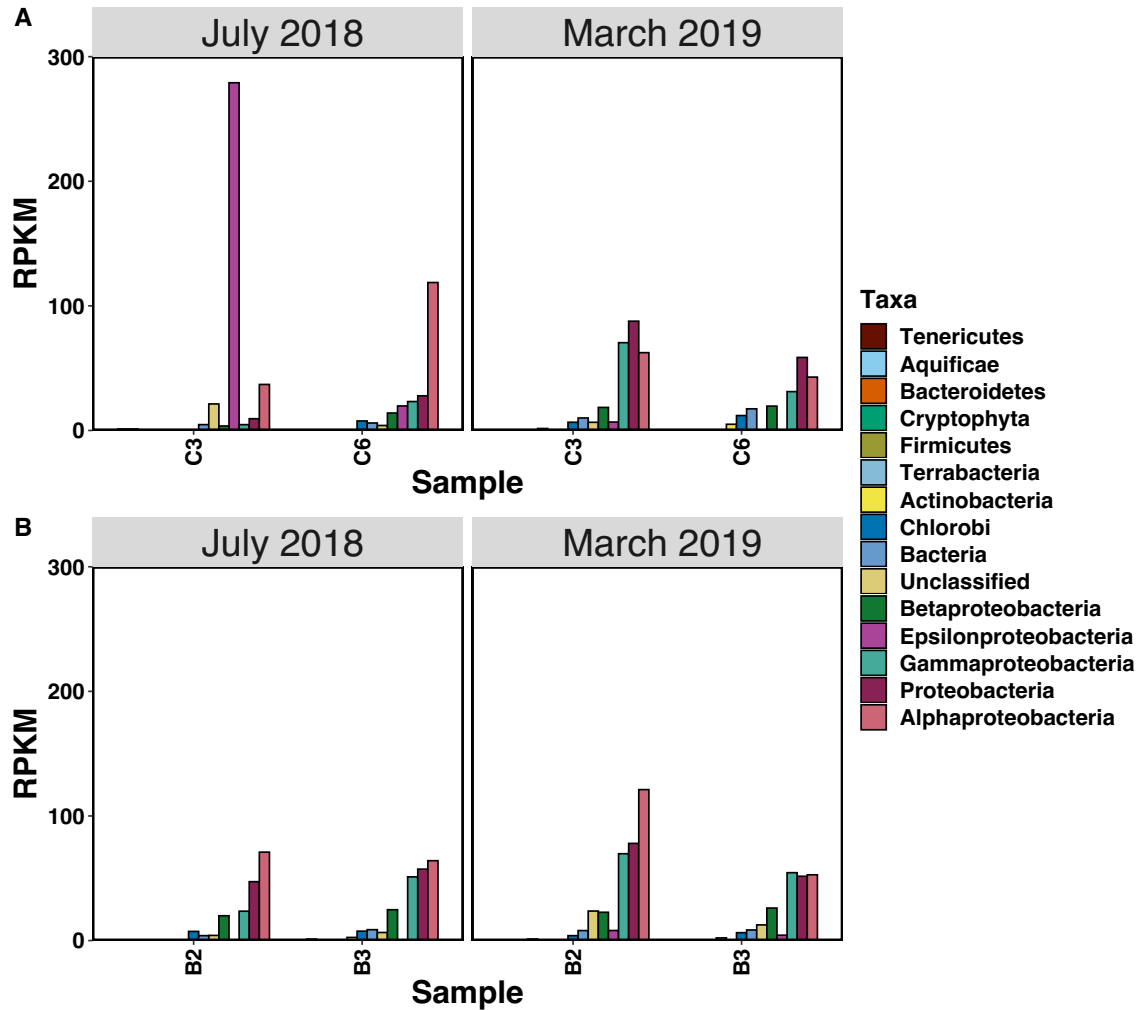


**Figure 3.9: Reads per kilobase million (RPKM) of the *soxB* gene separated by taxonomy before (July 2018) and during (March 2019) following in the A) cage sediments and B) buoy sediments. Reads are separated into reads per phylum aside from Proteobacteria which, when possible, were separated into the different classes due to abundance compared to other phyla.**

Breakdown of the top 10 most abundant Alphaproteobacteria showed that the majority of the *soxB* genes for this class were from *Rhodobacteraceae*, with higher relative abundance in July 2018 C6 and March 2019 B2 sediments (Figure 3.1, Figure S15).

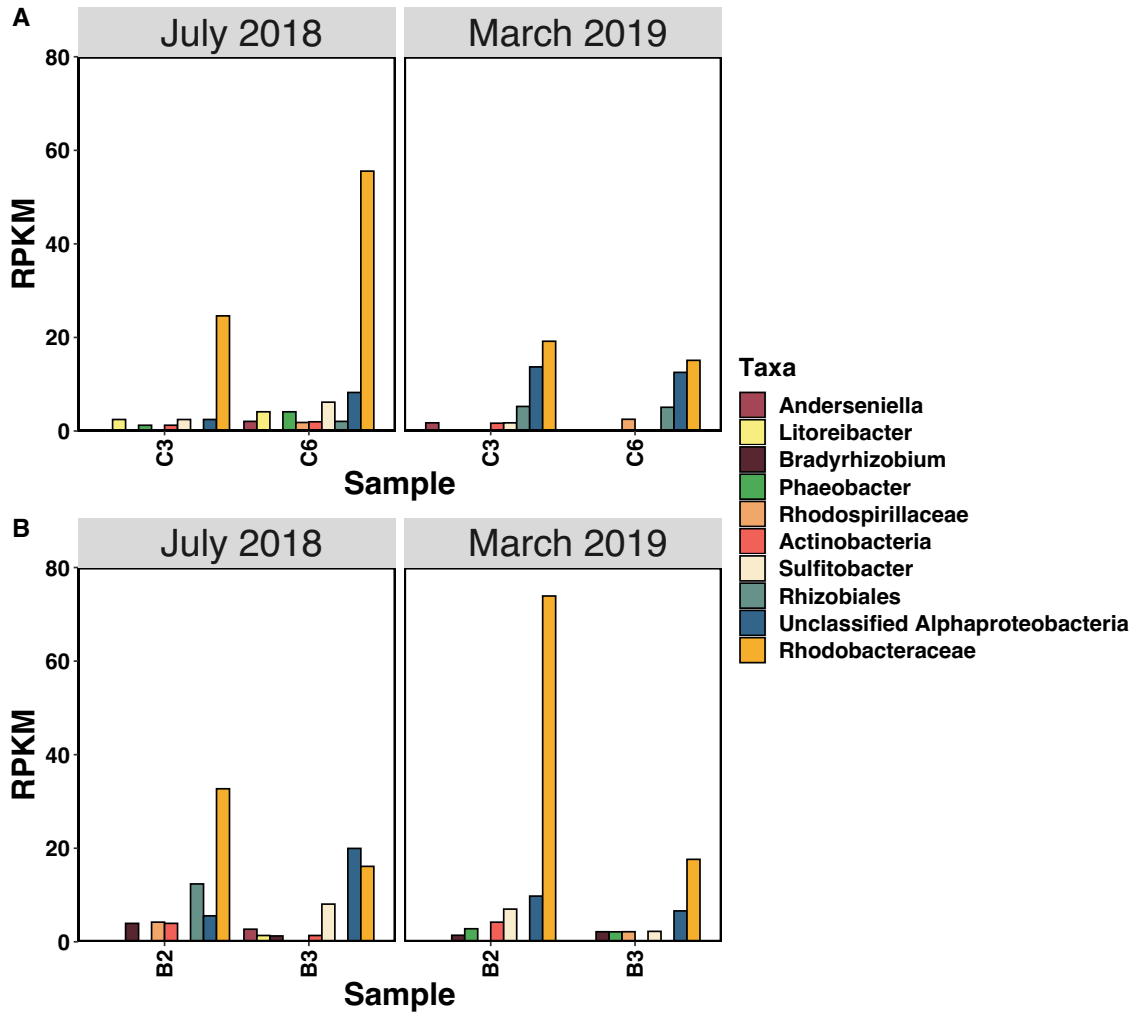


**Figure 3.10: Reads per kilobase million (RPKM) of Top 10 most abundant Alphaproteobacteria taxa that have the ability to perform sulfur oxidation via the *soxB* gene before (July 2018) and during (March 2019) following in the A) cage sediments and B) buoy sediments. Reads are separated into the lowest taxonomy level possible from the stratified table.**

The majority of the Gammaproteobacteria reads came from unclassified Gammaproteobacteria, though overall numbers were quite low (Figure 3.11). Like the *rdsrC* (Figure 3.6), the lowest number of *soxB* reads for Gammaproteobacteria was found in the pre-fallowing sediments, particularly the C3 sediments where there was only one of the top 10 taxa found: *Piscirickettsiaceae* (Figure 3.11). Interestingly, the number of raw reads as well as relative abundance of Unclassified Gammaproteobacteria *soxB* genes

was much lower in mid-fallowing C6 samples compared to the rest of the mid-fallowing samples (Figure 3.11, Figure S16). As well, although there was a noticeable increase in Unclassified Gammaproteobacteria reads in both buoy samples between July 2018 and March 2019 (Figure 3.11), the relative abundance of these reads did not change as noticeably (Figure S16). Lastly, 3 of the top 10 Gammaproteobacteria (*Chromatiales*, *Thioalkalivibrio*, Unclassified Gammaproteobacteria) were also in the *rdsrC* gene top 10 most abundant Gammaproteobacteria (Figure 3.6), indicating that these taxa may perform sulfur oxidation through both pathways.

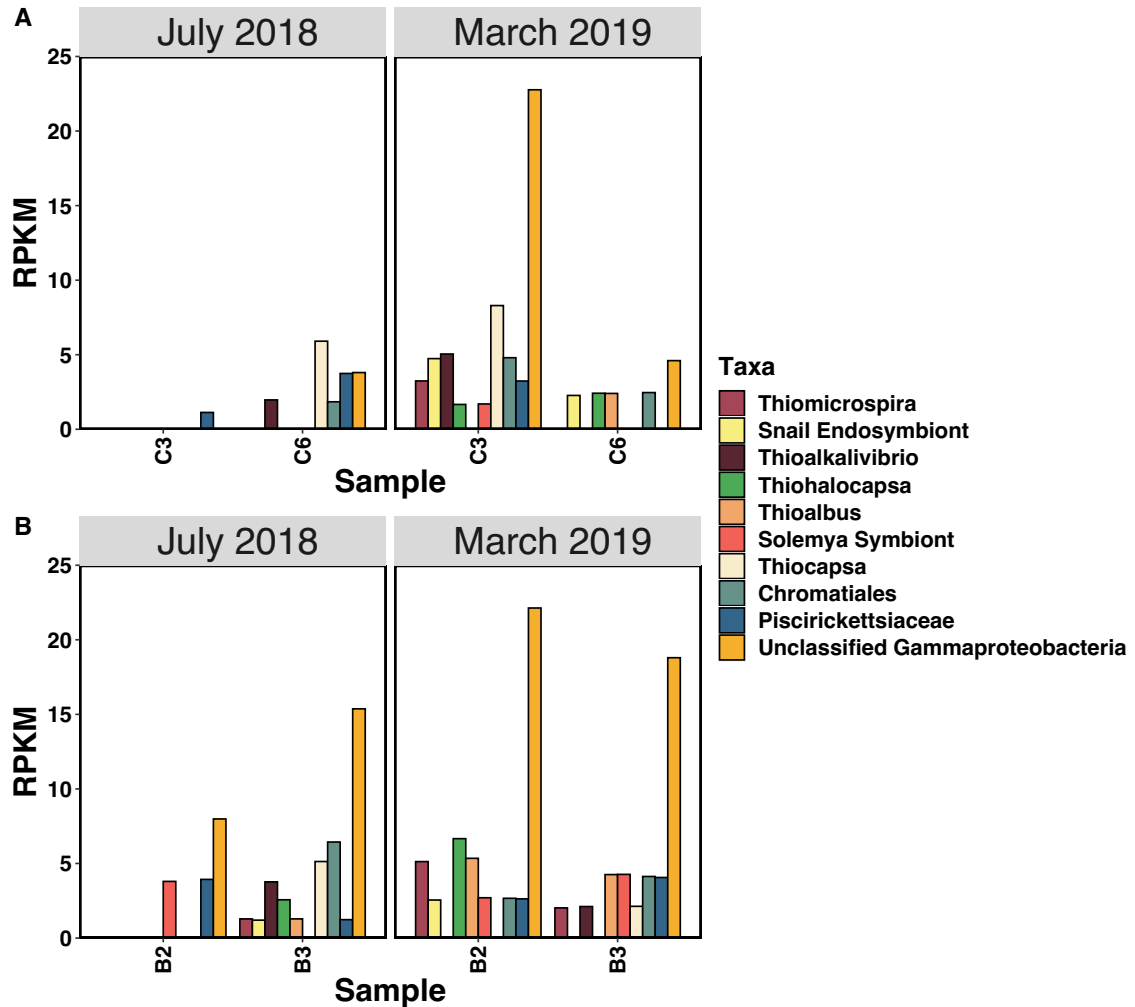


**Figure 3.11: Reads per kilobase million (RPKM) of Top 10 most abundant Gammaproteobacteria taxa that have the ability to perform sulfur oxidation via the *soxB* gene before (July 2018) and during (March 2019) following in the A) cage sediments and B) buoy sediments. Reads are separated into the lowest taxonomy level possible from the stratified table.**

### 3.4. DISCUSSION

#### 3.4.1. Metagenomic Results Relating back to Amplicon Sequencing

Overall, results show that Gammaproteobacteria and Deltaproteobacteria were the dominant sulfur cycling bacteria in the sediments at this aquaculture site. This reinforces the data found in the 16S amplicon sequencing, where many families with high relative abundance and potential bacterial indicators were from these two taxonomic classes (Figure 2.10, Figure 2.13, Figure S5, Figure S6). Although there was some overlap in the taxa identified from the metagenomic data and the amplicon sequencing data, there were important genera identified through metagenomics that were not resolved to the class or family level in the 16S amplicon data. These observations point out the additional benefit of metagenomic shotgun sequencing when targeting taxonomic groups involved in specific metabolic function such as sulfur metabolizing bacteria. Metagenomic data can provide a better taxonomic resolution, and more insight into which microbes are driving the sulfur cycle.

#### 3.4.2. SOB and SRB Identified Through the Dsr Pathway

Overall, the *dsrC* and *rdsrC* genes appear to be the genes whose presence was more affected by farm activity, compared to the *soxB* gene. Pre-fallowing farm sediments were characterized by much lower amounts of *rdsrC* and slightly elevated *dsrC*. In comparison, buoy sediments on the same day showed much higher levels of *rdsrC*. This pattern could also indicate low oxygen levels in the sediment under the cages, as sulfur reduction is an anoxic process (Pereira *et al.* 2011).

Unsurprisingly there was some variability among the pre-fallowing stations. Station C6 had a slightly higher abundance of *rdsrC* compared to C3, though not as high

as the buoy stations. This is likely due to the location of C6 the farm near the open ocean. As seen in Chapter 2, the sediments under the cages at the seaward end of the farm have a different microbial composition as determined by 16S amplicon sequencing, likely caused by the oxygenated water of the incoming tide (Burke *et al.* 2020) influencing the sediment surface in this shallow, but dynamic, coastal environment. In this case, the increased reads of *rdsrC* could be attributed to more aerobic SOB being present, due to the increased flushing with oxygenated water at each tidal cycle, in comparison with the C3 cages that are in the middle of the farm (Figure 3.2).

Similarly, in the buoy samples, station B3 had a higher level of *dsrC* compared to the other buoy station. This was likely because B3 was just off the middle of the farm and was more likely to be affected by the farm than the farther away B2 station. However, there was also a corresponding increase in *rdsrC* at B3, indicating that sediments were perhaps not experiencing low oxygen levels as might have been the case at cage sites directly on the farm. Overall, these results reinforce the important role of water circulation and farm orientation in determining how the farm will affect the benthic environment.

Deltaproteobacteria were the dominant SRB in all sediment samples and *Desulfobacter* in particular was elevated in the pre-fallowing farm sediments. The family that this genus belongs to was also seen to be a potential biomarker in the 16S amplicon sequencing data (Figure 2.10) and is known to be abundant in sediment under fish cages (Moncada *et al.* 2019).

Cage sediments during fallowing showed the opposite pattern as those from before fallowing with higher counts of *rdsrC* and fewer counts of *dsrC*, indicating that there may be some level of environmental recovery of the benthic communities occurring.

Further evidence of recovery through fallowing in the benthic communities below the cages was provided by the relative proportion of *rdsrC* and *dsrC* genes closer to that of the buoy samples. This pattern can also be seen in the 16S amplicon data where, in the same cage samples, there was a higher relative abundance of Deltaproteobacteria vs Gammaproteobacteria before fallowing, while in samples during fallowing, the ratio was more similar to the buoy samples (Figure S2). Interestingly, there is a higher amount of *dsrC* and *soxB* in the B2 mid-fallowing sediments that is unexplained.

Gammaproteobacteria were the drivers of Dsr sulfur oxidation, which is not surprising as the class consists of many known sulfur oxidizers including the purple sulfur bacteria, which can form mats on the surface of sediments, or perform chemolithotrophy in dark environments using sulfide or thiosulfide oxidation (Anantharaman *et al.* 2018, Hubas *et al.* 2013). In particular, the order Chromatiales, specifically the member *Thioalkalivibrio* appeared to be promising bioindicators of recovering or healthier sediments in the environment for this study. This has also been seen in other studies where various members of Chromatiales (*Thiotrichales*, *Thioalbus*, *Thioalkalivibrio* and *Thiohalomonas*) have been the dominant SOB affiliated with aquaculture farm sediment (Asami *et al.* 2005, Choi *et al.* 2018).

It should be noted that although there is a deep phylogenetic split between SOB and SRB *dsrC* genes (Crane 2019, Venceslau *et al.* 2014), it has recently been discovered that this distinction cannot always determine whether an organism will oxidize or reduce sulfur (Crane 2019). A recent study by Thorup *et al.* (2017) was the first to demonstrate an organism with (apparent) reductive *dsr* genes performing as a sulfur oxidizer (Crane 2019). Therefore, while metagenomics is a valid technique for investigating taxonomy and which organisms have apparent reductive vs oxidative *dsr* genes, care should be

taken when correlating presence of organisms and their activity in the environment (Crane 2019).

#### 3.4.3. SOB Identified Through the Sox Pathway

The overall amount of *soxB* present in samples did not vary as much as the *dsrC* and *rdsrC* genes, indicating that it was not as affected by fallowing. However, *soxB* was the dominant sulfur oxidation gene found in C3 sediments before fallowing as marked by a sharp increase in Epsilonproteobacteria, a class of Proteobacteria that plays a significant role in sulfur oxidation in highly sulfidic fish farm sediments (Choi *et al.* 2018). This further lends evidence to sub/anoxic sediments because while Gammaproteobacteria have an advantage when oxygen and sulfides are abundant, Epsilonproteobacteria are capable of the metabolic versatility needed to adapt to environments shifting from aerobic to anaerobic communities (Choi *et al.* 2018), and often live at the oxic/anoxic interface (Campbell *et al.* 2006).

The genus *Arcobacter* in particular contains diverse species from a wide variety of habitats and metabolisms, many of which originate from marine environments with an oxygen-sulfide chemocline (Campbell *et al.* 2006). Therefore, the presence of *soxB* genes from this genus could be used as a bioindicator for organic loading in sediments.

### 3.5. CONCLUSIONS

In conclusion, shotgun metagenomic sequencing of eDNA was used to further investigate taxa associated with genes involved in the sulfur cycle in the sediment environment under fish cages before and during fallowing. These results provided further

evidence that *Desulfobacter*, a bacterial genus discovered in the 16S amplicon sequencing, would be a good indicator organism, and also identified other genera (*Thioalkalivibrio* and *Arcobacter*) that have potential as indicator bacteria. As well, it was shown that *dsrC* and *rdsrC* genes followed a pattern of fewer reads of *rdsrC* and more reads of *dsrC* genes in cage sediments before fallowing, and the opposite pattern mid fallowing. *soxB* was present in all samples though did not show any patterns with respect to fallowing. While the presence of a functional gene does not necessarily reflect actual enzyme activity in the environment, the results of this study identify promising potential gene markers linked to their taxonomic assignment for further identifying and monitoring of environmentally important bacteria, which can be used in future eDNA environmental monitoring programs in Nova Scotia.

# **CHAPTER 4: EVALUATION OF QPCR ASSAYS FOR QUANTIFICATION OF *ALEXANDRIUM SP.* IN THE SEDIMENT SURROUNDING FINFISH AQUACULTURE IN SHELBURNE, NOVA SCOTIA**

## **4.1. INTRODUCTION**

### *4.1.1. Effect of HABs on Aquaculture in the North Atlantic*

Harmful algal species mainly belonging to cyanobacteria and dinoflagellates can produce a variety of biotoxins, and at high cell density can form harmful algal blooms (HABs). Increasing use of coastal marine environments for finfish aquaculture globally has led to an increased awareness of HABs and how they affect the farms both directly and indirectly (Hallegraeff 2002, Rensel and Whyte 2002). Algal blooms in general can directly harm fish in a number of ways, one of the most common being gill damage or irritation which can lead to excess mucus production and subsequent bacterial infection (Rensel and Whyte 2002). However, HABs can also cause toxigenic effects, blood hypoxia from depleted oxygen, and gas bubble trauma from oxygen supersaturation (Rensel and Whyte 2002). Indirect effects may occur when, despite no fish die offs, a bloom renders the farm unsafe for humans, leading to temporary closures (Anderson *et al.* 2000). Therefore, harmful algae have the potential to cause huge economic loss, as seen in the 80's and 90's when losses in British Columbia amounted up to 35 million USD due to *Heterosigma akashiwo* and *Chaetoceros sp.* (Rensel and Whyte 2002).

In the North Atlantic, the most prominent species of harmful algae belong to the *Alexandrium* genus, within which several species can produce saxitoxin, the toxin responsible for paralytic shellfish poisoning (PSP). Yearly blooms of *Alexandrium* have occurred from the Gulf of Maine to the Bay of Fundy, and the cyst stage of *Alexandrium*, which is viable for many years, can accumulate in patches along the shallow eastern coastlines of the United States and Canada (Anderson *et al.* 2002). Toxic species of *Alexandrium* have been responsible for shellfish aquaculture closures as well as finfish die offs along these coastal regions (Anderson *et al.* 2000).

#### 4.1.2. Monitoring HABs

Predicting when a HAB will occur, whether from cyst germination or from transport of planktonic cells from other regions, is challenging for numerous reasons. *In situ* distributions of phytoplankton are typically not spatially uniform, and the presence of a HAB species does not mean it will bloom (Smayda 2002). As well, there is a large variability in the cycles and trends from year to year, and the absence of a HAB species one year does not prevent its reoccurrence in future years (Smayda 2002). Environmental triggers for blooms via cyst germination also differ among species and geographic locations. For example, *Alexandrium sp.* appear unaffected by coastal eutrophication, however other species such as *Karenia mikimotoi* and *Gonyaulax polygramma* appear to increase in abundance with increasing eutrophication, particularly cultural eutrophication (Hallegraeff 2002). For temperate species such as *Alexandrium sp.* the primary stimulus is generally a temperature shift (a decrease in temperature in the case of *Alexandrium*), along with an absolute oxygen requirement that must be met (Anderson *et al.* 2002).

Burial of cysts below the oxygen layer within sediments has been suggested as an explanation for the absence of germination and bloom formation with a temperature shift (Anderson *et al.* 2002).

Due to the difficulty in predicting HABs, many monitoring techniques are more reactive than proactive, responding to a bloom event by identifying the HAB species and testing the level of toxin production. Approaches employed to monitor HABs include HAB species identification and cell density estimation by light microscopy, fluorescently labelled molecular probes, or immunoassays which test the toxicity of a bloom (Franks and Keafer 2002). However, these approaches are often time consuming and expensive, with the added difficulty of finding purified toxins and stable immunogens from low molecular weight toxins like saxitoxin (Cembella *et al.* 2002a). Recently, the development of qPCR based molecular monitoring strategies has been proposed in order to implement an additional tool for more rapid detection of HAB during monitoring. Although primers and probes would still need to be developed for each species in the region of interest, qPCR has the added advantages that only a small sample is needed, and it can detect HAB species at low concentrations (Scholin *et al.* 2002). This is important as even low concentrations of cells ( $< 5 \times 10^2$  cells/L for *Alexandrium sp.*) can be toxic (Franks and Keafer 2002). It can also offer an alternative for monitoring of cysts in sediments because identification of cysts based on morphological characters is not always reliable (Anderson *et al.* 2002).

#### 4.1.3. qPCR Monitoring

Quantitative PCR (qPCR) has many advantages over conventional PCR for monitoring because it provides quantitative results in real time (Scholin *et al.* 2002). Typically for PCR of eukaryotes, the small ribosomal subunit (SSU) rRNA is amplified in order to distinguish between species. However, for harmful algae, in particular *Alexandrium sp.*, primers and probes need to be more specific than the species level, as each species is comprised of a series of distinct strains at the genetic level, with only specific strains able to produce saxitoxin (Scholin *et al.* 2002). Therefore, many studies have amplified the D1-D2 region of the large ribosomal subunit (LSU), as it is one of the most rapidly evolving regions of the eukaryotic rRNA genes, allowing for more accurate quantification at the strain level (Scholin *et al.* 2002, Walsh *et al.* 1998).

Another gene for which qPCR assays are being developed is the *sxtA4* gene within the saxitoxin biosynthesis pathway. This gene in particular was chosen because while all *Alexandrium* species have a version of the saxitoxin biosynthesis pathway, non-toxic strains have a shorter isomer containing *sxtA1-A3*, while toxic strains have the extra *sxtA4* domain (Murray *et al.* 2019). However, an advantage to this type of assay over the LSU is that it is not species specific and could be useful in regions where different species occupy the same area, particularly before a monospecific bloom occurs (Murray *et al.* 2019). It also has the potential to quantify new species or strains that would not be captured by the LSU assays (Murray *et al.* 2019).

The purpose of this study was to assess published D1-D2 LSU and *sxtA4* (simplified to LSU and sxt in this paper) qPCR assays (Murray *et al.* 2019) to quantify

the amount of potentially harmful *Alexandrium* cysts in the sediment surrounding two finfish aquaculture farms off the coast of Nova Scotia, Canada

## **MATERIALS AND METHODS**

### *4.2.1. Sample Collection*

The area chosen for this study is a Cooke Aquaculture facility outside of Shelburne, NS (Figure 4.1). The site houses 2 farms, Hartz Point (HP) and Sandy Point (SP), each with 9-10 cages of rainbow trout (*Onchorhynchus mykiss*), as well as an onsite barge for staff. Sampling occurred intermittently from July 2019 – November 2019 (Table S7). Due to the sheltered nature of these sites, anchor reference points were able to be taken farther away from the farm site.

Sediment samples were taken at sites both next to cages, at surrounding buoys, and at reference anchor sites according to Figure 4.1 (Table S7). 2ml sediment samples were taken in triplicate, when possible, using a van der veen grab and immediately frozen on deck in a cryoshipper primed by liquid nitrogen the previous day.

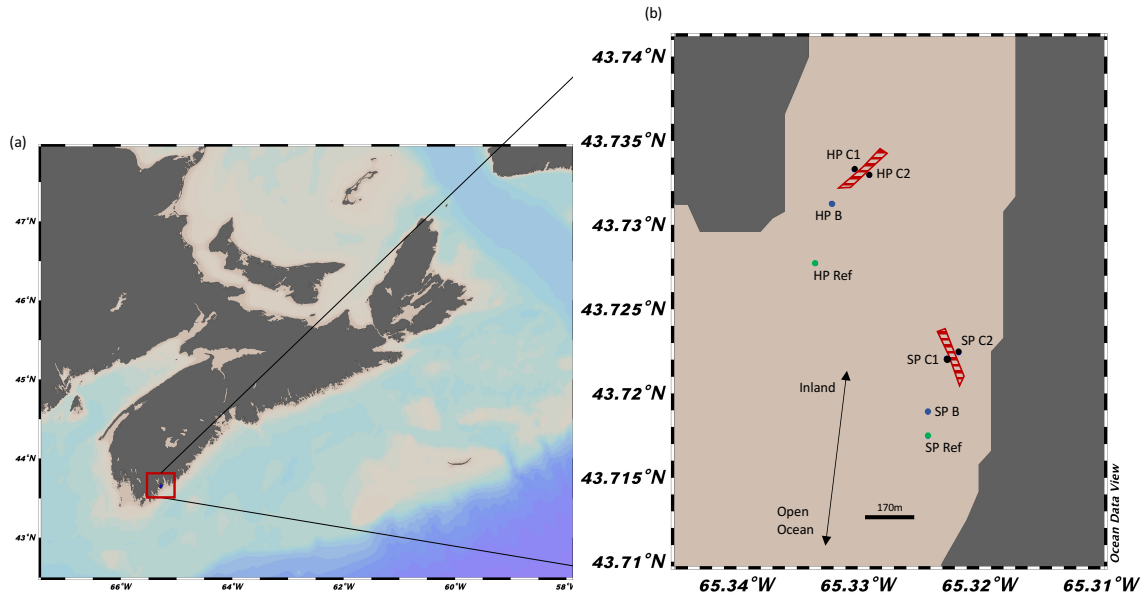


**Figure 4.1: Map of the sample areas (a) in relation to all of Nova Scotia and (b) close up of the farm areas, Hartz Point (HP) and Sandy Point (SP), indicated by red dashed lines, and sampling layout. In (b), stations beginning with C and marked by a black dot are cages, B and marked by a blue dot are farm buoys, and Ref represents off-site reference stations, marked by a green dot.**

#### 4.2.2. DNA Processing

DNA from both water and sediment samples was extracted, sequenced, and processed as described in Chapter 2.

#### 4.2.3. qPCR Optimization and Application

Primers for both LSU and sxt assays were described in Murray *et al.* (2019) (Table 4.1), and the qPCR protocol was adapted the same study. Initially 2X SYBR Green master mix (ThermoFisher Scientific) and 20,000 ng/ $\mu$ L BSA were diluted to 1X and 400 ng/ $\mu$ L final concentrations respectively per reaction. During the trials, the master mix was changed to PowerUp SYBR (ThermoFisher Scientific) as it is designed to prevent non-specific amplification (Table 4.2). Optimization of both assays was

performed through manipulation of primer concentrations, addition of BSA, and elongation time. Initial tests are reported in Table 4.2 and a full table of all optimization tests and parameters can be found in the supplemental material. Assays were run on Applied Biosystem's StepOnePlus system with the following conditions: 95°C for 10 minutes, 40 x 95°C for 15 seconds and 60°C for 30 seconds – 1 minute depending on trial (Table 6), followed by a melt curve analysis. Efficiency of assays was calculated from raw qPCR data using LinReg and gene copies were calculated using the standard curve.

**Table 4.1: LSU and *sxt44* qPCR primers from Murray *et al.* (2019).**

<b>Assay</b>	<b>Forward Primer</b>	<b>Reverse Primer</b>
LSU	5'GGCATTGGAATGCAAAGTG GGTGG 3'	5'GCAAGTGCAACACTCCCACCA AGCAA 3'
sxt	5' CTGAGCAAGGCGTTCAATC 3'	5' TACAGATMGGCCCTGTGARC 3'

**Table 4.2: Conditions for initial 2 optimization runs of each assay. Note: Only variables that differ amongst optimization runs are recorded in this table, mainly the concentration of primers, the addition of BSA and the elongation time.**

<b>Trial</b>	<b>Assay</b>	<b>Forward Primer Concentration (Final)</b>	<b>Reverse Primer Concentration (Final)</b>	<b>BSA</b>	<b>Elongation Time</b>
1	LSU	0.5 $\mu$ M	0.5 $\mu$ M	+	1 min
	sxt	0.5 $\mu$ M	0.5 $\mu$ M	+	1 min
2	LSU	0.5 $\mu$ M	0.5 $\mu$ M	+	30 sec
		0.025 $\mu$ M	0.025 $\mu$ M	+	30 sec
	sxt	0.5 $\mu$ M	0.5 $\mu$ M	+	30 sec
		0.025 $\mu$ M	0.025 $\mu$ M	+	30 sec
		0.5 $\mu$ M	0.5 $\mu$ M	-	30 sec
		0.025 $\mu$ M	0.025 $\mu$ M	-	30 sec

## 4.3. RESULTS

### 4.3.1. Initial Testing

Initial testing of the SYBR Green qPCR assays (Table 4.3) was performed using a dilution curve of a standard DNA molecule specific for each assay and the same primer concentration for both forward and reverse primers. After the first test of both assays, the LSU assay was shown to be 92% efficient, while the sxt was shown to be 86% efficient. The second trial was conducted in an attempt to increase the amplification efficiency of the assays. Assays were conducted with a range of forward and reverse primer

concentrations, elongation time, and presence/absence of BSA, which is generally added to our qPCR assays to reduce amplification inhibition. Wells with 0.025  $\mu\text{M}$  primers showed no amplification, while wells with 0.5  $\mu\text{M}$  primers yielded better results for the LSU assay (98% efficiency) but showed no improvement for the sxt assay (75% with BSA and 89% without BSA). After these initial runs, optimization was performed separately for each assay and despite the lower efficiency, BSA was kept in the sxt assay because it decreases amplification inhibition.

**Table 4.3: Primer combinations and the corresponding efficiencies for the first 2 tests of both assays. Primer concentrations recorded in this table are the stock concentrations.**

Trial	Assay	Forward Primer Concentration (Final)	Reverse Primer Concentration (Final)	BSA	Elongation Time	Efficiency
1	LSU	0.5 $\mu\text{M}$	0.5 $\mu\text{M}$	+	1 min	92%
	sxt	0.5 $\mu\text{M}$	0.5 $\mu\text{M}$	+	1 min	86%
2	LSU	0.5 $\mu\text{M}$	0.5 $\mu\text{M}$	+	30 sec	98%
		0.025 $\mu\text{M}$	0.025 $\mu\text{M}$	+	30 sec	-
	sxt	0.5 $\mu\text{M}$	0.5 $\mu\text{M}$	+	30 sec	75%
		0.025 $\mu\text{M}$	0.025 $\mu\text{M}$	+	30 sec	-
		0.5 $\mu\text{M}$	0.5 $\mu\text{M}$	-	30 sec	89%
		0.025 $\mu\text{M}$	0.025 $\mu\text{M}$	-	30 sec	-

#### 4.3.2. *sxtA4* Optimization

In the third test of the *sxt* assay, the concentration of the reverse primer was increased up to 4 times that of the forward primer in order to account for the degeneracy in the reverse primer (Table S9). Following this, various ratios of forward to reverse primers were tested in order to optimize the efficiency (Table S10). As the reverse primer was degenerate, it always had a higher concentration relative to the forward primer. The combination that gave the highest percent efficiency being 200nM forward primer and 3000nM reverse primer (Table S10). The last test of the *sxt* assay ran the full standard curve with 200nM forward primer and 3000nM reverse primer, however in this run the efficiencies ranged from 24-91% with the average efficiency for the curve being 71.6%. The lowest efficiencies often corresponded to the lowest two concentrations in the standard curve (1 and 10 copies/ $\mu$ L).

#### 4.3.3. *LSU* Optimization

After the success of the *LSU* assay in the 2<sup>nd</sup> test, the samples were run for both farms along with the standard curve (Figure 4.2). Amplification occurred in the majority of samples, with only 6 out of 75 samples showing no amplification of the *LSU* gene (Table S15). The samples with the highest average gene copy number were July 2018 for Hartz Point [ $3.45 \times 10^9$ ] and October 2019 for Sandy point [ $2.49 \times 10^9$ ], while those with the lowest average gene copy number were from August 2019 for both Hartz [ $1.05 \times 10^9$ ] and Sandy [ $3.25 \times 10^9$ ]. However, the average efficiency was only 77.5% (Table S11).

To account for the high concentration of DNA in the sediment samples, the next trial involved a tenfold dilution of two of the samples (Figure S17). The resulting average

efficiencies were 84.3% for the standard curve and 88.4% for the samples, with the undiluted samples curves looking no different to the diluted except in copy numbers. It's important to note that the elongation time was increased to 1 minute as a recommended time for the new SYBR (Table S11).

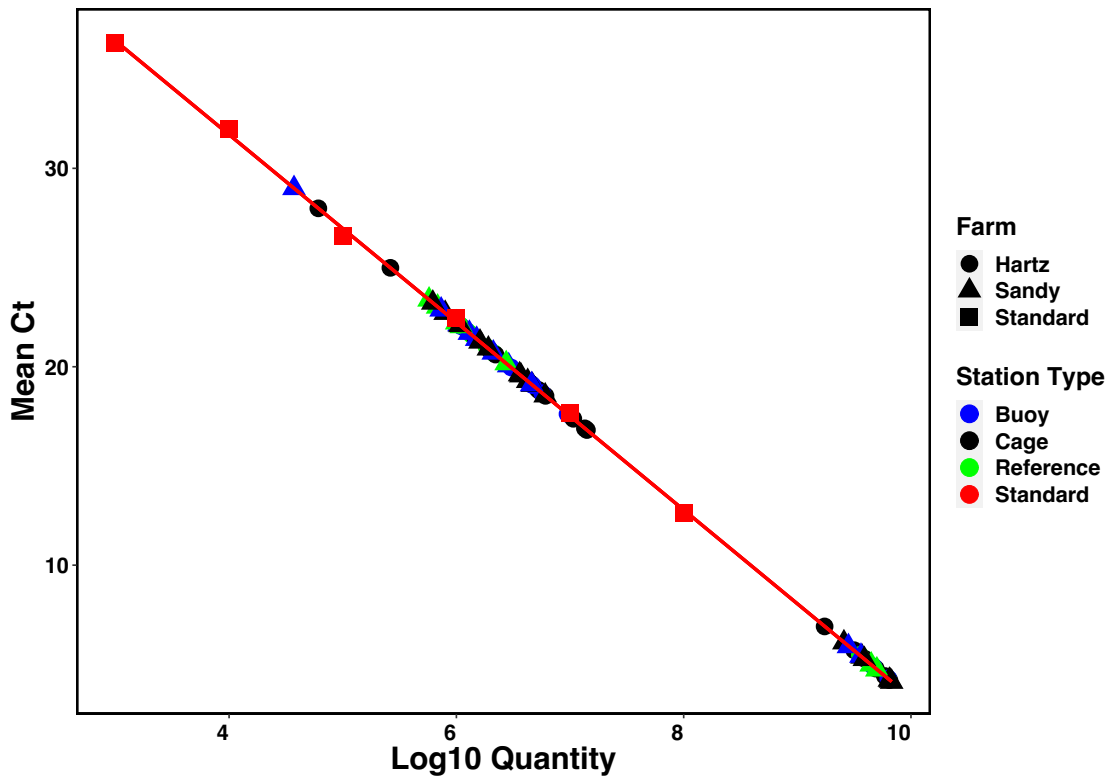


**Figure 4.2: Plot of the mean Ct values against the  $\log_{10}$  quantity of the standard curve for LSU assay test 3. The formula of the line of best fit ( $y = -4.7279x + 50.608$ ) was used to calculate the quantities in the samples from the Ct values.**

In order to try and get the efficiency back above 90%, the next two tests involved optimizing the primer concentration (Table S12, Table S13). The first primer optimization used concentrations recommended in the instructions from the SYBR manufacturer and yielded efficiencies ranging from 82.7% - 86.35% with the highest efficiency being the reactions with 800 nM forward primer and 300 nM reverse primer.

An additional test was carried out by increasing the forward primer to 1000 nM. Resulting efficiencies ranged from 84.05% - 87.25%, the highest efficiency being the 1000 nM forward and 800 nM reverse primer combination. Lastly, a run was done with the original 500 nM primer concentrations and the new 1000 nM/800 nM concentrations from the previous run with an elongation time down to 30 seconds, as was the original time (Table S14). Results from this showed an 83.2% efficiency for the 500 nM primer concentrations and an 86.9% efficiency for the 1000 nM/800 nM combination. Tables outlining each primer concentration and their efficiencies can be found in the supplemental material.

#### **4.4. DISCUSSION**

In the few runs that included samples, amplification of the *Alexandrium* D1-D2 region of the LSU was detected in the majority of sediments around the Hartz and Sandy Point farms including the reference sites away from the farms, indicating that the dinoflagellate may be endemic to the area and its presence is unlikely to be caused by the aquaculture farm. The presence of *Alexandrium* is not surprising as it has been well documented to occur in the North Atlantic around the Gulf of Maine and Bay of Fundy areas in both planktonic and cyst resting stages (Anderson *et al.* 2014). In particular, fish farms in the bay sampled for this study have had issues with *Alexandrium* blooms in the past (Cembella *et al.* 2002b). The farms sampled in this study are located in a sheltered, inland coastal setting over a soft, muddy bottom, characteristics known to favour *Alexandrium* cysts (Richlen *et al.* 2014). Despite these promising results that show the presence of *Alexandrium*, the difficulties encountered in optimization of both assays to

the MIQE standards (Bustin *et al.* 2009) indicate that the results provide initial estimates in terms of quantification, that will need to be further verified once the assays are performing more reproducibly.

Moving forward, there are issues that will be addressed in order to obtain a reliable assay for quantification of gene copy numbers in a sample. Additional primer optimization should be conducted with fresh primer and standard working stocks, reducing freeze-thaw cycles of primers and standards. In the case of the *sxtA4* assay, the degeneracy of the reverse primer may be causing the low efficiency, particularly the degenerate base near the 3' end of the primer. This is because in order for the polymerase to build a nucleotide chain, the 3' end of the primer has to bind securely to the DNA. Therefore, a review of the primer design may improve the assay overall, given that the presence of the 3' end degeneracy is not ideal. Lastly, Taqman assays are more specific than SYBR green assays and if the assays are re-designed, a Taqman assay may be considered instead of the SYBR assay.

#### **4.5. CONCLUSIONS**

In conclusion, the LSU assay demonstrated that *Alexandrium* is present in the sediment at the Hartz and Sandy Point farms, reinforcing both the amplicon sequencing results and the use of qPCR in monitoring HABs. However, these results also demonstrate the need for testing and developing specific primers to optimize the assays in order to obtain reliable quantifications.

## CHAPTER 5: CONCLUSIONS

Monitoring of the environment has become a focal point over the years with the expansion of open water aquaculture across the world. In particular, advances in DNA sequencing technology have led to the investigation of using eDNA to monitor the benthos under aquaculture farms in order to mitigate some of the pitfalls of traditional biological monitoring methods. The work described in this thesis demonstrates the potential of eDNA for monitoring multiple aspects of the environment around a fish farm outside of Shelburne, Nova Scotia.

In Chapter 2, I used amplicon sequencing of eDNA to track the changes in microbial and meiofaunal communities of both planktonic and benthic communities at the farm. Results show that changes in the planktonic communities were observed in the coastal waters at and near the farm location, and that seasonal changes dominated over changes due to the farm. In contrast, benthic communities were more affected by farm presence. Results from benthic meiofaunal and microbial communities also reinforce how farm orientation in respect to water/tidal flow is an important factor when addressing farm effect on the environment. Lastly, eDNA was able to show that sediment communities did change during the fallowing period and appeared to undergo a level of recovery. Through this, a few key organisms were identified as potential bioindicators for this site, including nematode worms and sulfur respiring bacteria.

Chapter 3 entailed the use of shotgun metagenomics, and results indicate that, overall, the benthos had a consistent composition of metabolic pathway types, though relative abundance of individual pathways varied, as seen in the nitrogen metabolism pathways. Results regarding the sulfur cycle show that the Dsr pathway was the sulfur

metabolizing pathway that was affected most by fallowing, while the Sox pathway did not show a similar pattern. Metagenomic results also provided better taxonomic resolution of sulfur metabolizing bacteria, and through this reinforced a potential indicator bacterium discovered in the 16S amplicon sequencing and uncovered others as well.

The last chapter, Chapter 4, demonstrated a practical approach to monitoring with eDNA could be used on fish farms that is different from the first two chapters: monitoring for potentially harmful organisms and pathogens. This research investigated the use of qPCR to quantify the potentially harmful algae *Alexandrium* on two fish farms further inland, but in the same bay as the farm discussed in the first two chapters. Of the two assays used, (LSU and sxt) results were informative only for the LSU qPCR assay and confirmed the presence of *Alexandrium* in the sediments. However, the efficiencies on both assays were lower than the accepted MIQE standards (Bustin *et al.* 2009) for determining the reliability and applicability of a qPCR assay, and therefore will need to be re-assessed in order to get reliable quantification.

Although each approach described in this thesis has the capability to be used for monitoring the environment around an aquaculture farm, there are situations when using one technique may be more advantageous than the others. For example, while shotgun metagenomics was able to identify more bacteria down to the genus level and monitor specific sulfur cycling genes, it is more expensive than amplicon sequencing and not as effective at identifying eukaryotes. Therefore, if the goal is to take many samples and focus on the community as a whole, including eukaryotes, amplicon sequencing may be the better choice. As well, qPCR involves a lot of work in advance to develop primers and probes and is therefore better suited to instances when knowing the absolute abundance instead of relative abundance is important. This could include the monitoring of HABs as

described in this thesis, or other harmful organisms such as sea lice or bacterial fish pathogens. While each technique has its advantages and disadvantages depending on the monitoring needs, overall, results from all chapters demonstrate the potential for eDNA to be used in many capacities on coastal aquaculture farms and it is the hope that, with continued research, eDNA can streamline and improve environmental monitoring and in the future help make aquaculture a more sustainable industry.

## REFERENCES

- Amir, A. *et al.* Deblur Rapidly Resolves Single-Nucleotide Community Sequence Patterns. *mSystems* 2. (2017).
- Anantharaman, K. *et al.* Expanded diversity of microbial groups that shape the dissimilatory sulfur cycle. *The ISME Journal* 12: 1715–1728 (2018).
- Anderson, D. M. Fukuyo, Y. & Matsouka, K. Cyst Methodologies. pp. 165-190. In, G.M. Hallegraeff, D.M. Anderson and A.D. Cembella [eds.] *Manual on Harmful Marine Microalgae*. IOC Manuals and Guides No. 11 UNESCO. (2002).
- Anderson, D. M., Hoagland, P., Kaoru, Y. & White, A. W. Estimated Annual Economic Impacts from Harmful Algal Blooms (HABs) in the United States. (2000). <https://apps.dtic.mil/docs/citations/ADA386861>.
- Andrews S. FastQC: a quality-control tool for high-throughput sequence data. Babraham Institute, Cambridge, United Kingdom. (2010). <http://www.bioinformatics.babraham.ac.uk/projects/fastqc/>.
- Antonella, P. & Luca, G. The quantitative real-time PCR applications in the monitoring of marine harmful algal bloom (HAB) species. *Environ Sci Pollut Res* 20: 6851–6862 (2013).
- Aquaculture Management Regulations - Fisheries and Coastal Resources Act (Nova Scotia). (2019). [https://novascotia.ca/just/regulations/regs/fcraquamgmt.htm#TOC3\\_1](https://novascotia.ca/just/regulations/regs/fcraquamgmt.htm#TOC3_1).
- Armstrong, E. G., Mersereau, J., Salvo, F., Hamoutene, D. & Dufour, S. C. Temporal change in the spatial distribution of visual organic enrichment indicators at aquaculture sites in Newfoundland, Canada. *Aquacult Int* (2019) doi:10.1007/s10499-019-00478-z.
- Asami, H., Aida, M. & Watanabe, K. Accelerated Sulfur Cycle in Coastal Marine Sediment beneath Areas of Intensive Shellfish Aquaculture. *AEM* 71: 2925–2933 (2005).
- Auguie B. gridExtra: Miscellaneous Functions for "Grid" Graphics. R package version 2.3. (2017). <https://CRAN.R-project.org/package=gridExtra>.
- Baillie, A.M., McGowan, C., May-McNally, S., Leggatt, R., Sutherland, B. J. G., Robinson, S. Environmental DNA and its applications to fisheries and oceans Canada: national needs and priorities. Canadian Technical Report of Fisheries and Aquatic Sciences 3329. Fisheries and Oceans Canada. (2019).
- Bastos Gomes, G. *et al.* Use of environmental DNA (eDNA) and water quality data to predict protozoan parasites outbreaks in fish farms. *Aquaculture* 479: 467–473 (2017).

Beentjes, K. K., Speksnijder, A. G. C. L., Schilthuizen, M., Hoogeveen, M. & Hoorn, B. B. van der. The effects of spatial and temporal replicate sampling on eDNA metabarcoding. *PeerJ* 7, e7335 (2019).

Bentzon-Tilia, M., Sonnenschein, E. C. & Gram, L. Monitoring and managing microbes in aquaculture - Towards a sustainable industry. *Microbial Biotechnology* 9: 576–584 (2016).

Black, K. D., Hansen, P. K. & Holmer, M. Salmon Aquaculture Dialogue Working Group Report on Benthic Impacts and Farm Siting. 55. (2008).

Boden, R. & Scott, K. M. Evaluation of the genus *Thiothrix* Winogradsky 1888 (Approved Lists 1980) emend. Aruga *et al.* 2002: reclassification of *Thiothrix disciformis* to *Thiolinea disciformis* gen. nov., comb. nov., and of *Thiothrix flexilis* to *Thiofilum flexile* gen. nov., comb. nov., with emended description of *Thiothrix*. *Int J Syst Evol Microbiol* 68: 2226–2239 (2018).

Bolyen E, Rideout JR, Dillon MR, *et al.* Reproducible, interactive, scalable and extensible microbiome data science using QIIME 2. *Nature Biotechnology* 37: 852–857. (2019) <https://doi.org/10.1038/s41587-019-0209-9>.

Bozo-Hurtado, L. *et al.* Identification of bacteria in enrichment cultures of sulfate reducers in the Cariaco Basin water column employing Denaturing Gradient Gel Electrophoresis of 16S ribosomal RNA gene fragments. *Aquat Biosyst* 9: 17 (2013).

Brunson, J. C. ggalluvial: Layered Grammar for Alluvial Plots. *Journal of Open-Source Software*, 5(49). 2017. (2020). <https://doi.org/10.21105/joss.02017>.

Burke, M., Grant, J., Filgueira, R. & Stone, T. Oceanographic processes control dissolved oxygen variability at a commercial Atlantic salmon farm: Application of a real-time sensor network. *Aquaculture* 736143. (2020). doi: 10.1016/j.aquaculture.2020.736143.

Bustin, S. A. *et al.* The MIQE Guidelines: Minimum Information for Publication of Quantitative Real-Time PCR Experiments. *Clin Chem* 55: 611–622 (2009).

Campbell, B. J., Engel, A. S., Porter, M. L. & Takai, K. The versatile  $\epsilon$ -proteobacteria: key players in sulphidic habitats. *Nature Reviews Microbiology* 4, 458–468 (2006).

Cao, H. *et al.* Microbial Sulfur Cycle in Two Hydrothermal Chimneys on the Southwest Indian Ridge. *mBio* 5, e00980-13 (2014).

Carroll, M. L., Cochrane, S., Fieler, R., Velvin, R. & White, P. Organic enrichment of sediments from salmon farming in Norway: environmental factors, management practices, and monitoring techniques. *Aquaculture* 226: 165–180 (2003).

Caspi, R. Altman, T. Billington. R, Dreher. K, Foerster. H, Fulcher. CA, Holland. TA, Keseler. IM, Kothari. A, Kubo. A, Krummenacker. M, Latendresse. M, Mueller. LA, Ong. Q, Paley. S, Subhraveti. P, Weaver. DS, Weerasinghe. D, Zhang P, and Karp, P.D. The MetaCyc Database of metabolic pathways and enzymes and the BioCyc collection of Pathway/Genome Databases *Nucleic Acids Research* 42(1): D459-D471. (2014).

Caspi, R. *et al.* The MetaCyc database of metabolic pathways and enzymes - a 2019 update. *Nucleic Acids Research* 48: D445–D453 (2020).

Cembella, A. D., Doucette, G. J. & Garthwrite, I. In vitro assays for phycotoxins. pp. 297-346. In, G.M. Hallegraeff, D.M. Anderson and A.D. Cembella [eds.] *Manual on Harmful Marine Microalgae*. IOC Manuals and Guides No. 11 UNESCO (2002a).

Cembella, A. D. *et al.* The toxigenic marine dinoflagellate *Alexandrium tamarense* as the probable cause of mortality of caged salmon in Nova Scotia. *Harmful Algae* 1: 313–325 (2002b).

Chen, W., Simpson, J., Levesque, C. A. RAM: R for Amplicon-Sequencing-Based Microbial-Ecology. R package version 1.2.1.7. (2018). URL: <https://cran.r-project.org/package=RAM>.

Choi, A. *et al.* Effects of finfish aquaculture on biogeochemistry and bacterial communities associated with sulfur cycles in highly sulfidic sediments. *Aquacult. Environ. Interact.* 10: 413–427 (2018).

Choi, A. *et al.* Impact of finfish aquaculture on biogeochemical processes in coastal ecosystems and elemental sulfur as a relevant proxy for assessing farming condition. *Marine Pollution Bulletin* 150: 110635 (2020).

Comeau, A. M., Douglas, G. M. & Langille, M. G. I. Microbiome Helper: a Custom and Streamlined Workflow for Microbiome Research. *mSystems* 2. (2017).

Comeau, A. M., Li, W. K. W., Tremblay, J.-É., Carmack, E. C. & Lovejoy, C. Arctic Ocean Microbial Community Structure before and after the 2007 Record Sea Ice Minimum. *PLOS ONE* 6: e27492 (2011).

Crane, E. J. Sulfur-dependent microbial lifestyles: deceptively flexible roles for biochemically versatile enzymes. *Current Opinion in Chemical Biology* 49: 139–145 (2019).

Dahl, C., Friedrich, C. & Kletzin, A. Sulfur Oxidation in Prokaryotes. in eLS (2008). doi:10.1002/9780470015902.a0021155.

Day, J., Chopin, T., Cooper, J. A. Comparative study of the aquaculture environmental monitoring programs for marine finfish in Canada and other jurisdictions: time to go beyond sediment related impact monitoring and consider appropriate tools for water column and ecosystem related impact monitoring. *Aquaculture Canada 2014 Proceedings of Contributed Papers*, Aquaculture Association of Canada. (2014).

De Caceres, M., Legendre, P. Associations between species and groups of sites: indices and statistical inference. *Ecology*. (2019). <http://sites.google.com/site/miqueldecaceres/>.

Dully, V. *et al.* Robustness, sensitivity and reproducibility of eDNA metabarcoding as an environmental biomonitoring tool in coastal salmon aquaculture – An inter-laboratory study. *Ecological Indicators* 107049. (2020). doi: 10.1016/j.ecolind.2020.107049.

Ewels, P., Magnusson, M., Lundin, S. & Källér, M. MultiQC: summarize analysis results for multiple tools and samples in a single report. *Bioinformatics* 32: 3047–3048 (2016).

Fernandes, T. F. *et al.* The scientific principles underlying the monitoring of the environmental impacts of aquaculture. *J. Appl. Ichthyol.* 17: 181-193. (2001).

Franks, P. J. S. & Keafer, A. Sampling techniques and strategies for coastal phytoplankton blooms. pp. 51-76. In, G.M. Hallegraeff, D.M. Anderson and A.D. Cembella [eds.] *Manual on Harmful Marine Microalgae*. IOC Manuals and Guides No. 11 UNESCO (2002).

Franzosa, E. A., McIver, L. J., Rahnavaard, G., Thompson, L. R., Schirmer, M., Weingart, G., Schwarzberg Lipson, K., Knight, R., Caporaso, J. G., Segata, N., Huttenhower, C. Species-level functional profiling of metagenomes and metatranscriptomes. *Nat Methods* 15: 962-968 (2018).

Fuhrman, J. A., Cram, J. A. & Needham, D. M. Marine microbial community dynamics and their ecological interpretation. *Nature Reviews Microbiology* 13: 133–146 (2015).

Garlapati, D., Charankumar, B., Ramu, K., Madeswaran, P. & Ramana Murthy, M. V. A review on the applications and recent advances in environmental DNA (eDNA) metagenomics. *Rev Environ Sci Biotechnol.* (2019). doi:10.1007/s11157-019-09501-4.

Garnier, S. viridis: Default Color Maps from matplotlib. R package version 0.5.1. (2018). <https://CRAN.R-project.org/package=viridis>

Glöckner, F. O. *et al.* 25 years of serving the community with ribosomal RNA gene reference databases and tools. *Journal of Biotechnology* 261: 169–176 (2017).

Goodwin, K. D. *et al.* DNA Sequencing as a Tool to Monitor Marine Ecological Status. *Frontiers in Marine Science* 4: 107 (2017).

Government of Canada, F. and O. C. Aquaculture statistics. (2013). <https://www.dfo-mpo.gc.ca/aquaculture/sector-secteur/stats-eng.htm>.

Government of Canada, F. and O. C. Aquaculture Activities Regulations guidance document. (2015a). <https://www.dfo-mpo.gc.ca/aquaculture/management-gestion/aar-raa-gd-eng.htm>.

Government of Canada, F. and O. C. Aquaculture Monitoring Standard. (2015b). <https://www.dfompo.gc.ca/aquaculture/management-gestion/aar-raa-ann7-eng.htm>.

Gribben, P. E. *et al.* Microbial communities in marine sediments modify success of an invasive macrophyte. *Scientific Reports* 7: 9845 (2017).

Grolemund G, Wickham H. Dates and Times Made Easy with lubridate. *Journal of Statistical Software*, 40(3): 1-25. (2011). <http://www.jstatsoft.org/v40/i03/>.

Guo, L., Li, Z., Xie, P. & Ni, L. Assessment effects of cage culture on nitrogen and phosphorus dynamics in relation to fallowing in a shallow lake in China. *Aquacult Int* 17: 229–241 (2009).

Hallegraeff, G. Harmful algal blooms: a global overview. pp. 25-50. In, G.M. Hallegraeff, D.M. Anderson and A.D. Cembella [eds.] Manual on Harmful Marine Microalgae. IOC Manuals and Guides No. 11 UNESCO (2002).

Hargrave, B. T. *et al.* Assessing Benthic Impacts of Organic Enrichment from Marine Aquaculture. *Water, Air, & Soil Pollution* 99: 641–650 (1997).

Holmer, M., Wildish, D. & Hargrave, B. Organic Enrichment from Marine Finfish Aquaculture and Effects on Sediment Biogeochemical Processes. in *Environmental Effects of Marine Finfish Aquaculture* (ed. Hargrave, B. T.) 181–206 (2005). doi:10.1007/b136010.

Hornick, K. M. & Buschmann, A. H. Insights into the diversity and metabolic function of bacterial communities in sediments from Chilean salmon aquaculture sites. *Ann Microbiol* 68: 63–77 (2018).

Hubas, C. *et al.* Proliferation of Purple Sulphur Bacteria at the Sediment Surface Affects Intertidal Mat Diversity and Functionality. *PLoS One* 8, (2013).

IMR. Integrated Microbiome Resource (IMR): Protocols. (2014). <https://imr.bio/protocols.html>.

Kassambara A. ggpubr: 'ggplot2' Based Publication Ready Plots. R package version 0.3.0. (2020). <https://CRAN.R-project.org/package=ggpubr>.

Kawahara, N., Shigematsu, K., Miyadai, T. & Kondo, R. Comparison of bacterial communities in fish farm sediments along an organic enrichment gradient. *Aquaculture* 287: 107–113 (2009).

Kojima, H. & Fukui, M. *Sulfuriflexus mobilis* gen. nov., sp. nov., a sulfur-oxidizing bacterium isolated from a brackish lake sediment. *International Journal of Systematic and Evolutionary Microbiology* 66: 3515–3518 (2016).

Kolda, A. Profiling of bacterial assemblages in the marine cage farm environment, with implications on fish, human and ecosystem health. *Ecological Indicators* 12 (2020).

König, S. *et al.* Nitrogen fixation in a chemoautotrophic lucinid symbiosis. *Nature Microbiology* 2: 1–10 (2016).

Kuever, J. The Family Desulfobacteraceae. in *The Prokaryotes: Deltaproteobacteria and Epsilonproteobacteria* (eds. Rosenberg, E., DeLong, E. F., Lory, S., Stackebrandt, E. & Thompson, F.) 45–73. (2014). doi:10.1007/978-3-642-39044-9\_266.

Langmead, B., Trapnell, C., Pop, M. & Salzberg, S. L. Ultrafast and memory-efficient alignment of short DNA sequences to the human genome. *Genome Biology* 10: R25 (2009).

Lavy, A. *et al.* A novel Chromatiales bacterium is a potential sulfide oxidizer in multiple orders of marine sponges. *Environ Microbiol* 20: 800–814 (2018).

Leon, S. M. S. S., Nuñal, S. N., Wei, H., Yoshikawa, T. & Maeda, H. Bacterial community composition shifts in sediments influenced by fish feeds. *Aquaculture Research* 48: 4380–4389 (2017).

Li, J., Li, F., Yu, S., Qin, S. & Wang, G. Impacts of Mariculture on the Diversity of Bacterial Communities within Intertidal Sediments in the Northeast of China. *Microb Ecol* 66: 861–870 (2013).

Lin, D. T. & Bailey-Brock, J. H. Partial recovery of infaunal communities during a fallow period at an open-ocean aquaculture. *Marine Ecology Progress Series* 371: 65–72 (2008).

Macleod, C. K., Moltschaniwskyj, N. A. & Crawford, C. M. Evaluation of short-term fallowing as a strategy for the management of recurring organic enrichment under salmon cages. *Marine Pollution Bulletin* 52: 1458–1466 (2006).

McBride, M. J. The Family Flavobacteriaceae. in *The Prokaryotes: Other Major Lineages of Bacteria and The Archaea* (eds. Rosenberg, E., DeLong, E. F., Lory, S., Stackebrandt, E. & Thompson, F.) 643–676 (2014). doi:10.1007/978-3-642-38954-2\_130.

McIlroy, S. J. & Nielsen, P. H. The Family Saprospiraceae. in *The Prokaryotes: Other Major Lineages of Bacteria and The Archaea* (eds. Rosenberg, E., DeLong, E. F., Lory, S., Stackebrandt, E. & Thompson, F.) 863–889 (2014). doi:10.1007/978-3-642-38954-2\_138.

- Mirto, S., La Rosa, T., Gambi, C., Danovaro, R. & Mazzola, A. Nematode community response to fish-farm impact in the western Mediterranean. *Environmental Pollution* 116: 203–214 (2002).
- Moncada, C., Hassenrück, C., Gärdes, A. & Conaco, C. Microbial community composition of sediments influenced by intensive mariculture activity. *FEMS Microbiol Ecol* 95 (2019).
- Murray, S. A., Ruvindy, R., Kohli, G. S., Anderson, D. M. & Brosnahan, M. L. Evaluation of sxtA and rDNA qPCR assays through monitoring of an inshore bloom of *Alexandrium catenella* Group 1. *Scientific Reports* 9: 1–12 (2019).
- Muyzer, G. & Stams, A. J. M. The ecology and biotechnology of sulphate-reducing bacteria. *Nature Reviews Microbiology* 6: 441–454 (2008).
- Oksanen, J., Guillaume Blanchet, F., Friendly, M., Kindt, R., Legendre, P., McGlinn, D., Minchin, P. R., O'Hara, R. B., Simpson, G. L., Solymos, P., Stevens, M. H. H., Szoecs, E., Wagner, H. *vegan: Community Ecology Package*. R package version 2.5-6. (2019). <https://CRAN.R-project.org/package=vegan>.
- Parada, A. E., Needham, D. M. & Fuhrman, J. A. Every base matters: assessing small subunit rRNA primers for marine microbiomes with mock communities, time series and global field samples. *Environmental Microbiology* 18: 1403–1414. (2016).
- Paterson, A. T. The Distribution and Diversity of Functional Gene Pathways Controlling Sulfur Speciation in Lower Kane Cave, Wyoming. 117.
- Pearson, T.H. & Rosenberg, R. Macrobenthic succession in relation to organic enrichment and pollution of the marine environment. *Oceanogr. Mar. Biol. Ann. Rev.* 16, 229-311 (1978).
- Pereira, I. A. C. *et al.* A Comparative Genomic Analysis of Energy Metabolism in Sulfate Reducing Bacteria and Archaea. *Front. Microbiol.* 2. (2011).
- Petersen, J. M. *et al.* Chemosynthetic symbionts of marine invertebrate animals are capable of nitrogen fixation. *Nature Microbiology* 2: 1–11 (2016).
- Pohlner, M. *et al.* The Majority of Active Rhodobacteraceae in Marine Sediments Belong to Uncultured Genera: A Molecular Approach to Link Their Distribution to Environmental Conditions. *Front. Microbiol.* 10. (2019).
- Probandt, D. *et al.* Permeability shapes bacterial communities in sublittoral surface sediments: Permeability shapes benthic bacterial communities. *Environ Microbiol* 19: 1584–1599 (2017).
- Quast, C. *et al.* The SILVA ribosomal RNA gene database project: improved data processing and web-based tools. *Nucleic Acids Research* 41: D590–D596 (2013).

R Core Team. R: A language and environment for statistical computing. R Foundation for Statistical Computing, Vienna, Austria. (2020). <https://www.R-project.org/>.

Rensel, J. E. & Whyte, J. N. C. Finfish mariculture and harmful algal blooms. pp. 693-722. In, G.M. Hallegraeff, D.M. Anderson and A.D. Cembella [eds.] Manual on Harmful Marine Microalgae. IOC Manuals and Guides No. 11 UNESCO (2002).

Richlen, M. L. *et al.* Distribution of *Alexandrium fundyense* (Dinophyceae) cysts in Greenland and Iceland, with an emphasis on viability and growth in the Arctic. *Mar Ecol Prog Ser* 547: 33–46 (2016).

Rubio-Portillo, E., Villamor, A., Fernandez-Gonzalez, V., Antón, J. & Sanchez-Jerez, P. Exploring changes in bacterial communities to assess the influence of fish farming on marine sediments. *Aquaculture* 506: 459–464 (2019).

Salman-Carvalho, V., Fadeev, E., Joye, S. B. & Teske, A. How Clonal Is Clonal? Genome Plasticity across Multicellular Segments of a “*Candidatus Marithrix* sp.” Filament from Sulfidic, Briny Seafloor Sediments in the Gulf of Mexico. *Front. Microbiol.* 7 (2016).

Schmidt, T. M., Arieli, B., Cohen, Y., Padan, E. & Strohl, W. R. Sulfur metabolism in *Beggiatoa alba*. *J Bacteriol* 169: 5466–5472 (1987).

Scholin, C. A., Vrieling, E., Peperzak, L., Rhodes, L. & Rublee, P. Detection of HAB species using lectin, antibody and DNA probes. pp. 131-164. In, G.M. Hallegraeff, D.M. Anderson and A.D. Cembella [eds.] Manual on Harmful Marine Microalgae. IOC Manuals and Guides No. 11 UNESCO (2002).

Sharpton, T. J. An introduction to the analysis of shotgun metagenomic data. *Front. Plant Sci.* 5 (2014).

Smayda, T. J. Environmental monitoring, with examples from Narragansett Bay, pp. 595-626. In, G.M. Hallegraeff, D.M. Anderson and A.D. Cembella [eds.] Manual on Harmful Marine Microalgae. IOC Manuals and Guides No. 11 UNESCO (2002).

Stoeck, T. *et al.* Environmental DNA metabarcoding of benthic bacterial communities indicates the benthic footprint of salmon aquaculture. *Marine Pollution Bulletin* 127: 139–149 (2018a).

Stoeck, T., Kochems, R., Forster, D., Lejzerowicz, F. & Pawlowski, J. Metabarcoding of benthic ciliate communities shows high potential for environmental monitoring in salmon aquaculture. *Ecological Indicators* 85: 153–164 (2018b).

Strain, P. M. & Hargrave, B. T. Salmon Aquaculture, Nutrient Fluxes and Ecosystem Processes in Southwestern New Brunswick. in *Environmental Effects of Marine Finfish Aquaculture* (ed. Hargrave, B. T.) vol. 5M 29–57 (2005).

- Suzek, B. E. *et al.* UniRef clusters: a comprehensive and scalable alternative for improving sequence similarity searches. *Bioinformatics* 31: 926–932 (2015).
- Thorup, C., Schramm, A., Findlay, A. J., Finster, K. W. & Schreiber, L. Disguised as a Sulfate Reducer: Growth of the Deltaproteobacterium *Desulfurivibrio alkaliphilus* by Sulfide Oxidation with Nitrate. *mBio* 8 (2017).
- Tsallagov, S. I., Sorokin, D. Y., Tikhonova, T. V., Popov, V. O. & Muyzer, G. Comparative Genomics of *Thiohalobacter thiocyanaticus* HRh1T and *Guyparkeria* sp. SCN-R1, Halophilic Chemolithoautotrophic Sulfur-Oxidizing Gammaproteobacteria Capable of Using Thiocyanate as Energy Source. *Front Microbiol* 10 (2019).
- Venceslau, S. S., Stockdreher, Y., Dahl, C. & Pereira, I. A. C. The “bacterial heterodisulfide” DsrC is a key protein in dissimilatory sulfur metabolism. *Biochimica et Biophysica Acta (BBA) - Bioenergetics* 1837: 1148–1164 (2014).
- Verhoeven, J. T. P., Salvo, F., Knight, R., Hamoutene, D. & Dufour, S. C. Temporal Bacterial Surveillance of Salmon Aquaculture Sites Indicates a Long Lasting Benthic Impact With Minimal Recovery. *Front. Microbiol.* 9 (2018).
- Vigneron, A. *et al.* Beyond the tip of the iceberg; a new view of the diversity of sulfite- and sulfate-reducing microorganisms. *The ISME Journal* 12: 2096–2099 (2018).
- Wade, J., Jackson, T., Brewer, K. *et al.* Aquaculture Canada 2014 proceedings of contributed papers. 2015(1): 1-46. (2015).
- Waite, D. *et al.* Comparative Genomic Analysis of the Class Epsilonproteobacteria and Proposed Reclassification to Epsilonbacteraeota (phyl. nov.). *Frontiers in Microbiology* 8 (2017).
- Walsh, D. *et al.* Heterogeneity of SSU and LSU rDNA sequences of *Alexandrium* species. *Biochemical Systematics and Ecology* 26: 495–509 (1998).
- Walters, W. *et al.* Improved Bacterial 16S rRNA Gene (V4 and V4-5) and Fungal Internal Transcribed Spacer Marker Gene Primers for Microbial Community Surveys. *mSystems* 1 (2016).
- Wang, Z.-J., Liu, Q.-Q., Zhao, L.-H., Du, Z.-J. & Chen, G.-J. *Bradymonas sediminis* gen. nov., sp. nov., isolated from coastal sediment, and description of *Bradymonadaceae* fam. nov. and *Bradymonadales* ord. nov. *International Journal of Systematic and Evolutionary Microbiology* 65: 1542-1549 (2015).
- Wickham H. Reshaping Data with the reshape Package. *Journal of Statistical Software*, 21(12), 1-20 (2007). <http://www.jstatsoft.org/v21/i12/>.

Wickham H. *ggplot2: Elegant Graphics for Data Analysis*. Springer-Verlag New York. (2016).

Wickham H. *et al.* Welcome to the tidyverse. *Journal of Open-Source Software*, 4(43): 1686. (2019). <https://doi.org/10.21105/joss.01686>.

Wildish, D. J. & Pohle, G. W. Benthic Macrofaunal Changes Resulting from Finfish Mariculture. in *Environmental Effects of Marine Finfish Aquaculture* (ed. Hargrave, B. T.) 275–304 (2005). doi:10.1007/b136015.

Wilke CO. *cowplot: Streamlined Plot Theme and Plot Annotations for 'ggplot2'*. R package version 1.0.0. (2019). <https://CRAN.R-project.org/package=cowplot>.

Yilmaz, P. *et al.* The SILVA and “All-species Living Tree Project (LTP)” taxonomic frameworks. *Nucleic Acids Research* 42: D643–D648 (2014).

Zhulay, I., Reiss, K. & Reiss, H. Effects of aquaculture fallowing on the recovery of macrofauna communities. *Marine Pollution Bulletin* 97: 381–390 (2015).

Zorz, J. *et al.* Drivers of Regional Bacterial Community Structure and Diversity in the Northwest Atlantic Ocean. *Front. Microbiol.* 10 (2019).

## APPENDIX A: SUPPLEMENTAL MATERIAL

**Table S1: Outline of McNutt's stations sampled at each timepoint for sediment.**

Date	Number of Cage Stations	Number of Buoy Stations	Replicates	Total Sent for sequencing	Remaining after Qiime2 Analysis
2018-07-26	6	4	1	10	18S: 10 V6V8: 10
2018-09-18	3	0	1	3	18S: 3 V6V8: 3
2019-03-29	7	4	3	33	18S: 33 V6V8: 33
2019-07-18	7	3	1-3	12	18S: 12 V6V8: 12
2019-08-27	6	3	3	27	18S: 27 V6V8: 27
2019-10-08	6	3	3	26	18S: 24 V6V8: 26
2019-11-26	7	3	3	30	18S: 23 V6V8: 30

**Table S2: Outline of McNutt's stations sampled at each timepoint for water.**

Date	Number of Cage Stations	Number of Buoy Stations	Replicates	Total Sent for sequencing	Remaining after Qiime2 Analysis
2018-07-26	5	4	2	20	18S: 20 V6V8: 20
2018-09-18	3	0	2	6	18S: 6 V6V8: 6
2019-03-29	7	5	2	23	18S: 23 V6V8: 23
2019-07-18	6	3	2	18	18S: 18 V6V8: 18
2019-08-27	7	3	2	20	18S: 14 V6V8: 20
2019-10-08	6	3	2	18	18S: 14 V6V8: 18
2019-11-26	7	3	2	20	18S: 3 V6V8: 19

**Table S3: Overview of sediment samples taken at the McNutt’s site on each sampling day. Highlighted and bolded samples were sequenced using shotgun metagenomics.**

Station	Sampling Date						
	July 2018	September 2018	March 2019	July 2019	August 2019	October 2019	November 2019
B1	✓			✓			
B2	✓		✓	✓	✓	✓	✓
B3	✓		✓				
B4			✓		✓	✓	✓
B5	✓		✓	✓	✓	✓	✓
B6							
Bg	✓	✓	✓	✓	✓	✓	✓
C1	✓		✓	✓	✓	✓	✓
C2		✓	✓	✓	✓	✓	✓
C3	✓		✓	✓			✓
C4	✓	✓	✓		✓	✓	✓
C5	✓		✓		✓	✓	✓
C6	✓		✓	✓	✓	✓	✓
C7				✓			

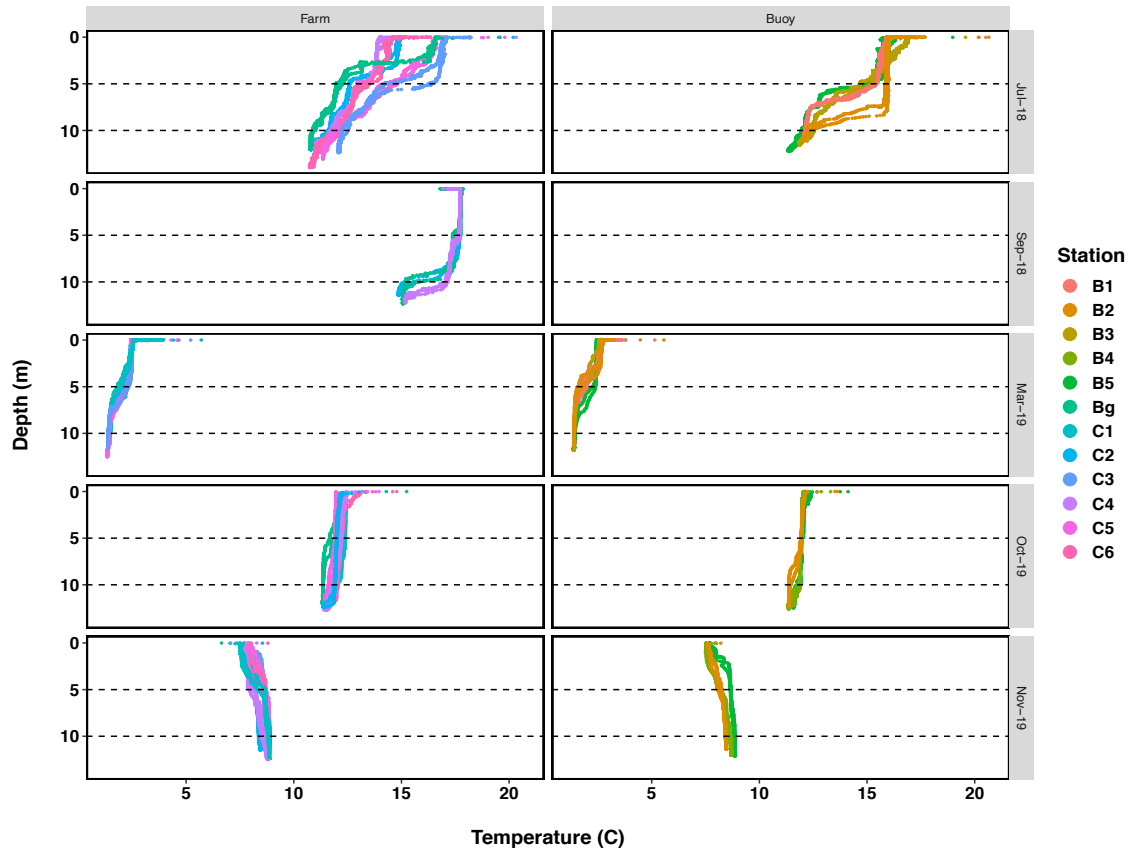


**Figure S1: Depth profile of temperature collected using a seacast ctd. Dotted lines at 5m and 10m indicate depths at which samples were taken.**

**Table S4: Most significant bacterial ASV for the different station types on each sampling date as determined by indiciespecies analysis. No ASVs were found to be significantly associated with any station type on Day 2, nor with barge or buoy stations on Day 3.**

Day	Station	Most Significant ASV	Taxonomy
July 2018	barge	c711e20466cd03fef484676537d9a819	Bacteroidetes; Bacteroidia; Flavobacteriales; <i>Flavobacteriaceae</i>
	buoy	a89abcb240137e7e6164d567de8f9cf0	Bacteroidetes; Bacteroidia; Flavobacteriales; <i>Flavobacteriaceae</i>
	cage	891d85468f1e4e570ab996a06c17083e	Bacteroidetes; Bacteroidia; Chitinophagales; <i>Saprospiraceae</i> ; uncultured
March 2019	cage	059b048bb4362d4a9c5bbd08bef49611	Bacteroidetes; Bacteroidia; Bacteroidales; Bacteroidetes BD2-2
July 2019	barge	5744c2078c28609dbd3a85f6e35dae95	Epsilonbacteraeota; Campylobacteria; Campylobacterales; <i>Sulfurovaceae</i> ; <i>Sulfurovum</i>
	buoy	62376838588c3db9b3f6db5d3aa6da8b	Bacteroidetes; Bacteroidia; Chitinophagales; <i>Saprospiraceae</i> ; uncultured
	cage	5a91a8b3b821cfa391d8b8d131ff5230	Bacteroidetes; Bacteroidia; Flavobacteriales; <i>Flavobacteriaceae</i> ; <i>Maribacter</i> ; uncultured bacterium
August 2019	barge	a90a49cea02f8c3dda2256fee6c46b38	Proteobacteria; Deltaproteobacteria; Bradymonadales
	buoy	93c6eaf26402f43b67665f766c1a5136	Proteobacteria; Gammaproteobacteria; BD7-8
	cage	00557a9f1a8dbef5907c4471aa29b4b5	Proteobacteria; Gammaproteobacteria; Chromatiales; <i>Sedimenticolaceae</i> ; <i>Sedimenticola</i>
October 2019	barge	aa6279ee927784caa9f78379cfae8928	Bacteroidetes; Bacteroidia; Bacteroidales
	buoy	a1a48bb64cf82bb76e0625b2ddd587e4	Proteobacteria; Gammaproteobacteria
	cage	8a3bd060fab834b018b4d9a848bc3544	Bacteroidetes; Bacteroidia; Flavobacteriales; <i>Flavobacteriaceae</i> ; <i>Polaribacter</i>

<b>Day</b>	<b>Station</b>	<b>Most Significant ASV</b>	<b>Taxonomy</b>
November 2019	barge	9c023ed20ed259d85dcb0a9721c0e983	Cloacimonetes; Cloacimonadia; Cloacimonadales; MSBL8
	buoy	93c6eaf26402f43b67665f766c1a5136	Proteobacteria; Gammaproteobacteria; BD7-8
	cage	e14621f46c401cf8be2a8a7578601d2d	Epsilonbacteraeota; Campylobacteria; Campylobacterales; <i>Sulfurovaceae; Sulfurovum</i>

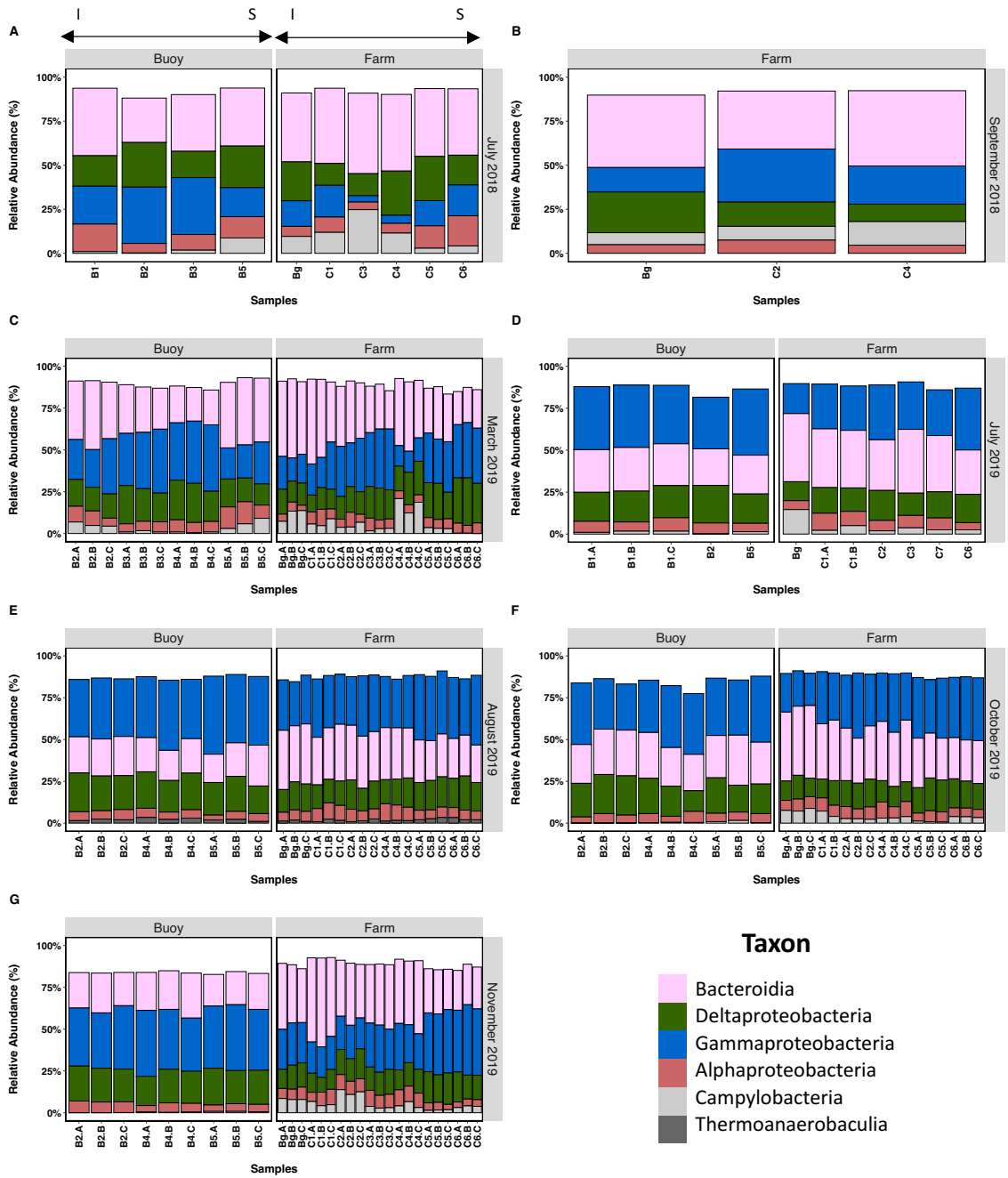


**Figure S2: Relative abundance of the top 5 prokaryotic taxonomic classes present in the sediment on each sample date as determined by 16S V6V8 sequencing. Buoy and Farm samples are ordered left to right from inland (I) to seaward (S). ASV's unclassified to the family level were excluded and represented by white space on the y-axis. The letters ABC in x-axis labels indicate sediment replicates. Plots A-B are from time period P1, C from time period F, and D-G from time period P2.**

**Table S5: Prokaryotic taxa from Figure 2.13 and the taxonomic families they belong to. Families denoted by a \* are plotted in the previous sediment taxonomic bar plot (Figure 2.10).**

<b>Genus</b>	<b>Family</b>
<i>Desulfobacterium</i>	<i>Desulfobacteraceae*</i>
<i>Desulfoconvexum</i>	<i>Desulfobacteraceae*</i>
<i>Desulforopalus</i>	<i>Desulfobulbaceae*</i>
<i>Desulfotalea</i>	<i>Desulfobulbaceae*</i>
<i>Draconibacterium</i>	<i>Prolixibacteraceae</i>
<i>Fusibacter</i>	<i>Clostridiales Family XII</i>
<i>Marinifilum</i>	<i>Marinifilaceae*</i>
<i>Psychromonas</i>	<i>Psychromonadaceae</i>
<i>Sediminispirochaeta</i>	<i>Spirochaetaceae</i>
<i>Spirochaeta</i>	<i>Spirochaetaceae</i>
<i>Sulfurimonas</i>	<i>Thiovulaceae</i>
<i>Sulfurovum</i>	<i>Sulfurovaceae*</i>

**Table S6: Prokaryotic taxonomic families found in the sediment (Figure 2.10) and the phylum to which they belong, as well as a description of their metabolism and other relevant information.**

<b>Family</b>	<b>Phylum</b>	<b>Description</b>
<i>Flavobacteriaceae</i> (sediment) (McBride <i>et al.</i> 2014)	Bacteroidetes	<ul style="list-style-type: none"> <li>• most, but not all, are aerobic</li> <li>• highly diverse family of chemoorganotrophs</li> <li>• some are fish pathogens: <i>F. columnare</i>, <i>F. psychrophilum</i>, <i>F. branchiophilum</i>, <i>T. maritimum</i></li> </ul>
<i>Desulfobulbaceae</i> (Gribben <i>et al.</i> 2017, Vigneron <i>et al.</i> 2018)	Proteobacteria (Delta)	<ul style="list-style-type: none"> <li>• generally associated with sulfur reduction</li> <li>• often reported as abundant sulfate reducing bacteria in the surface sediment</li> </ul>
<i>Rhodobacteraceae</i> (sediment) (Pohlner <i>et al.</i> 2019)	Proteobacteria (Alpha)	<ul style="list-style-type: none"> <li>• one of the most widely distributed bacteria</li> <li>• contains sulfur oxidizers</li> </ul>
<i>Desulfobacteraceae</i> (Kuever 2014)	Proteobacteria (Delta)	<ul style="list-style-type: none"> <li>• contains mesophilic and psychrophilic sulfate reducing bacteria</li> <li>• strictly anaerobic</li> </ul>
<i>Sulfurovaceae</i> (Waite <i>et al.</i> 2017)	Epsilonproteobacteria	<ul style="list-style-type: none"> <li>• contains sulfur oxidizers</li> </ul>
<i>Thiotrichaceae</i> (Boden and Scott 2018, Schmidt <i>et al.</i> 1987)	Proteobacteria (Gamma)	<ul style="list-style-type: none"> <li>• family contains <i>Beggiatoa</i> and other sulfur-oxidizing bacteria</li> <li>• some capable of sulfur reduction under extreme anaerobic conditions (produces H<sub>2</sub>S)</li> </ul>
<i>Saprospiraceae</i> (McIlroy and Nielsen 2014)	Bacteroidetes	<ul style="list-style-type: none"> <li>• some specialize in the breakdown and utilization of complex carbon sources</li> <li>• often associated with the epibacterial community of macroalgae</li> </ul>
<i>Sandaracinaceae</i> (Probandt <i>et al.</i> 2017)	Proteobacteria (Delta)	<ul style="list-style-type: none"> <li>• play a role in organic decomposition</li> </ul>
<i>Marinifilaceae</i> (Bozo-Hurtado <i>et al.</i> 2013)	Bacteroidetes	<ul style="list-style-type: none"> <li>• most members are facultatively anaerobic or even aerobic</li> <li>• involved in sulfur coupling</li> </ul>

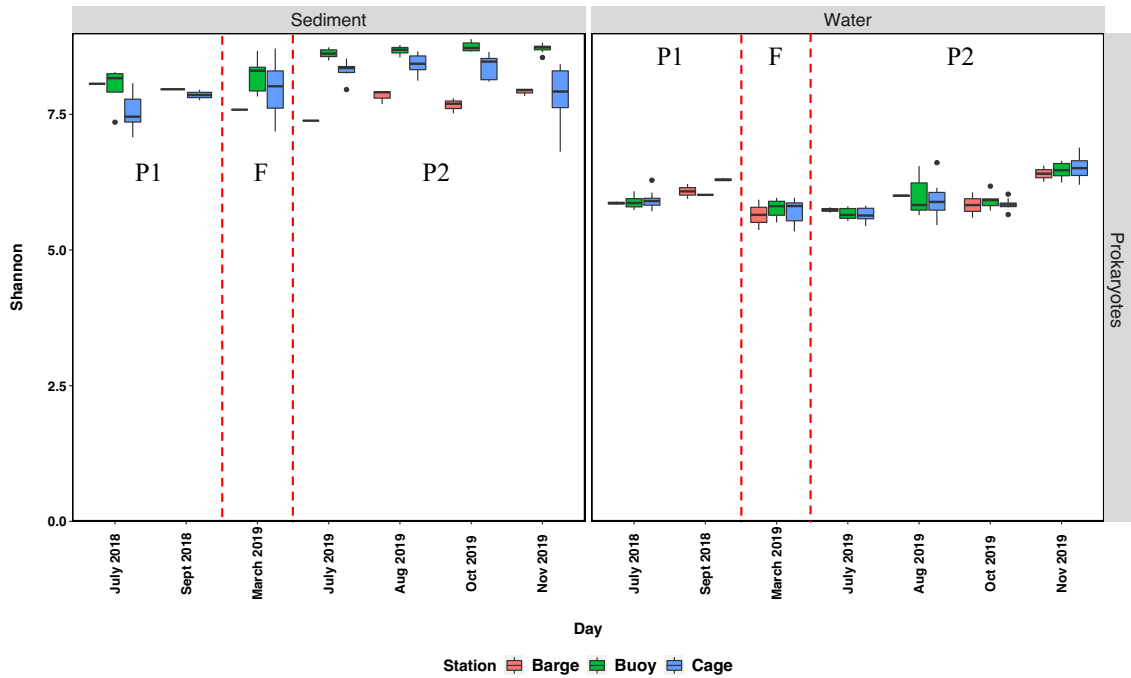


**Figure S3: Shannon diversity index of prokaryotes (16S V4V5) in the water column and sediment across the sampling period. Red dotted lines show the approximate time fallowing occurred. Labels in plots represent the 3 time periods outlined in the methods: production cycle 1 (P1), mid-fallowing (F), and production cycle 2 (P2).**

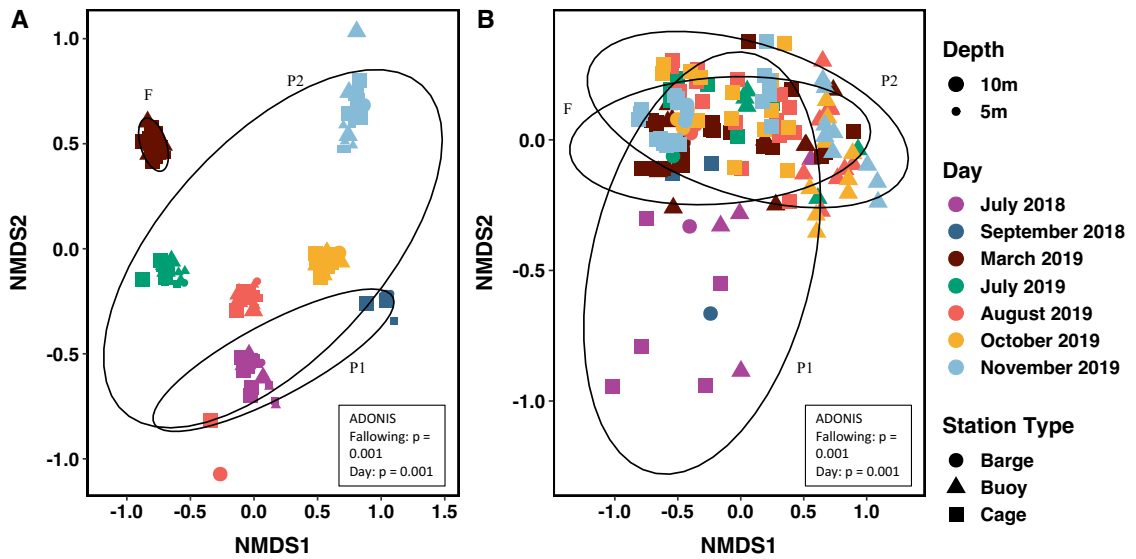


**Figure S4: nMDS plots of A) water column 16S V4V5 and B) sediment 16S V4V5 amplicon sequencing for all days of sampling. Ellipses in plots represent the 3 time periods outlined in the methods: production cycle 1 (P1), mid-fallowing (F), and production cycle 2 (P2). Note: depth only applies to water column samples as all sediment samples are from approximately the same depth.**

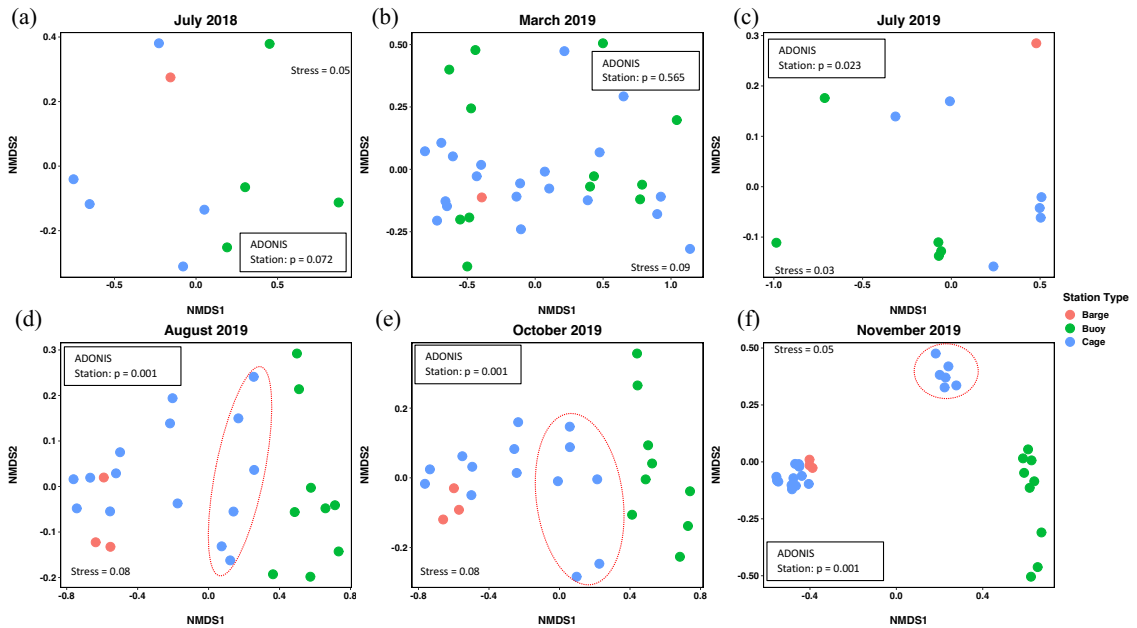


**Figure S5: nMDS plots of 16S V4V5 amplicon sequencing of sediment samples by day, with the exception of September 2018 as there were too few samples to conduct a robust nMDS analysis. Red ellipses on plots (d), (e), and (f) indicate samples from the two cages at the open-ocean end of the farm (C5 & C6). Plot A is from time period P1, B from time period F, and C-F from time period P2.**

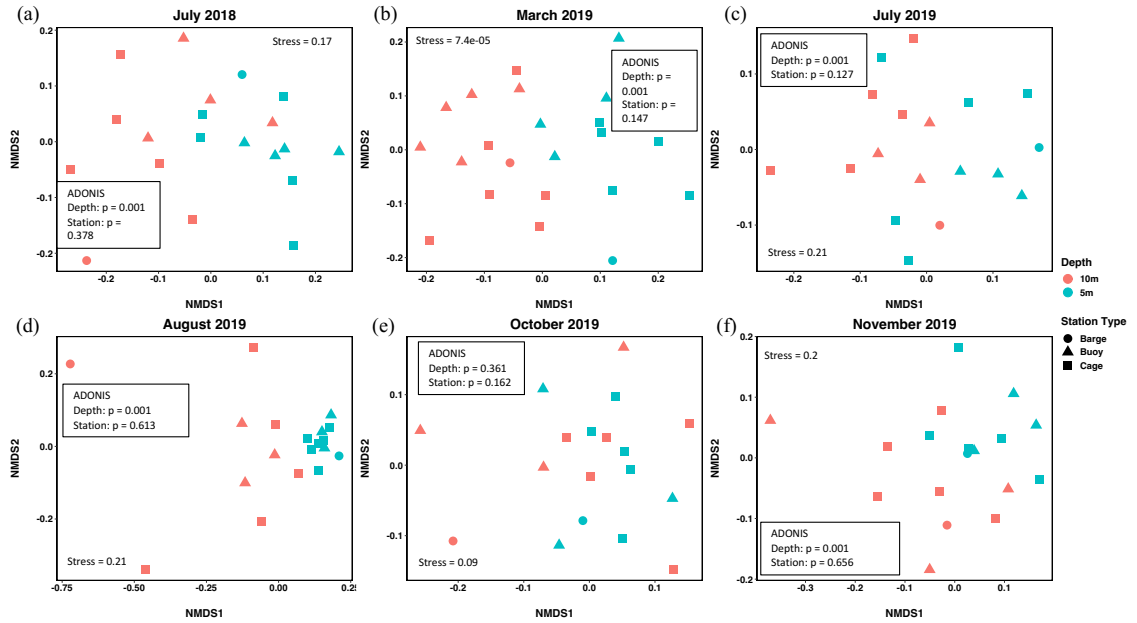


**Figure S6: nMDS plots of 16S V4V5 amplicon sequencing of water column samples by day, with the exception of September 2018 as there were too few samples to conduct a robust nMDS analysis. Plot A is from time period P1, B from time period F, and C-F from time period P2.**

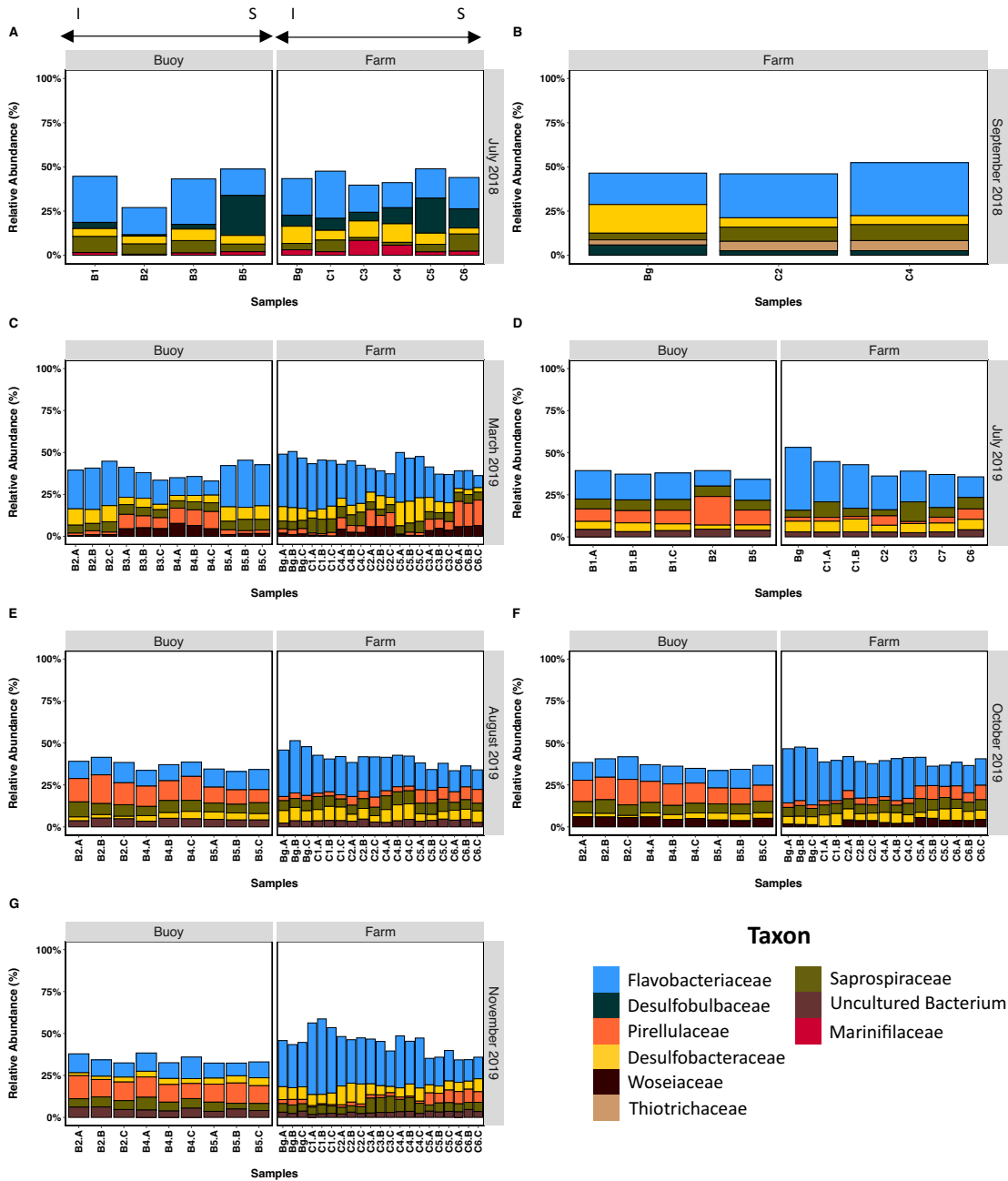


**Figure S7: Relative abundance of the top 5 prokaryotic taxonomic families present in the sediment on each sample date as determined by 16S V4V5 sequencing. Buoy and Farm samples are ordered left to right from inland (I) to seaward (S). ASV's unclassified to the family level were excluded and represented by white space on the y-axis. The letters ABC in x-axis labels indicate sediment replicates. Plots A-B are from time period P1, C from time period F, and D-G from time period P2.**

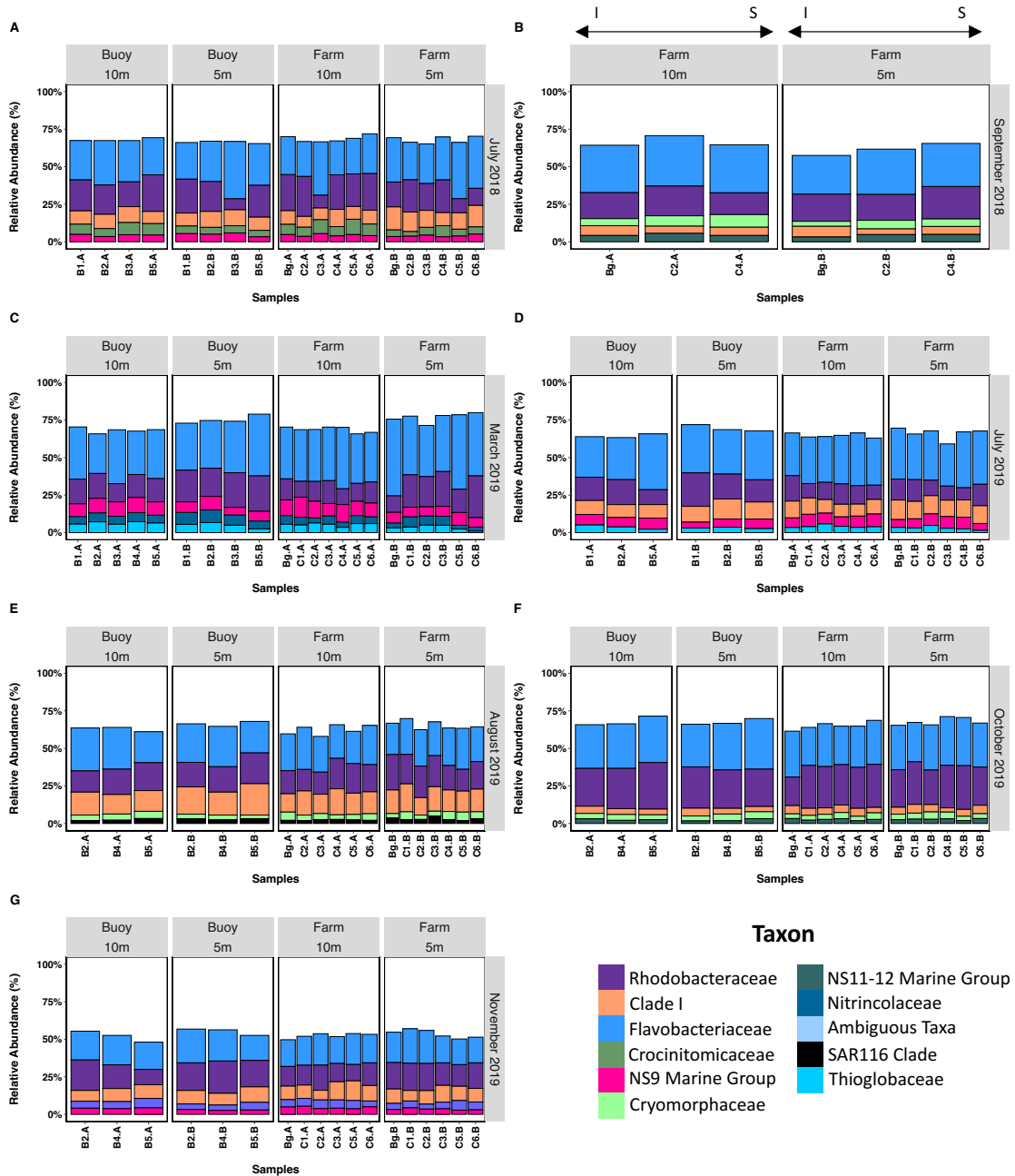


**Figure S8: Relative abundance of the top 5 prokaryotic taxonomic families present in the water column on each sample date as determined by 16S V4V5 sequencing. In each section, samples are ordered left to right from inland to open ocean. ASV's unclassified to the class levels were excluded and represented by white space on the y-axis. In the x-axis labels, samples ending in A are from 10m water, and those ending in B are from 5m water. Plots A-B are from time period P1, C from time period F, and D-G from time period P2.**

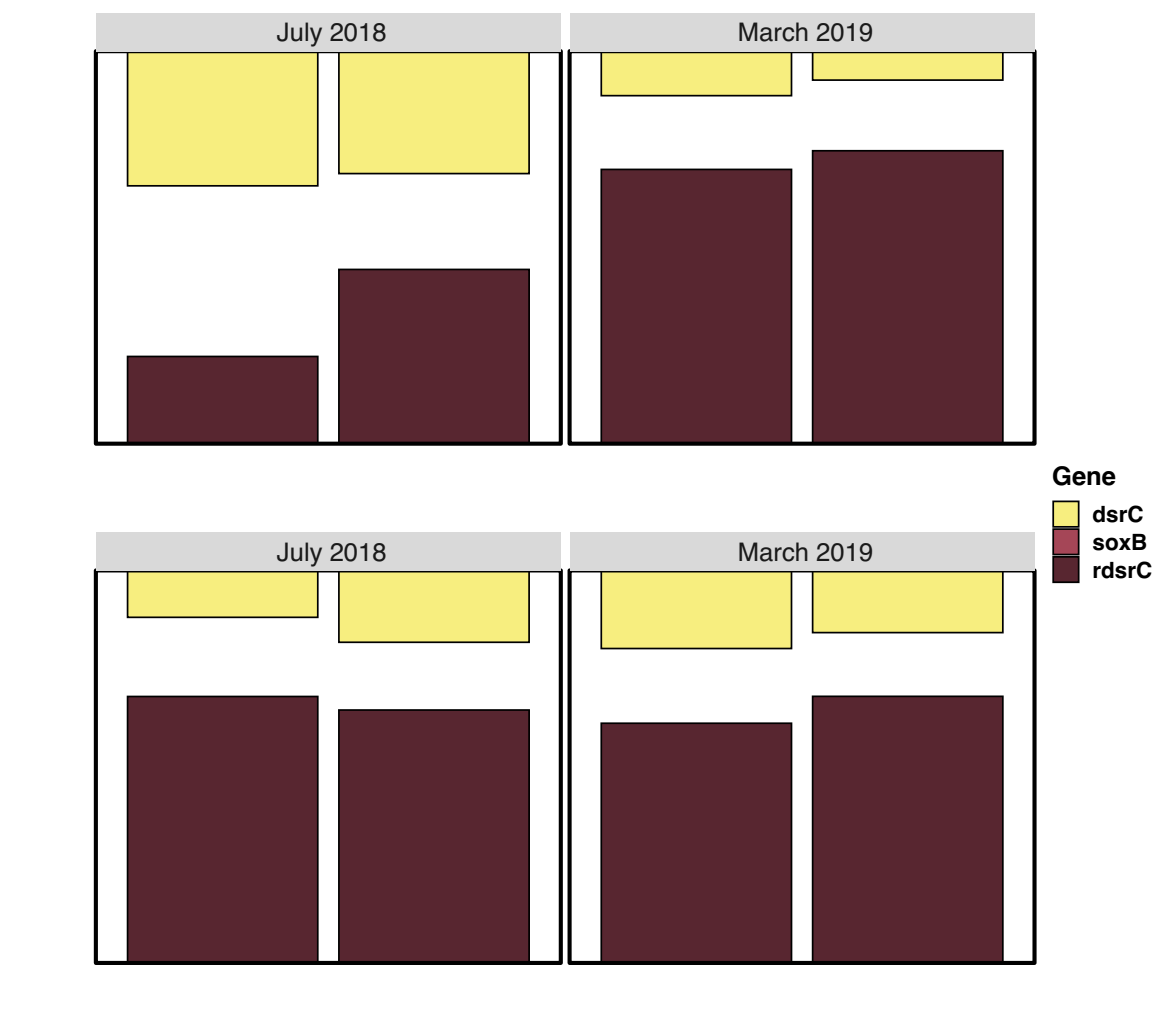


**Figure S9: Percent relative abundance of unstratified sulfur cycling genes before (July 2018) and during (March 2019) following in the A) cage sediments and B) buoy sediments. Relative abundance was calculated for each sample by adding together raw reads of all pathways and determining the percentage of each pathway.**

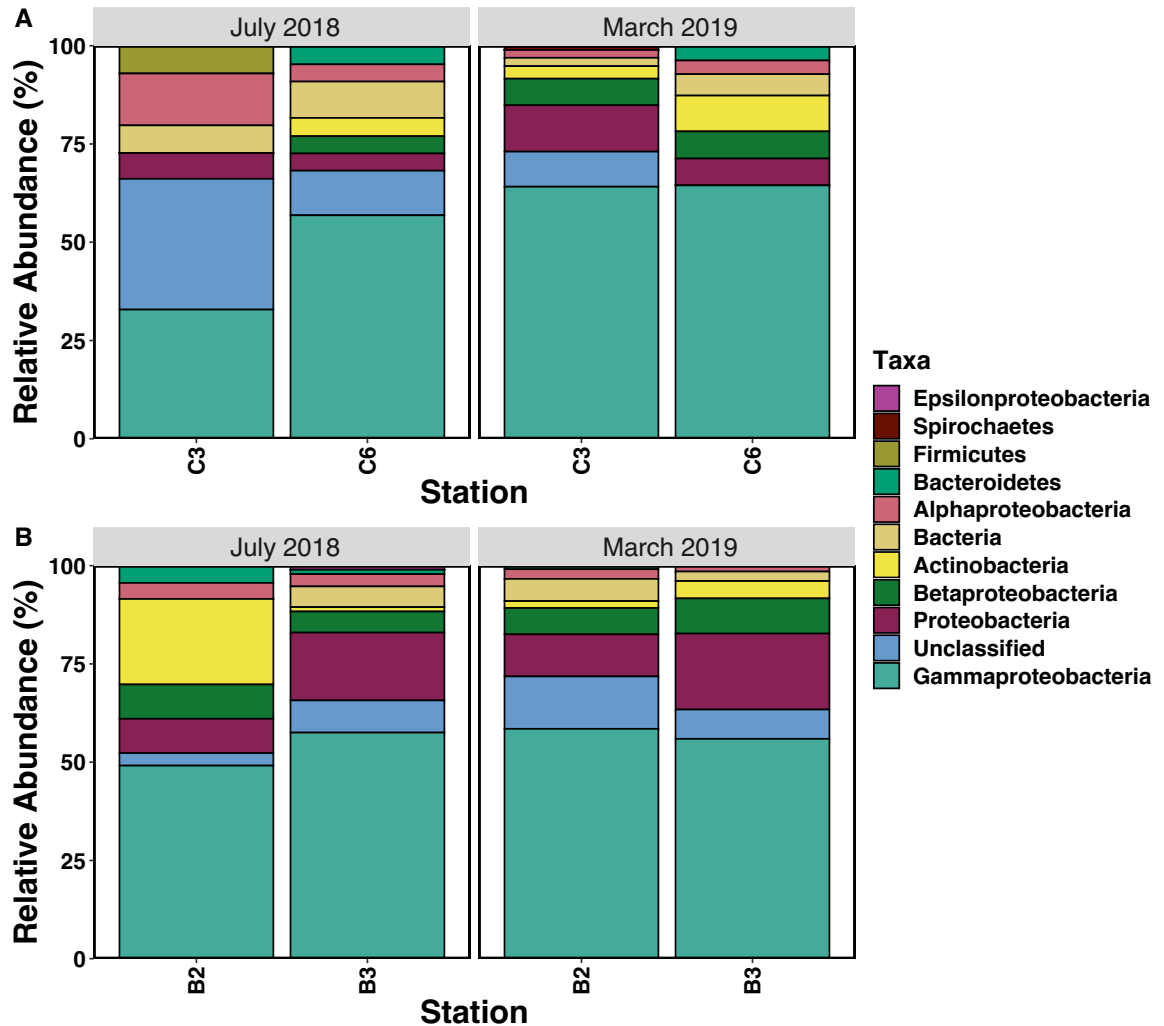


**Figure S10: Percent relative abundance of the *rdsrC* gene separated by taxonomy before (July 2018) and during (March 2019) following in the A) cage sediments and B) buoy sediments. Reads are separated into reads per phylum aside from Proteobacteria which, when possible, were separated into the different classes due to abundance compared to other phyla. Relative abundance was calculated for each sample by adding together raw reads of all pathways and determining the percentage of each pathway.**

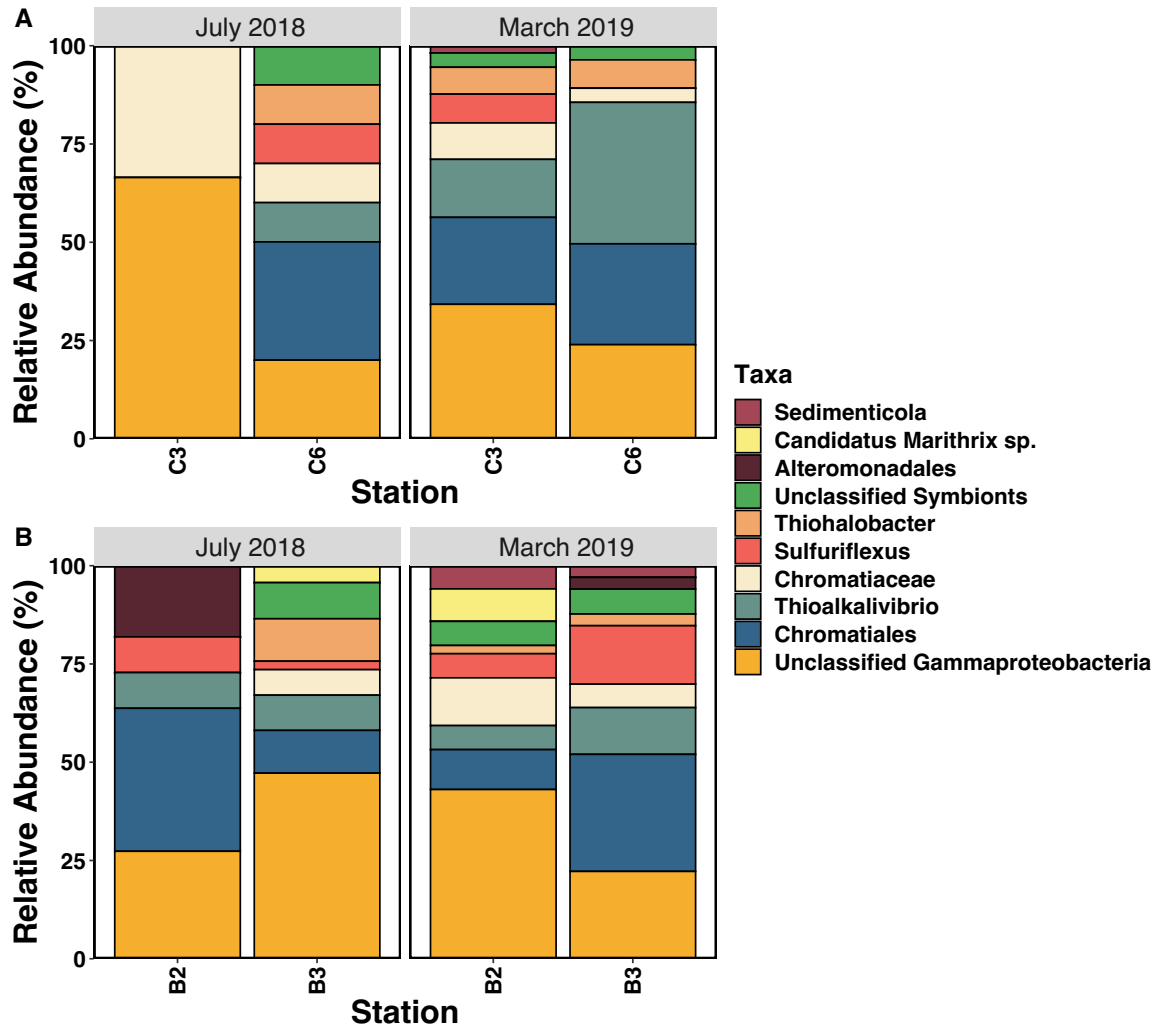


**Figure S11: Percent relative abundance of Top 10 most abundant Gammaproteobacteria taxa that have the ability to perform sulfur oxidation via the *rdsrC* gene before (July 2018) and during (March 2019) following in the A) cage sediments and B) buoy sediments. Reads are separated into the lowest taxonomy level possible from the stratified table. References confirming these taxa are oxidizers can be found in Table 3.1. Relative abundance was calculated for each sample by adding together raw reads of all pathways and determining the percentage of each pathway.**

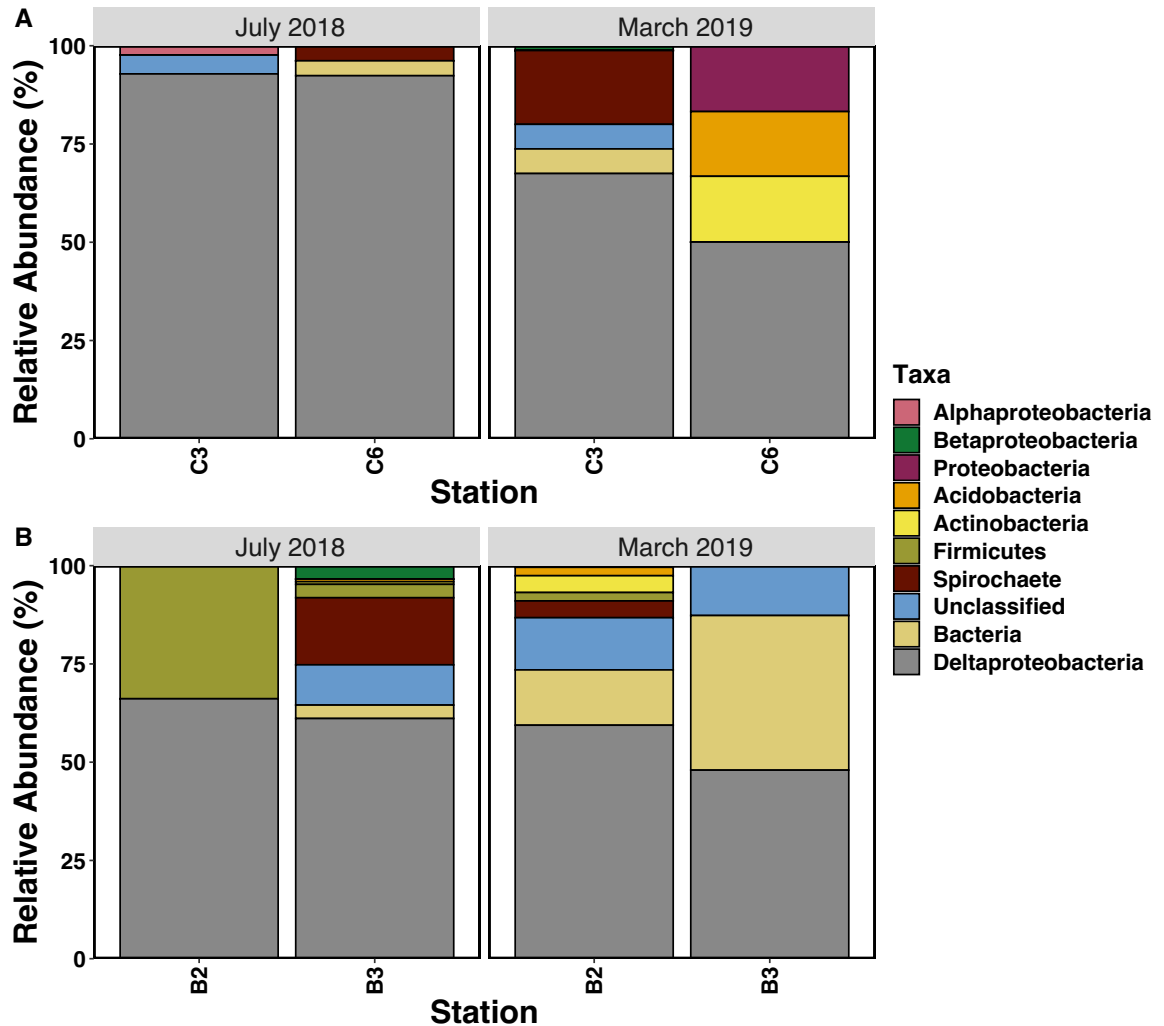


**Figure S12: Percent relative abundance of the *dsrC* gene separated by taxonomy before (July 2018) and during (March 2019) following in the A) cage sediments and B) buoy sediments. Reads are separated into reads per phylum aside from Proteobacteria which, when possible, were separated into the different classes due to abundance compared to other phyla. Relative abundance was calculated for each sample by adding together raw reads of all pathways and determining the percentage of each pathway.**

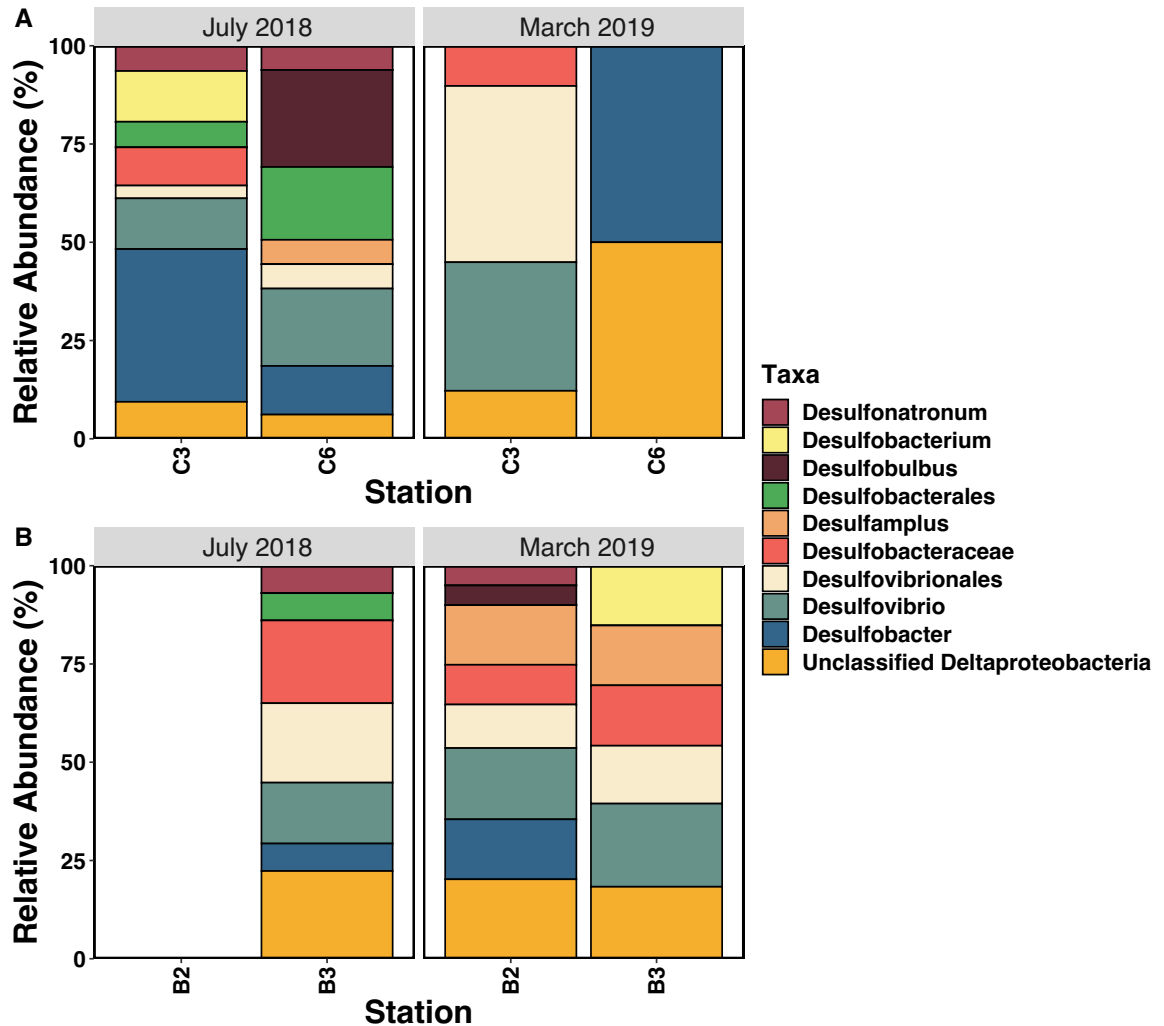


**Figure S13: Percent relative abundance of Top 10 most abundant Deltaproteobacteria taxa that have the ability to perform sulfur reduction via the *dsrC* gene before (July 2018) and during (March 2019) following in the A) cage sediments and B) buoy sediments. Reads are separated into the lowest taxonomy level possible from the stratified table. References confirming these taxa are reducers can be found in Table 3.1. Relative abundance was calculated for each sample by adding together raw reads of all pathways and determining the percentage of each pathway.**

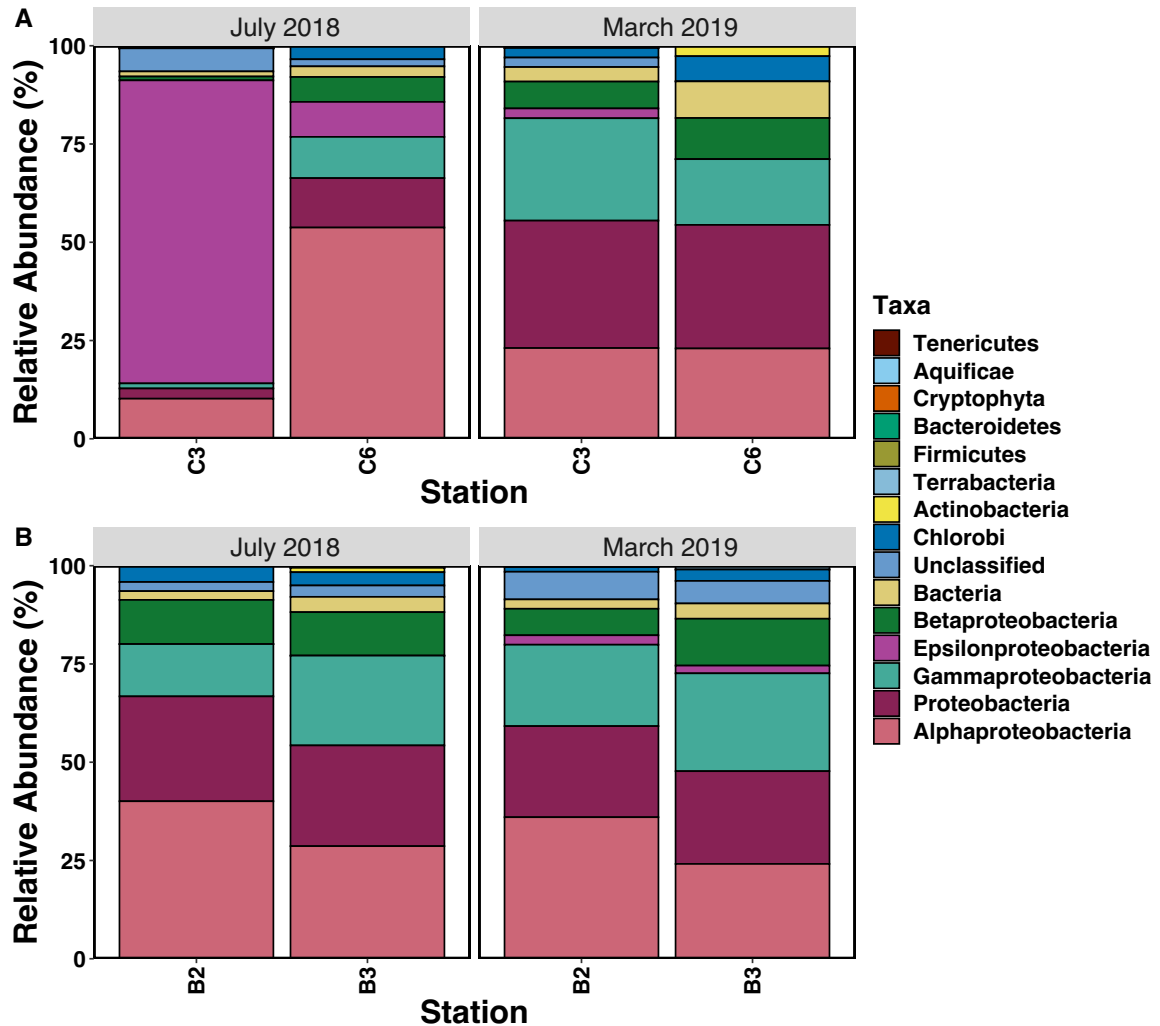


**Figure S14: Percent relative abundance of the *soxB* gene separated by taxonomy before (July 2018) and during (March 2019) following in the A) cage sediments and B) buoy sediments. Reads are separated into reads per phylum aside from Proteobacteria which, when possible, were separated into the different classes due to abundance compared to other phyla. Relative abundance was calculated for each sample by adding together raw reads of all pathways and determining the percentage of each pathway.**

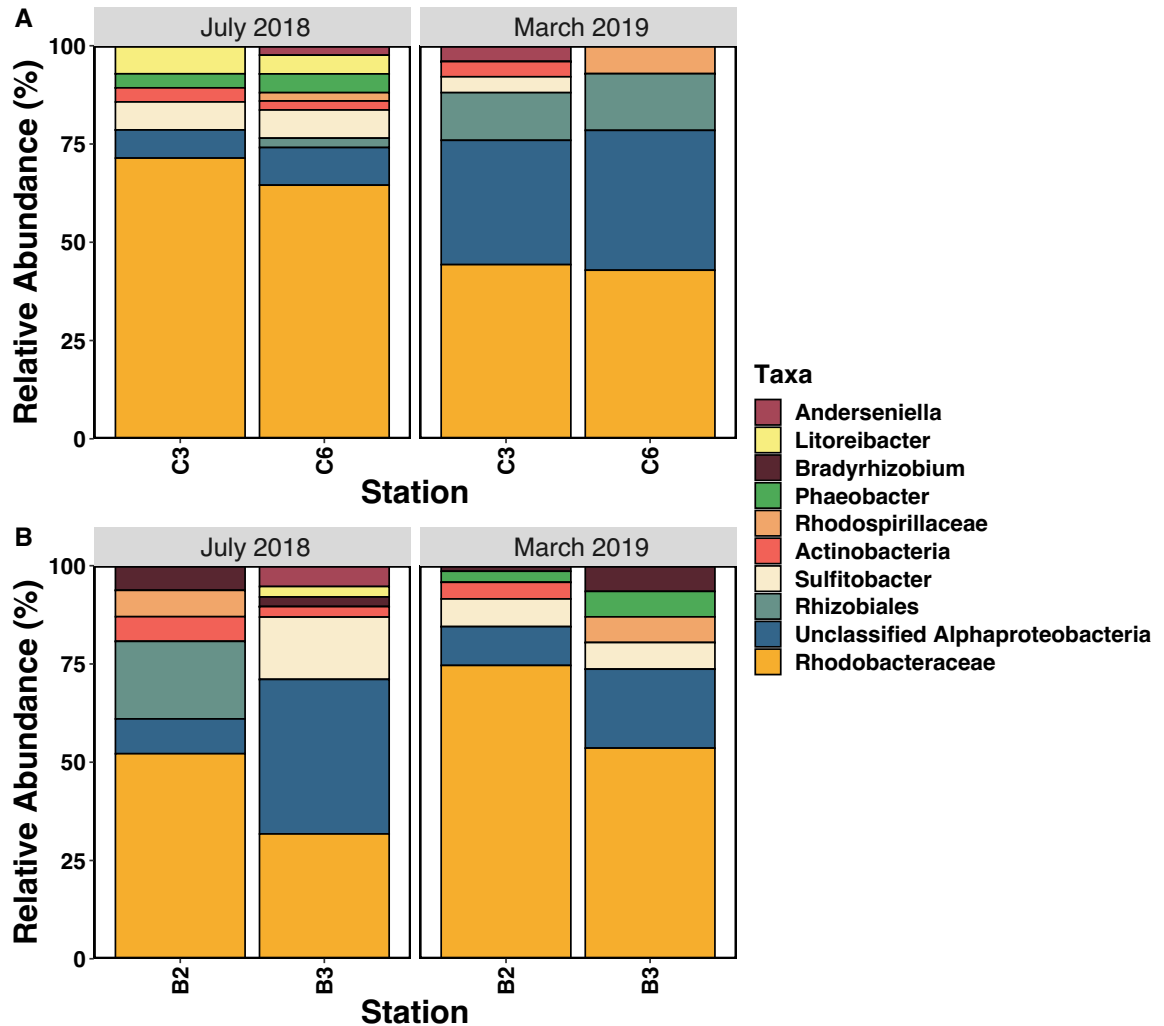


**Figure S15: Percent relative abundance of Top 10 most abundant Alphaproteobacteria taxa that have the ability to perform sulfur oxidation via the *soxB* gene before (July 2018) and during (March 2019) following in the A) cage sediments and B) buoy sediments. Reads are separated into the lowest taxonomy level possible from the stratified table. Relative abundance was calculated for each sample by adding together raw reads of all pathways and determining the percentage of each pathway.**

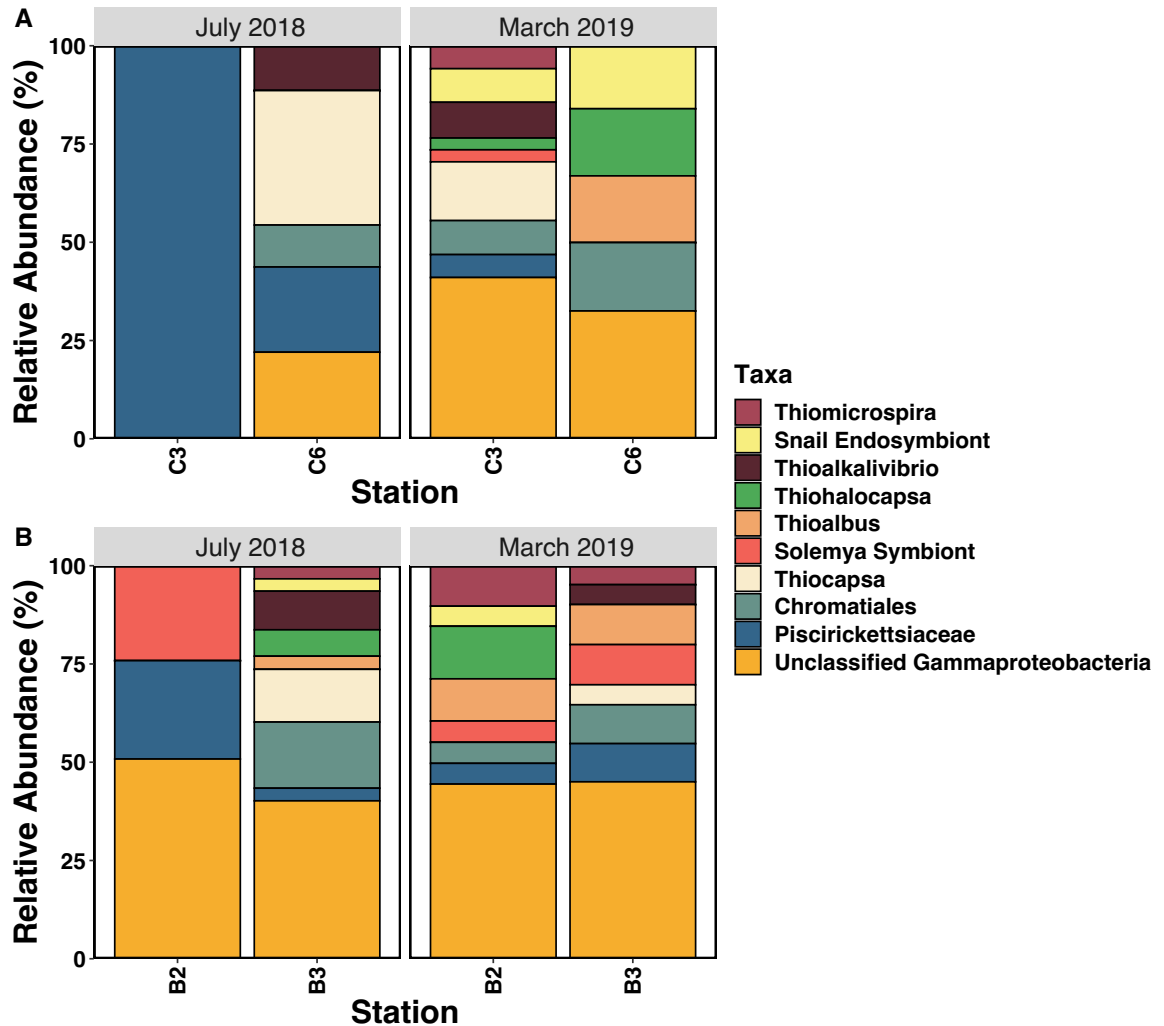


**Figure S16: Percent relative abundance of Top 10 most abundant Gammaproteobacteria taxa that have the ability to perform sulfur oxidation via the *soxB* gene before (July 2018) and during (March 2019) following in the A) cage sediments and B) buoy sediments. Reads are separated into the lowest taxonomy level possible from the stratified table. Relative abundance was calculated for each sample by adding together raw reads of all pathways and determining the percentage of each pathway.**

**Table S7: Outline of Hartz and Sandy Points stations sampled at each timepoint for sediment.**

Date	Farm	Number of Cage Stations	Number of Buoy Stations	Number of Reference Stations	Replicates
2019-07-17	Hartz	2	1	0	1
	Sandy	2	1	0	1
2019-08-26	Hartz	2	1	1	3
	Sandy	2	1	1	3
2019-10-07/08	Hartz	2	1	1	3
	Sandy	1	1	1	3
2019-11-25/26	Hartz	2	1	1	3
	Sandy	2	1	1	3

**Table S8: Conditions for each optimization run of each assay. Note: Only variables that differ amongst optimization runs are recorded in this table. \* Denotes runs where PowerUp SYBR was used.**

Assay	Trial	Forward Primer Concentration (Final)	Reverse Primer Concentration (Final)	BSA	Elongation Time
LSU	1	0.5 $\mu$ M	0.5 $\mu$ M	+	1 min
	2	0.5 $\mu$ M	0.5 $\mu$ M	+	30 sec
		0.025 $\mu$ M	0.025 $\mu$ M	+	30 sec
	3	0.5 $\mu$ M	0.5 $\mu$ M	+	30 sec
	4*	0.5 $\mu$ M	0.5 $\mu$ M	+	1 min
	5*	0.3 $\mu$ M	0.3 $\mu$ M	+	1 min
		0.3 $\mu$ M	0.5 $\mu$ M	+	1 min
		0.3 $\mu$ M	0.8 $\mu$ M	+	1 min

<b>Assay</b>	<b>Trial</b>	<b>Forward Primer Concentration (Final)</b>	<b>Reverse Primer Concentration (Final)</b>	<b>BSA</b>	<b>Elongation Time</b>	
LSU	5*	0.5 $\mu$ M	0.3 $\mu$ M	+	1 min	
		0.5 $\mu$ M	0.5 $\mu$ M	+	1 min	
		0.5 $\mu$ M	0.8 $\mu$ M	+	1 min	
		0.3 $\mu$ M	0.5 $\mu$ M	+	1 min	
		0.8 $\mu$ M	0.5 $\mu$ M	+	1 min	
		0.8 $\mu$ M	0.8 $\mu$ M	+	1 min	
	6*	1.0 $\mu$ M	0.3 $\mu$ M	+	1 min	
		1.0 $\mu$ M	0.5 $\mu$ M	+	1 min	
		1.0 $\mu$ M	0.8 $\mu$ M	+	1 min	
		0.8 $\mu$ M	0.3 $\mu$ M	+	1 min	
		0.8 $\mu$ M	0.5 $\mu$ M	+	1 min	
	7*	1.0 $\mu$ M	0.8 $\mu$ M	+	30 sec	
		0.5 $\mu$ M	0.5 $\mu$ M	+	30 sec	
	sxt	1	0.5 $\mu$ M	0.5 $\mu$ M	+	1 min
			0.5 $\mu$ M	0.5 $\mu$ M	+	30 sec
2		0.5 $\mu$ M	0.5 $\mu$ M	-	30 sec	
		0.025 $\mu$ M	0.025 $\mu$ M	+	30 sec	
		0.5 $\mu$ M	0.5 $\mu$ M	-	30 sec	
3		0.5 $\mu$ M	0.5 $\mu$ M	+	30 sec	
		0.5 $\mu$ M	0.75 $\mu$ M	+	30 sec	
		0.5 $\mu$ M	1 $\mu$ M	+	30 sec	

<b>Assay</b>	<b>Trial</b>	<b>Forward Primer Concentration (Final)</b>	<b>Reverse Primer Concentration (Final)</b>	<b>BSA</b>	<b>Elongation Time</b>
sxt	3	0.5 $\mu$ M	1.5 $\mu$ M	+	30 sec
		0.5 $\mu$ M	2 $\mu$ M	+	30 sec
	4	0.5 $\mu$ M	0.5 $\mu$ M	+	1 min
		0.5 $\mu$ M	1.5 $\mu$ M	+	1 min
		0.5 $\mu$ M	3 $\mu$ M	+	1 min
		0.5 $\mu$ M	5 $\mu$ M	+	1 min
		0.25 $\mu$ M	0.5 $\mu$ M	+	1 min
		0.25 $\mu$ M	1.5 $\mu$ M	+	1 min
		0.25 $\mu$ M	3 $\mu$ M	+	1 min
		0.2 $\mu$ M	0.5 $\mu$ M	+	1 min
		0.2 $\mu$ M	1.5 $\mu$ M	+	1 min
		0.2 $\mu$ M	3 $\mu$ M	+	1 min
	5	0.2 $\mu$ M	3 $\mu$ M	+	1 min

**Table S9: Primer combinations and the corresponding efficiencies for the 3<sup>rd</sup> test of the sxt assay. Primer concentrations recorded in this table are the final concentration in the PCR tube.**

<b>Trial</b>	<b>Assay</b>	<b>Forward Primer Concentration (Final)</b>	<b>Reverse Primer Concentration (Final)</b>	<b>Efficiency</b>
3	sxt	0.5 $\mu$ M	0.5 $\mu$ M	74%
		0.5 $\mu$ M	0.75 $\mu$ M	74%
		0.5 $\mu$ M	1 $\mu$ M	73%
		0.5 $\mu$ M	1.5 $\mu$ M	76%
		0.5 $\mu$ M	2 $\mu$ M	77%

**Table S10: Primer combinations and the corresponding efficiencies for the 4<sup>th</sup> test of the sxt assay. Primer concentrations recorded in this table are the final concentration in the PCR tube.**

<b>Trial</b>	<b>Assay</b>	<b>Forward Primer Concentration (Final)</b>	<b>Reverse Primer Concentration (Final)</b>	<b>Efficiency</b>
4	sxt	0.5 $\mu$ M	0.5 $\mu$ M	81.3%
		0.5 $\mu$ M	1.5 $\mu$ M	78.7%
		0.5 $\mu$ M	3 $\mu$ M	80.2%
		0.25 $\mu$ M	0.5 $\mu$ M	82.5%
		0.25 $\mu$ M	1.5 $\mu$ M	91.6%
		0.25 $\mu$ M	3 $\mu$ M	95.8%
		0.2 $\mu$ M	0.5 $\mu$ M	73.9%
		0.2 $\mu$ M	1.5 $\mu$ M	80.6%
		0.2 $\mu$ M	3 $\mu$ M	96%

**Table S11: Primer combinations and the corresponding efficiencies for the 3<sup>rd</sup> and 4<sup>th</sup> tests of the LSU assay. Primer concentrations recorded in this table are the final concentration in the PCR tube.**

<b>Trial</b>	<b>Assay</b>	<b>Forward Primer Concentration (Final)</b>	<b>Reverse Primer Concentration (Final)</b>	<b>BSA</b>	<b>Elongation Time</b>	<b>Efficiency</b>
3	LSU	0.5 $\mu$ M	0.5 $\mu$ M	+	30 sec	77.5% average
4	LSU	0.5 $\mu$ M	0.5 $\mu$ M	+	1 min	84.3% std curve 88.4% Samples

**Table S12: Primer combinations and the corresponding efficiencies for the 5<sup>th</sup> test of the LSU assay. Primer concentrations recorded in this table are the final concentration in the PCR tube.**

<b>Trial</b>	<b>Assay</b>	<b>Forward Primer Concentration (Final)</b>	<b>Reverse Primer Concentration (Final)</b>	<b>Efficiency</b>
5	LSU	0.3 $\mu$ M	0.3 $\mu$ M	83.05%
		0.3 $\mu$ M	0.5 $\mu$ M	82.7%
		0.3 $\mu$ M	0.8 $\mu$ M	83.95%
		0.5 $\mu$ M	0.3 $\mu$ M	84.65%
		0.5 $\mu$ M	0.5 $\mu$ M	83.9%
		0.5 $\mu$ M	0.8 $\mu$ M	84.85%
		0.8 $\mu$ M	0.3 $\mu$ M	86.35%
		0.8 $\mu$ M	0.5 $\mu$ M	84.7%
		0.8 $\mu$ M	0.8 $\mu$ M	85.75%

**Table S13: Primer combinations and the corresponding efficiencies for the 6<sup>th</sup> test of the LSU assay. Primer concentrations recorded in this table are the final concentration in the PCR tube.**

<b>Trial</b>	<b>Assay</b>	<b>Forward Primer Concentration (Final)</b>	<b>Reverse Primer Concentration (Final)</b>	<b>Efficiency</b>
6	LSU	1 $\mu$ M	0.3 $\mu$ M	85.55%
		1 $\mu$ M	0.5 $\mu$ M	84.35%
		1 $\mu$ M	0.8 $\mu$ M	87.25%
		0.8 $\mu$ M	0.3 $\mu$ M	84.05%
		0.8 $\mu$ M	0.5 $\mu$ M	85.1%

**Table S14: Primer combinations and the corresponding efficiencies for the 7<sup>th</sup> test of the LSU assay. Primer concentrations recorded in this table are the final concentration in the PCR tube.**

<b>Trial</b>	<b>Assay</b>	<b>Forward Primer Concentration (Final)</b>	<b>Reverse Primer Concentration (Final)</b>	<b>Elongation Time</b>	<b>Efficiency</b>
7	LSU	0.5 $\mu$ M	0.5 $\mu$ M	30 sec	83.2%
		1 $\mu$ M	0.8 $\mu$ M	30 sec	86.9%

**Table S15: Results from LSU assay test 3. Quantities were calculated using the formula from the line of best fit for the standard curve.**

<b>Day</b>	<b>Farm</b>	<b>Station</b>	<b>Type</b>	<b>Gene Copies</b>
July 2019	Hartz	HP C1	Cage	6529085549
July 2019	Hartz	HP B	Buoy	1105265.98
July 2019	Hartz	HP C2	Cage	3849129858
August 2019	Hartz	HP C1	Cage	262711.023
August 2019	Hartz	HP C1	Cage	1462754.25
August 2019	Hartz	HP C1	Cage	60995.7676
August 2019	Hartz	HP B	Buoy	4679264.7
August 2019	Hartz	HP B	Buoy	4669156817
August 2019	Hartz	HP B	Buoy	6257232528
August 2019	Hartz	HP C2	Cage	5228660.21
August 2019	Hartz	HP C2	Cage	1747089064
August 2019	Hartz	HP C2	Cage	6085238.98
August 2019	Hartz	HP Ref	Reference	1845531.17
August 2019	Hartz	HP Ref	Reference	1257160.29
August 2019	Hartz	HP Ref	Reference	2134142.24
October 2019	Hartz	HP C1	Cage	4912654768
October 2019	Hartz	HP C1	Cage	5554261.17
October 2019	Hartz	HP C1	Cage	4270793
October 2019	Hartz	HP B	Buoy	4314848.49
October 2019	Hartz	HP B	Buoy	5696851.95
October 2019	Hartz	HP B	Buoy	9502036.67

<b>Day</b>	<b>Farm</b>	<b>Station</b>	<b>Type</b>	<b>Gene Copies</b>
October 2019	Hartz	HP C2	Cage	4522128.55
October 2019	Hartz	HP C2	Cage	3130525525
October 2019	Hartz	HP C2	Cage	0
October 2019	Hartz	HP Ref	Reference	6314325631
October 2019	Hartz	HP Ref	Reference	1060802.79
October 2019	Hartz	HP Ref	Reference	1057989.27
November 2019	Hartz	HP C1	Cage	10684788.6
November 2019	Hartz	HP C1	Cage	13513908.9
November 2019	Hartz	HP C1	Cage	14079685.9
November 2019	Hartz	HP B	Buoy	3032423.63
November 2019	Hartz	HP B	Buoy	0
November 2019	Hartz	HP B	Buoy	0
November 2019	Hartz	HP C2	Cage	5900606931
November 2019	Hartz	HP C2	Cage	2209428.52
November 2019	Hartz	HP C2	Cage	1936061.3
November 2019	Hartz	HP Ref	Reference	1349479.41
November 2019	Hartz	HP Ref	Reference	4697792146
November 2019	Hartz	HP Ref	Reference	3515093956
July 2019	Sandy	SP C1	Cage	6486610202
July 2019	Sandy	SP C2	Cage	797285.053
July 2019	Sandy	SP B	Buoy	734406.33
August 2019	Sandy	SP C1	Cage	1075841.12

<b>Day</b>	<b>Farm</b>	<b>Station</b>	<b>Type</b>	<b>Gene Copies</b>
August 2019	Sandy	SP C1	Cage	620107.292
August 2019	Sandy	SP C1	Cage	1613168.6
August 2019	Sandy	SP C2	Cage	3901417238
August 2019	Sandy	SP C2	Cage	0
August 2019	Sandy	SP C2	Cage	1911751.01
August 2019	Sandy	SP B	Buoy	1301261.4
August 2019	Sandy	SP B	Buoy	37256.9925
August 2019	Sandy	SP B	Buoy	1055025.41
August 2019	Sandy	SP Ref	Reference	0
August 2019	Sandy	SP Ref	Reference	683416.673
August 2019	Sandy	SP Ref	Reference	1105093.51
October 2019	Sandy	SP C2	Cage	6642636918
October 2019	Sandy	SP C2	Cage	3679992419
October 2019	Sandy	SP C2	Cage	2593109775
October 2019	Sandy	SP B	Buoy	2113099.94
October 2019	Sandy	SP B	Buoy	2886669.74
October 2019	Sandy	SP B	Buoy	1509289.01
October 2019	Sandy	SP Ref	Reference	5046081063
October 2019	Sandy	SP Ref	Reference	2743929.64
October 2019	Sandy	SP Ref	Reference	4467526565
November 2019	Sandy	SP C1	Cage	6828919010
November 2019	Sandy	SP C1	Cage	4240511.97

<b>Day</b>	<b>Farm</b>	<b>Station</b>	<b>Type</b>	<b>Gene Copies</b>
November 2019	Sandy	SP C1	Cage	6044535.04
November 2019	Sandy	SP C2	Cage	4662984.44
November 2019	Sandy	SP C2	Cage	3695057.19
November 2019	Sandy	SP C2	Cage	3600727.39
November 2019	Sandy	SP B	Buoy	4595344.83
November 2019	Sandy	SP B	Buoy	3604274755
November 2019	Sandy	SP B	Buoy	2847486945
November 2019	Sandy	SP Ref	Reference	574882.787
November 2019	Sandy	SP Ref	Reference	1007253.81
November 2019	Sandy	SP Ref	Reference	0

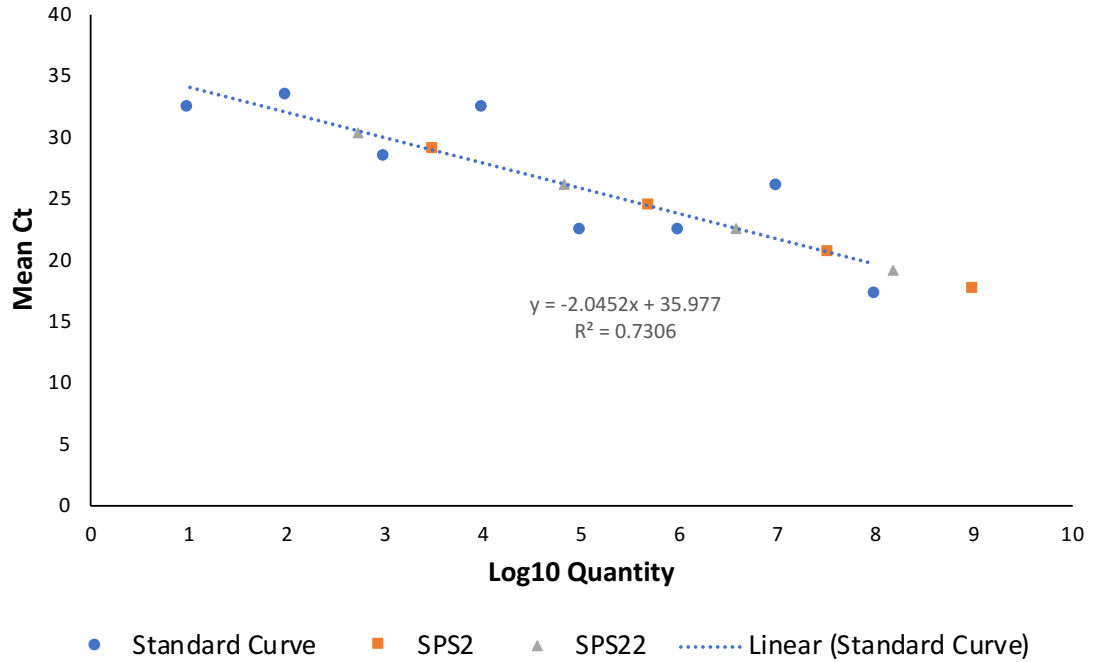


**Figure S17: Plot of the mean Ct values against the log<sub>10</sub> quantity of the standard curve for the LSU assay test 4. The formula of the line of best fit was used to calculate the quantities in the sample dilutions from the Ct values. SPS2 corresponds to Sandy Point station C2 in July 2018, while SPS22 corresponds to Sandy Point reference station in October 2019.**

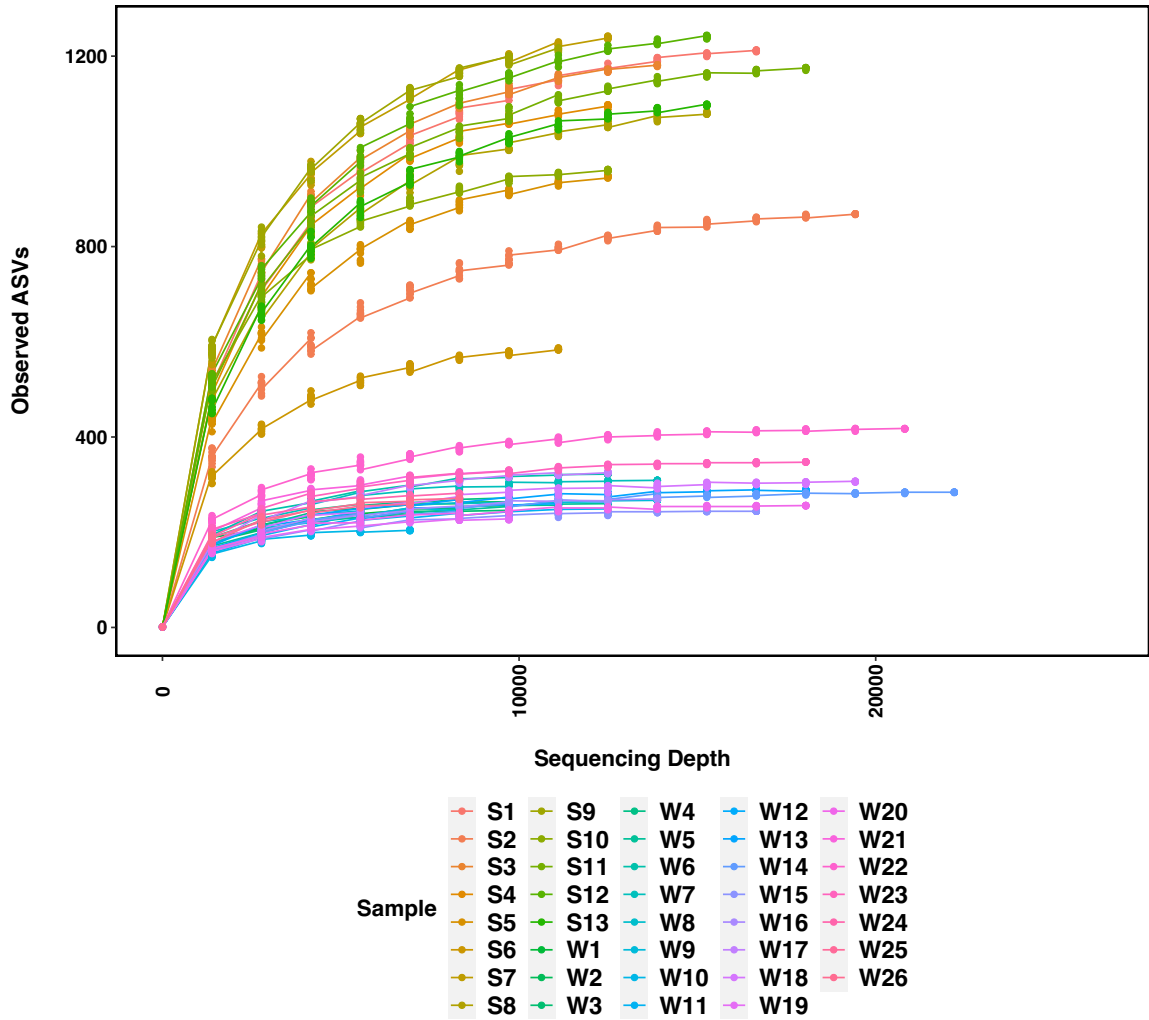


**Figure S18: Alpha rarefaction curves for sediment (S) and water column (W) samples from Run 1 of 16S V4V5 sequencing.**

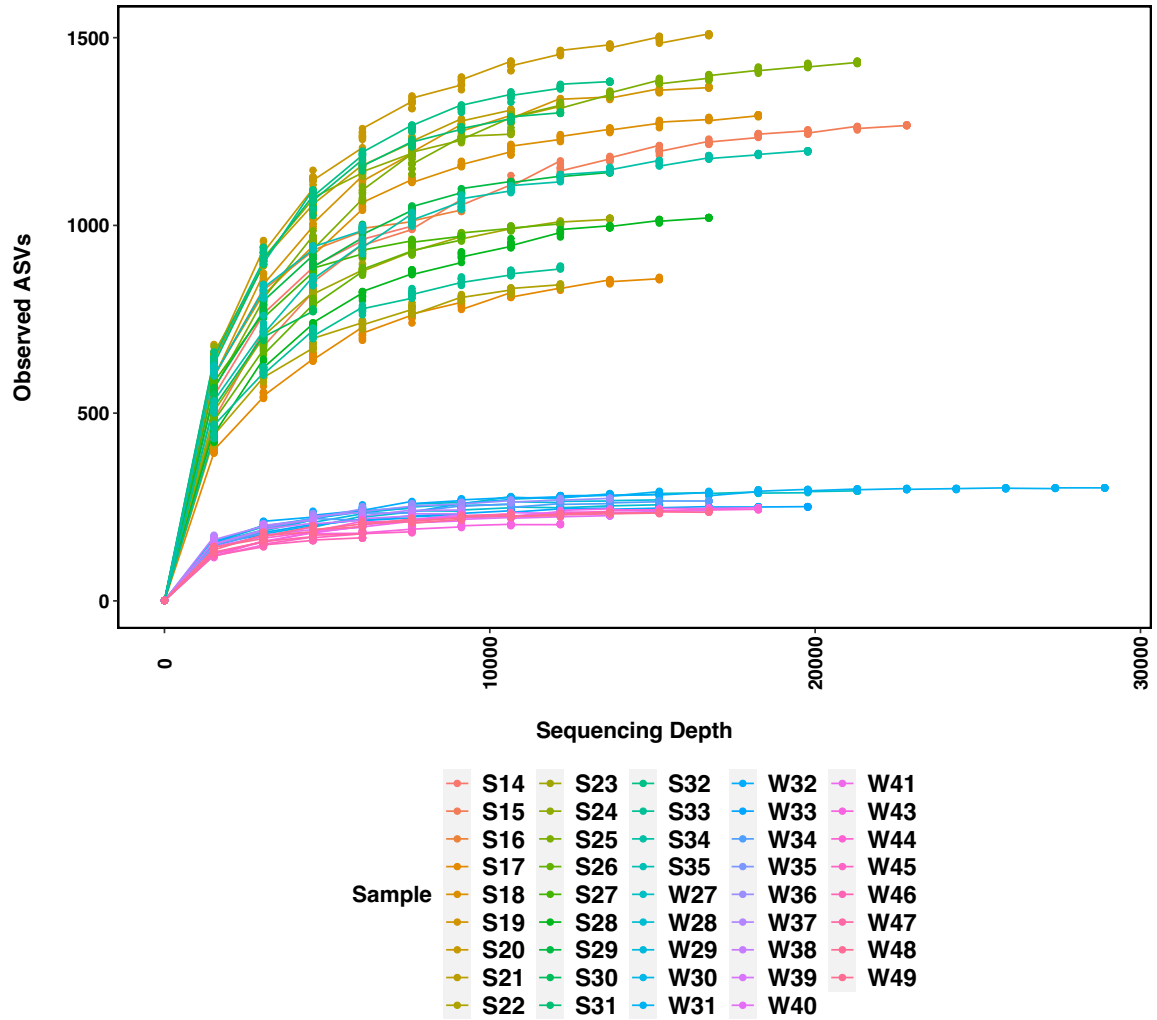


**Figure S19: Alpha rarefaction curves for sediment (S) and water column (W) samples from Run 2 of 16S V4V5 sequencing.**

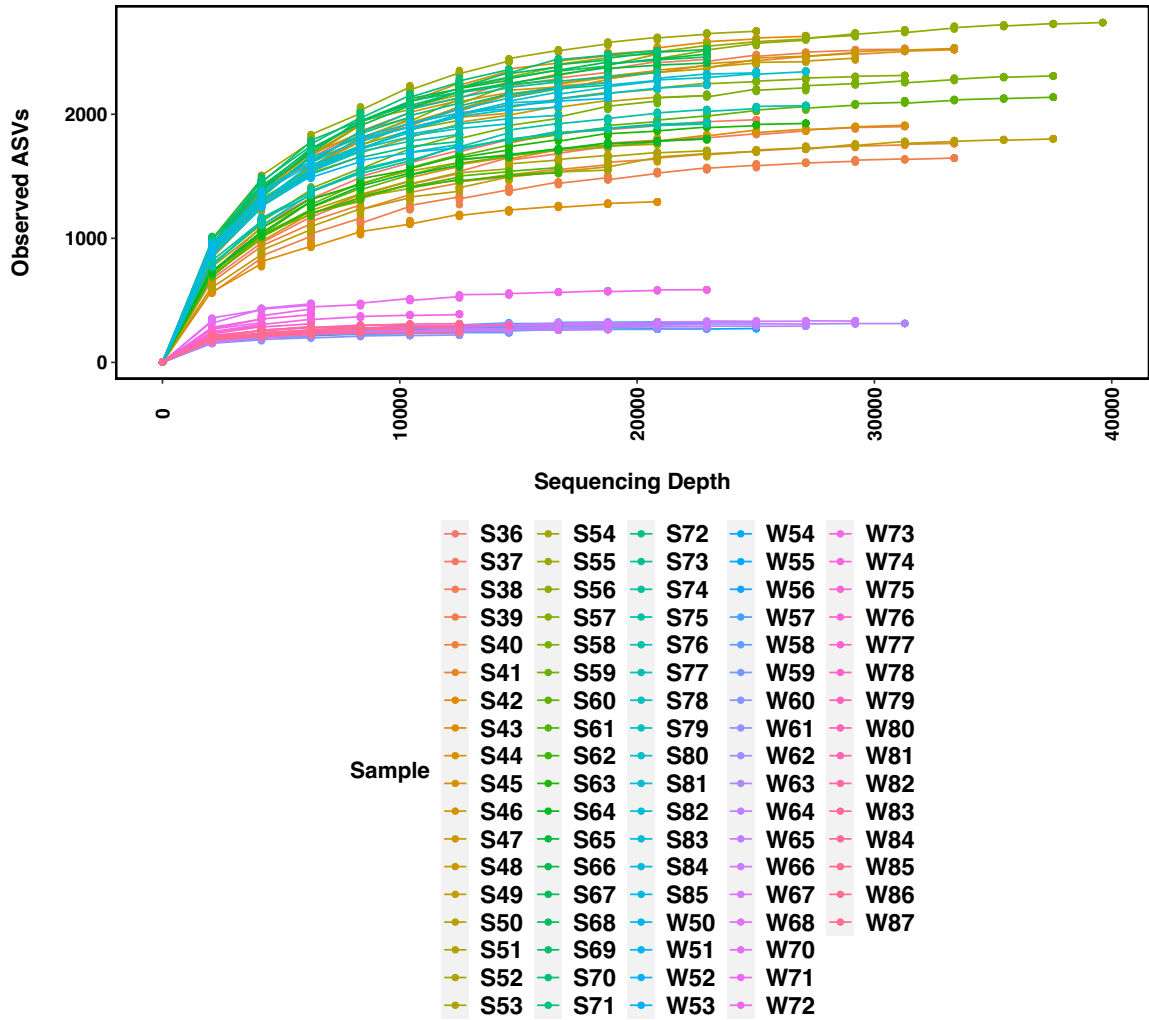


**Figure S20: Alpha rarefaction curves for sediment (S) and water column (W) samples from Run 3 of 16S V4V5 sequencing.**

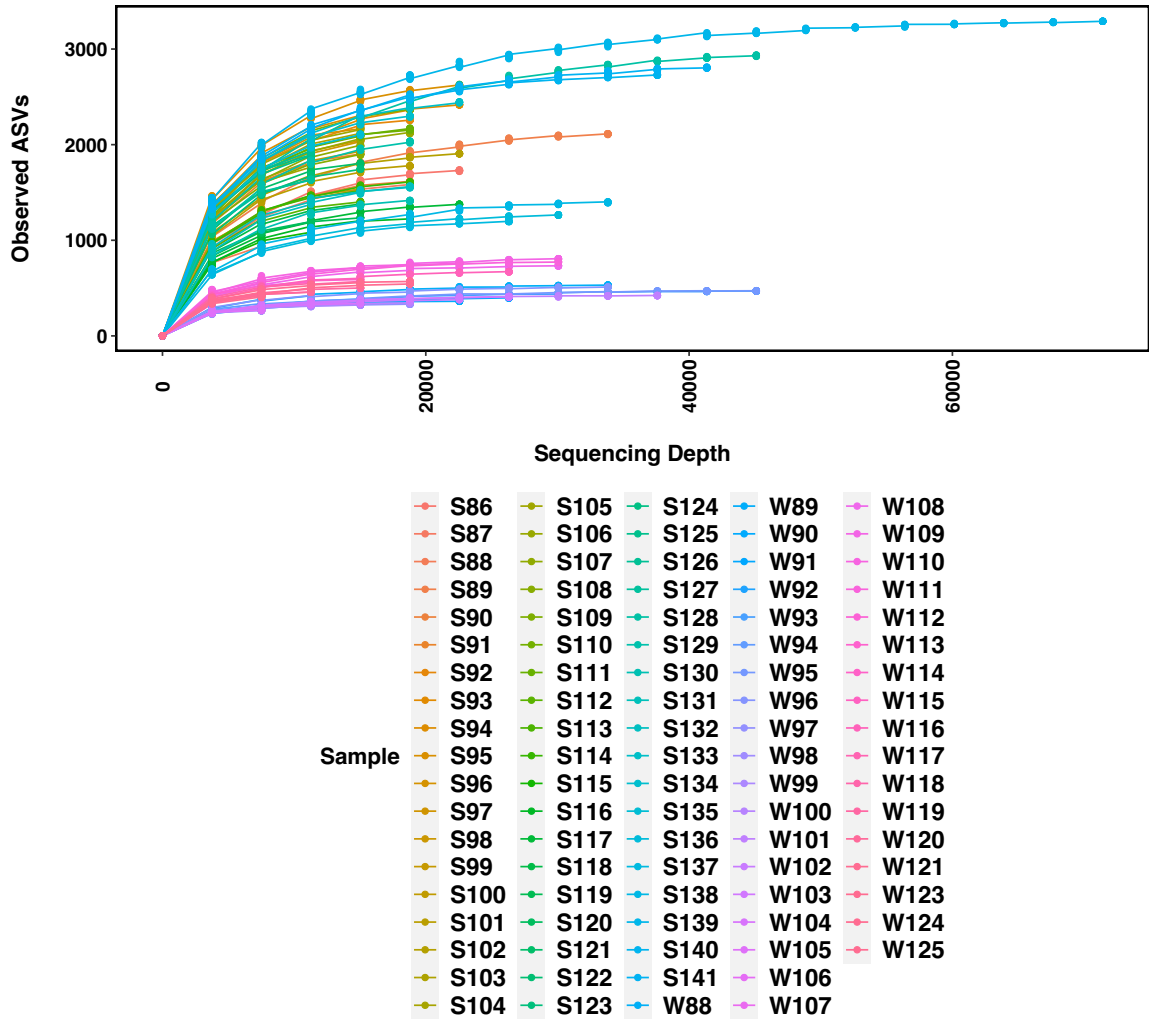


**Figure S21: Alpha rarefaction curves for sediment (S) and water column (W) samples from Run 4 of 16S V4V5 sequencing.**

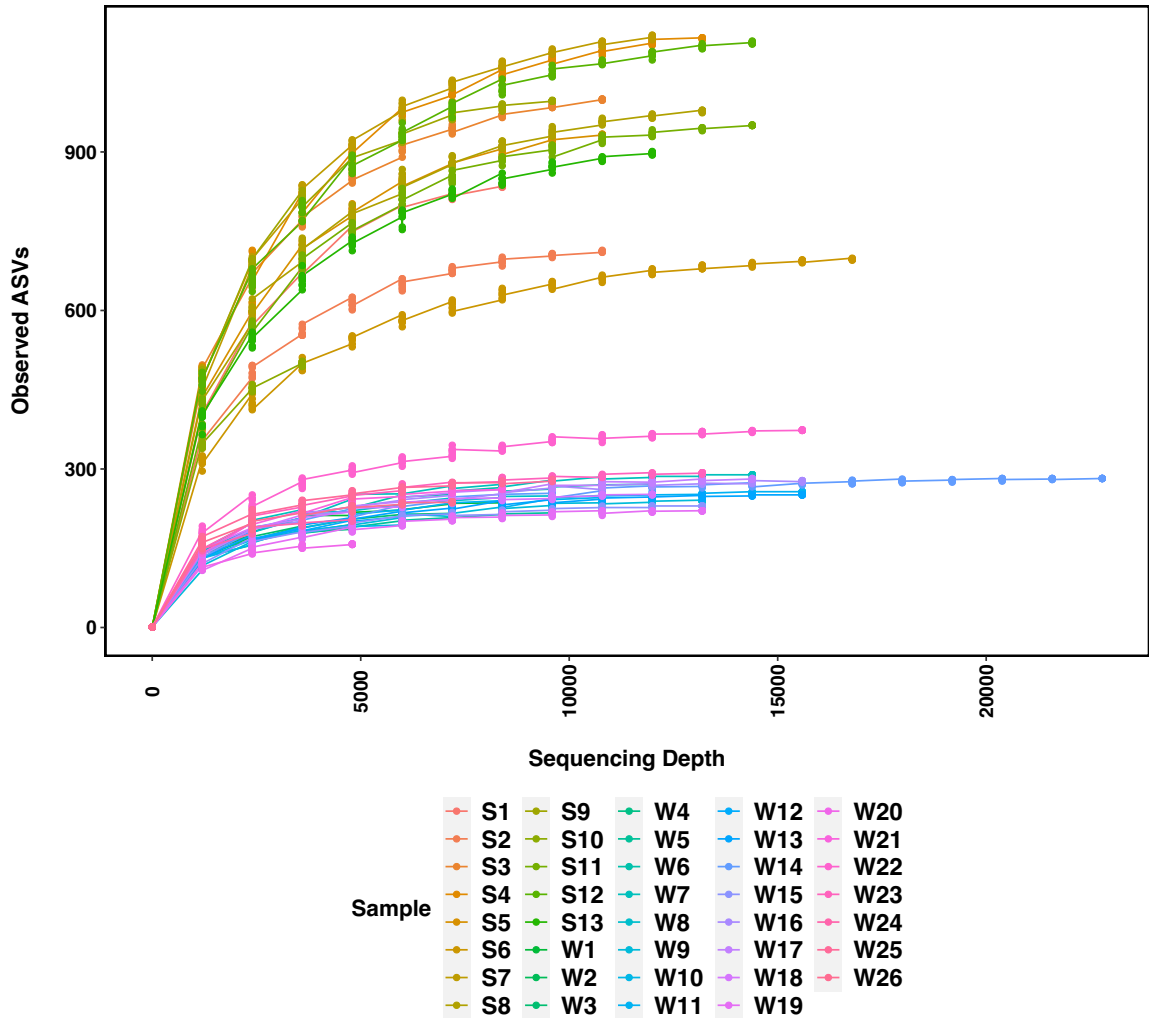


**Figure S22: Alpha rarefaction curves for sediment (S) and water column (W) samples from Run 1 of 16S V6V8 sequencing.**





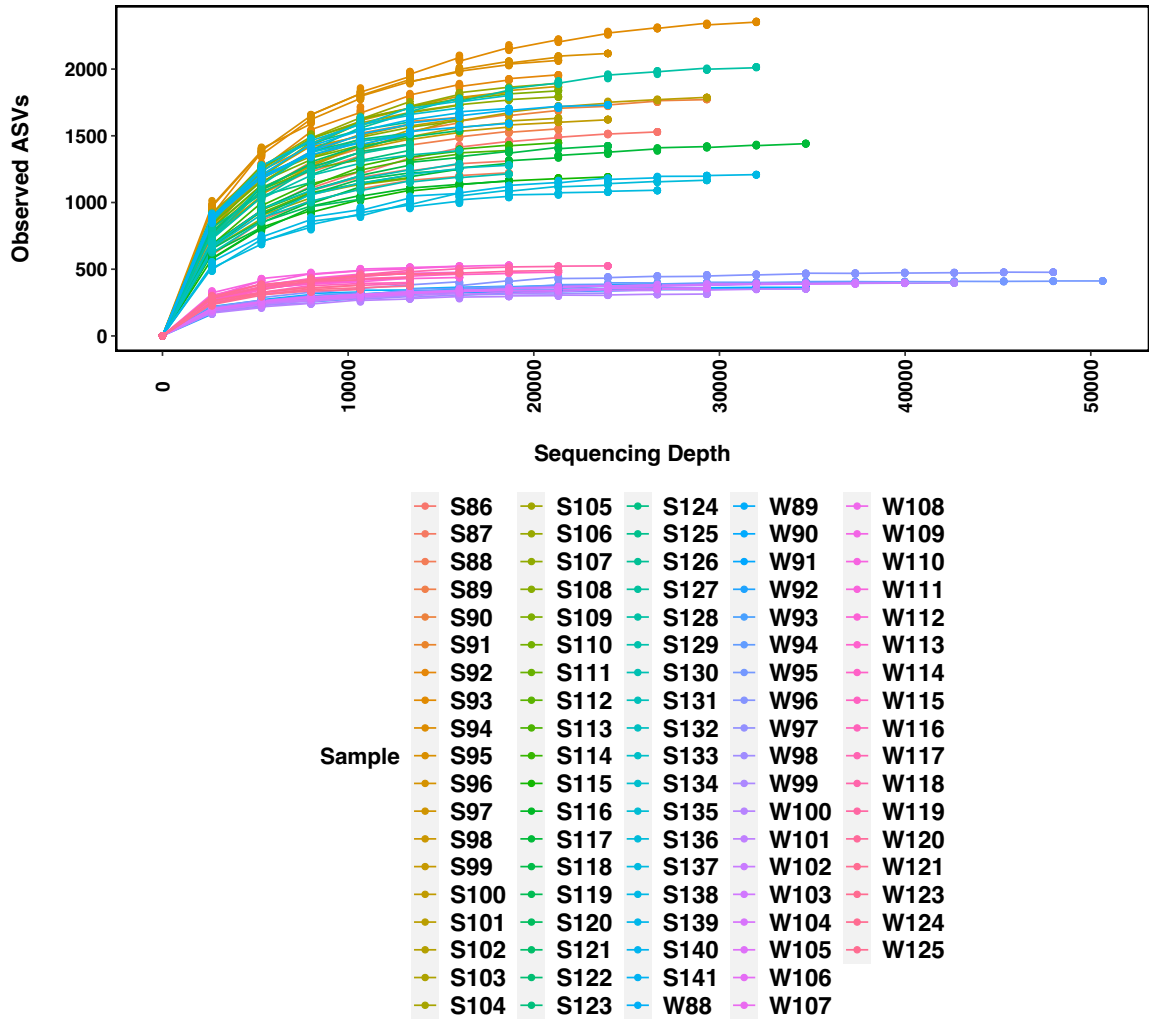
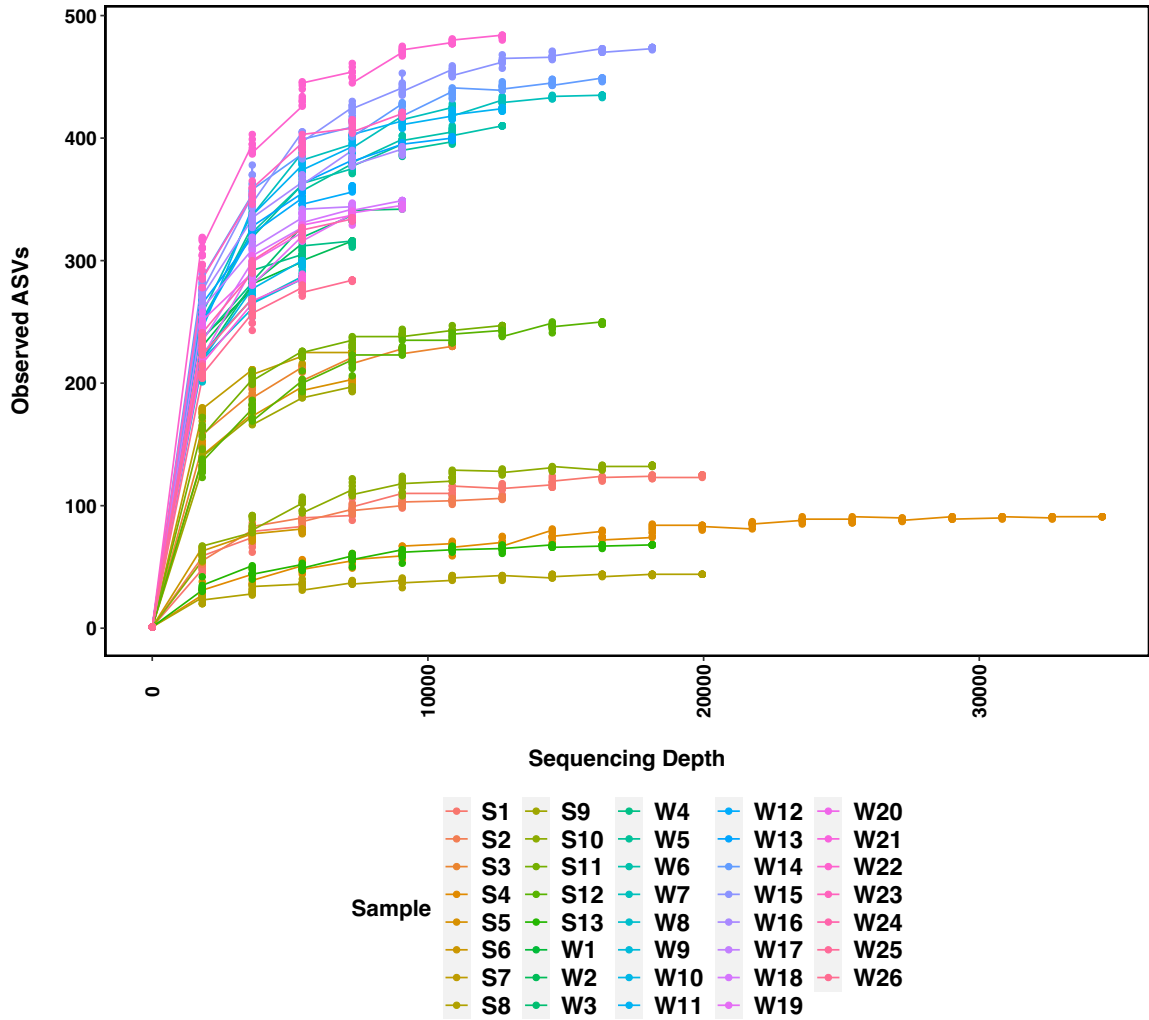
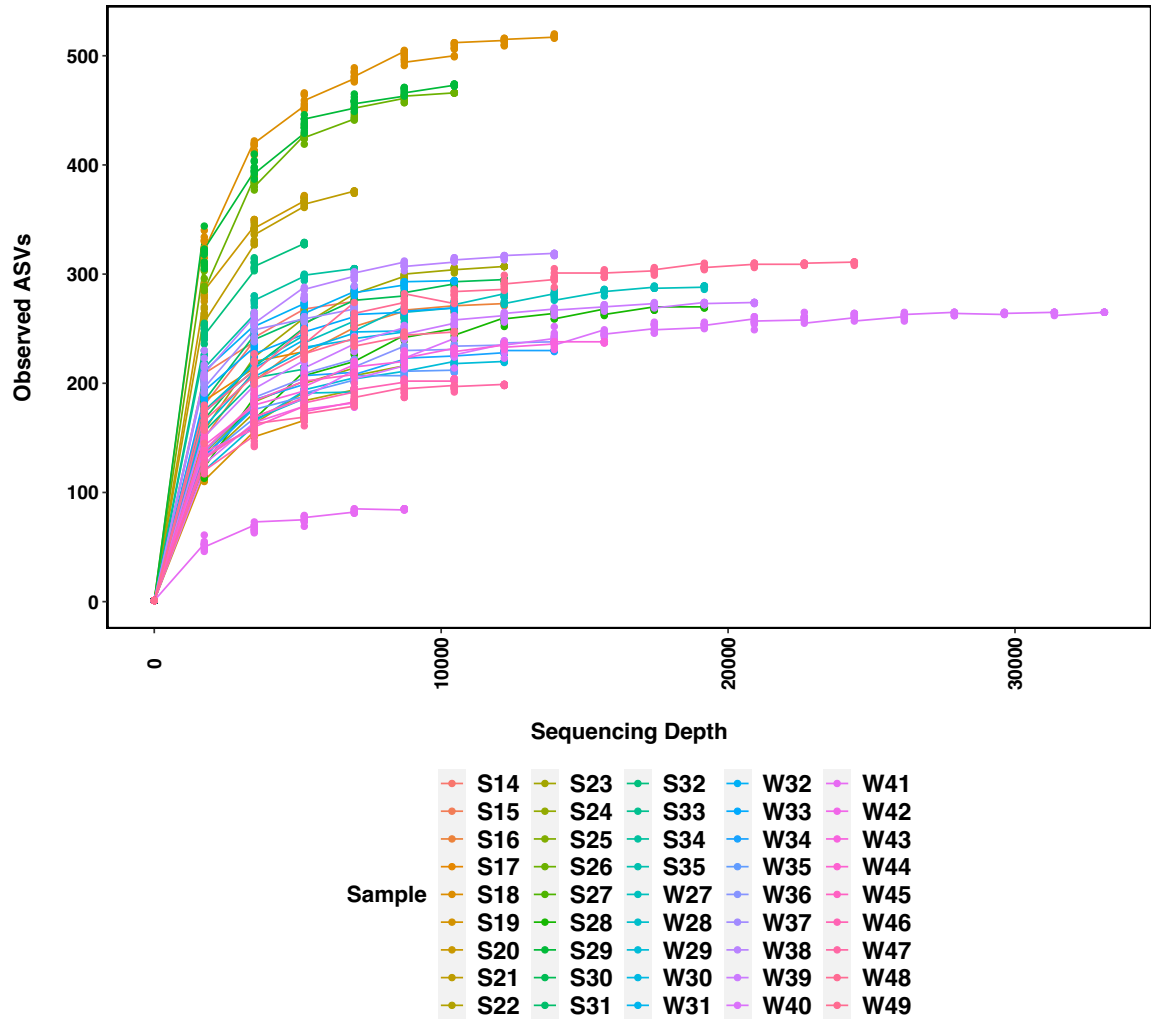


Figure S25: Alpha rarefaction curves for sediment (S) and water column (W) samples from Run 4 of 16S V6V8 sequencing.



**Figure S26: Alpha rarefaction curves for sediment (S) and water column (W) samples from Run 1 of 18S V4 sequencing.**



**Figure S27: Alpha rarefaction curves for sediment (S) and water column (W) samples from Run 2 of 18S V4 sequencing.**

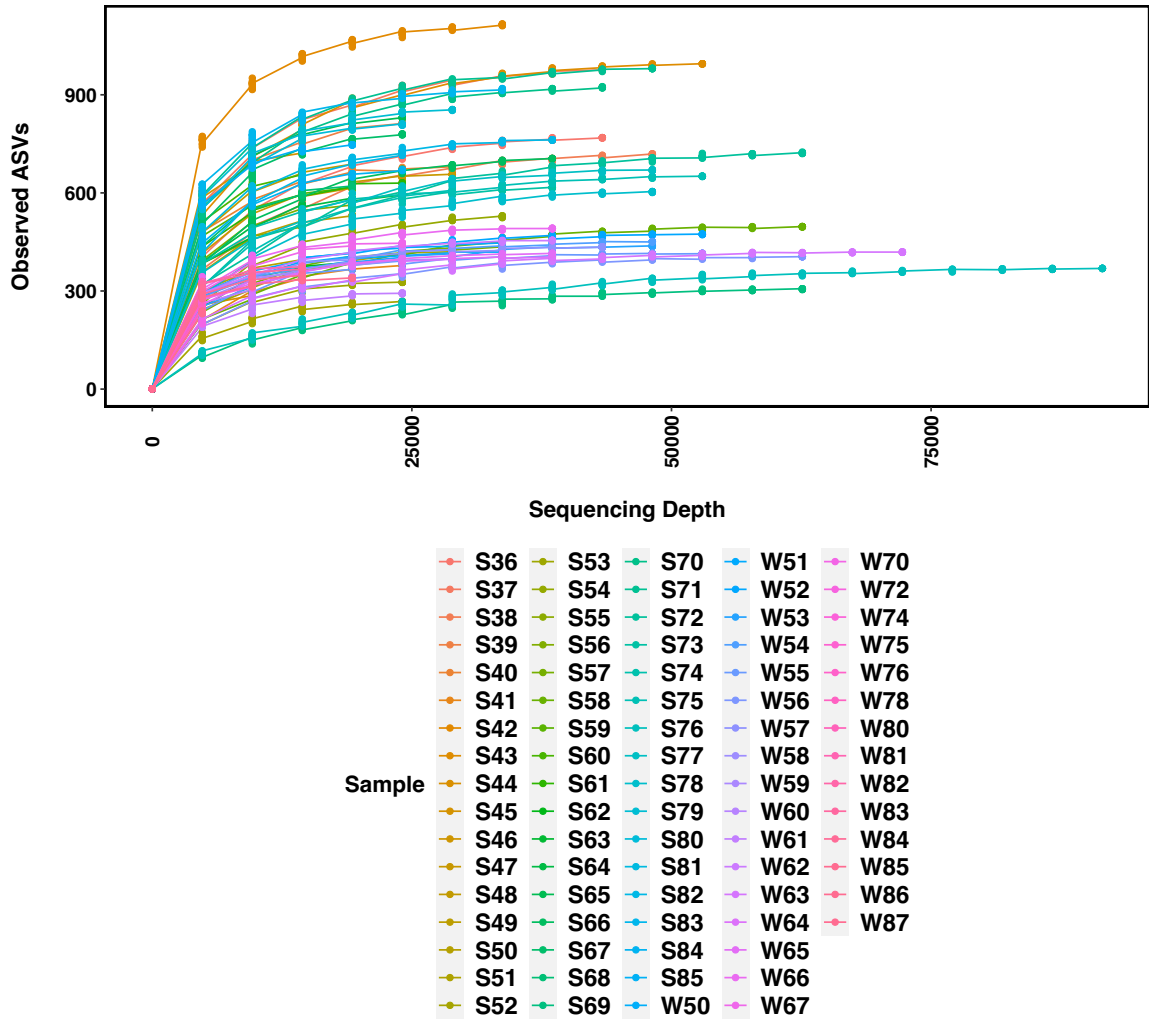


**Figure S28: Alpha rarefaction curves for sediment (S) and water column (W) samples from Run 3 of 18S V4 sequencing.**

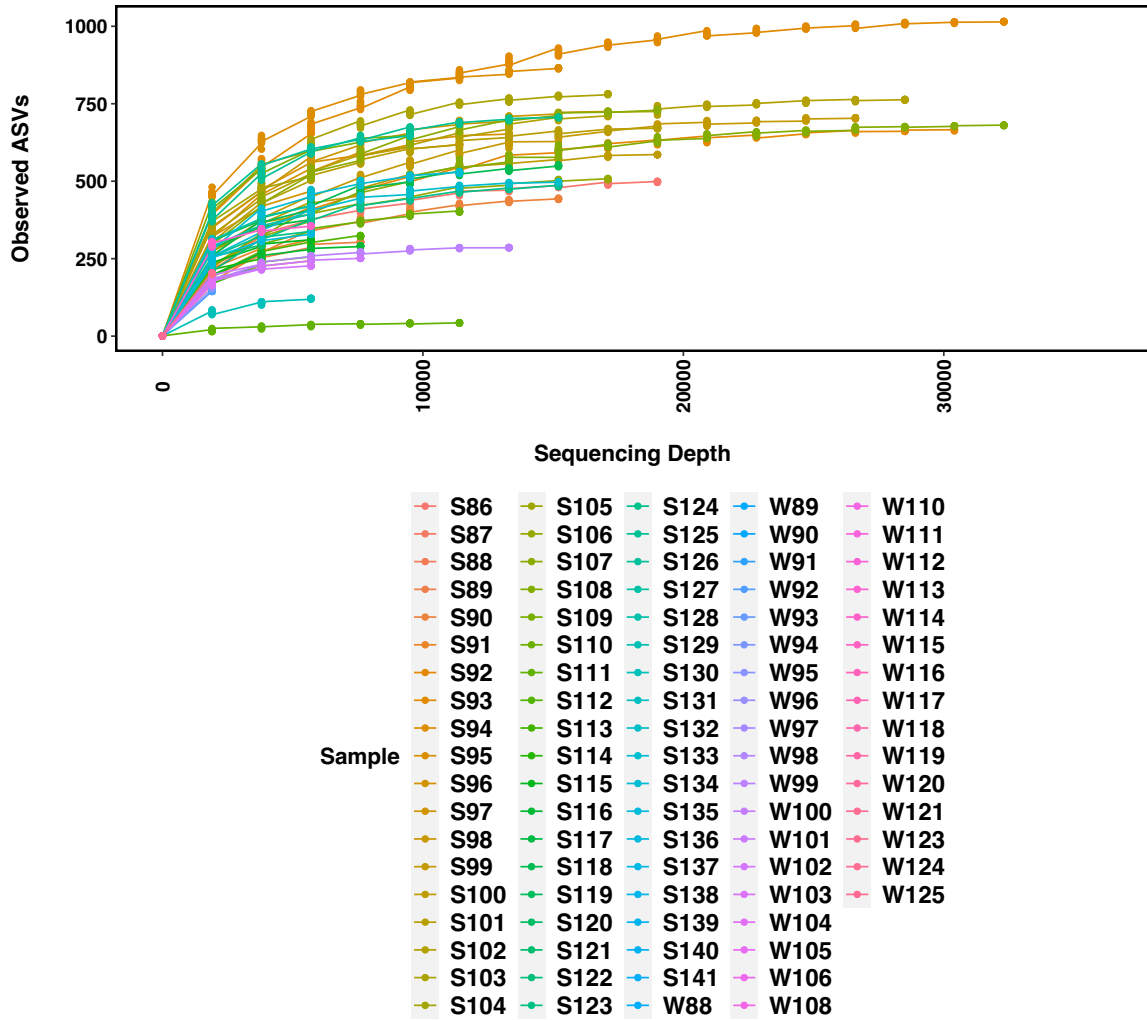


**Figure S29: Alpha rarefaction curves for sediment (S) and water column (W) samples from Run 4 of 18S V4 sequencing.**